12
B.S.

Convective Burning in Propellant Defects: A Literature Review

by

Harold H. Bradley, Jr.
Thomas L. Boggs

Aerothermochemistry Division

Research Department

FEBRUARY 1978

Naval Weapons Center
CHINA LAKE, CALIFORNIA 93555

Naval Weapons Center

AN ACTIVITY OF THE NAVAL MATERIAL COMMAND

FOREWORD

This work was performed during the period 1 April through 30 September 1977. The purpose was to conduct a survey of the literature describing the transition from purely conductive combustion (laminar surface regression) to convective combustion (combustion within the sample) of propellants.

This report has been reviewed for technical accuracy by Dr. R. L. Derr and Mr. Jack L. Prentice.

Approved by
E. B. ROYCE, *Head*
Research Department
15 February 1978

Under authority of
W. L. HARRIS, JR.
RAdm., U.S. Navy
Commander

Released for publication by
R. M. HILLYER
Technical Director (Acting)

NWC Technical Publication 6007

Published by ..... Technical Information Department
Collation ..... Cover, 51 leaves
Firsting printing ..... 210 unnumbered copies

1 Universal Propulsion Company, Riverside, CA (H. J. McSpadden)
1 University of California, Lawrence Radiation Laboratory, Livermore, CA (P. Urtiew)
1 University of California, San Diego, La Jolla, CA (AMES Dept, Forman A. Williams)
1 University of Delaware, Newark, DE (Department of Chemistry, T. C. Brill)
1 University of Illinois, Urbana, IL (AAE Dept, Herman Krier)
1 University of Massachusetts, Amherst, MA (Dept of Mechanical Engineering, Karl Jakus)
1 University of Southern California, Los Angeles, CA (Mechanical Engineering Dept/OHE200, M. Gerstein)
2 University of Texas, Austin, TX
  E. Becker (1)
  Dr. Jack Turner (1)
3 University of Utah, Salt Lake City, UT
  Dept of Chemical Engineering, Alva D. Baer (1)
  G. A. Flandro (1)
  S. Swanson (1)
1 University of Washington, Seattle, WA (G. Duvall)
2 Whittaker Corporation, Bermite Division, Saugus, CA
  L. Bloom (1)
  L. LoFiego (1)

UNCLASSIFIED

SECURITY CLASSIFICATION OF THIS PAGE (When Data Entered)

REPORT DOCUMENTATION PAGE

READ INSTRUCTIONS BEFORE COMPLETING FORM

1. REPORT NUMBER: (14) NWC-TP-6007
2. GOVT ACCESSION NO.
3. RECIPIENT'S CATALOG NUMBER

4. TITLE (and Subtitle): (6) CONVECTIVE BURNING IN PROPELLANT DEFECTS: A LITERATURE REVIEW.

5. TYPE OF REPORT & PERIOD COVERED: (9) Final Report 1 Apr [redacted] 30 Sep [redacted]77

6. PERFORMING ORG. REPORT NUMBER

7. AUTHOR(s): (10) Harold H. Bradley, Jr.
Thomas L. Boggs

8. CONTRACT OR GRANT NUMBER(s)

9. PERFORMING ORGANIZATION NAME AND ADDRESS
Naval Weapons Center
China Lake, California 93555

10. PROGRAM ELEMENT, PROJECT, TASK AREA & WORK UNIT NUMBERS

11. CONTROLLING OFFICE NAME AND ADDRESS
Naval Weapons Center
China Lake, California 93555

12. REPORT DATE: (11) Feb [redacted]78

13. NUMBER OF PAGES: 100 (12) 94

14. MONITORING AGENCY NAME & ADDRESS (if different from Controlling Office)

15. SECURITY CLASS. (of this report): UNCLASSIFIED

15a. DECLASSIFICATION/DOWNGRADING SCHEDULE

16. DISTRIBUTION STATEMENT (of this Report)

Approved for public release; distribution unlimited.

17. DISTRIBUTION STATEMENT (of the abstract entered in Block 20, if different from Report)

18. SUPPLEMENTARY NOTES

19. KEY WORDS (Continue on reverse side if necessary and identify by block number)

Combustion
Combustion in cracks
Conductive burning
Convective burning
Deflagration-to-detonation transition
Development of convective combustion
High energy propellants
Ignition rates
Onset of convective combustion
Porous propellants
Propellant defects

20. ABSTRACT (Continue on reverse side if necessary and identify by block number)

(See back of form.)

DD FORM 1 JAN 73 1473 EDITION OF 1 NOV 65 IS OBSOLETE
S/N 0102-014-6601

UNCLASSIFIED

SECURITY CLASSIFICATION OF THIS PAGE (When Data Entered)

(U) *Convective Burning in Propellant Defects: A Literature Review*, by Harold H. Bradley, Jr. and Thomas L. Boggs. China Lake, Calif., Naval Weapons Center, February 1978. 100 pp. (NWC TP 6007, publication UNCLASSIFIED.)

(U) This report presents a survey of literature describing the onset and development of convective combustion--one of the first steps associated with the transition of deflagration-to-detonation of solid propellants. It contains results from experiments using various single pore (or channel) geometry and porous bed geometry, as well as damaged propellant samples. A section describes the results from various analytical models as applied to single pore and porous bed geometries.

(U) Attributes that favor convective combustion are presented in the context of: attributes favoring gas flow into the defects, attributes favoring ignition of the pore surfaces, and attributes favoring acceleration of the convective front.

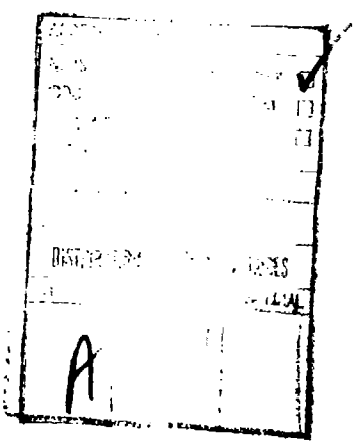

CONTENTS

1.0 INTRODUCTION

Solid rocket propellants, being highly energetic compounds, may, upon exposure to suitable stimulus, deflagrate or detonate. For rocket propulsion, these energetic compounds must deflagrate in a predictable and controllable manner, converting the stored potential chemical energy into high temperature gases which, when exhausted, result in a thrust imparted to the missile. Unfortunately, this same stored chemical energy can also be released as a detonation. Usually, the stimulus causing detonation is provided by mechanical action and is referred to as shock-to-detonation initiation (SDI) (analogous to initiation by a small amount of primary explosive). However, detonation can also occur as a transition from deflagration without any external mechanical initiating source. In this case, called deflagration-to-detonation transition (DDT), the initiating energy originates in the deflagration itself as a result of the synergistic interaction between pressure and mass burning rate, leading to abnormally high rates of pressure rise. This transition is thought to occur as follows:

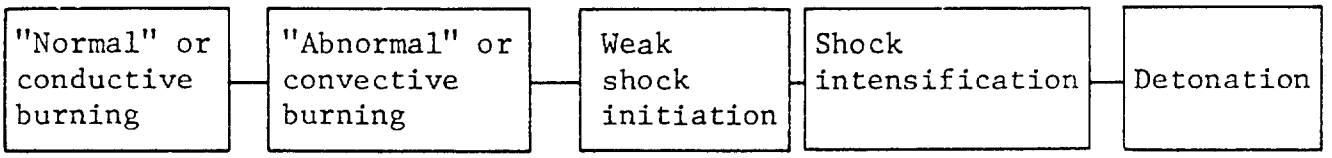

The first transition might be thought of as the change from normal conductive (layerwise) combustion to the more rapid abnormal convective combustion (burning "within" the sample). Pressure generation rate is a function of the mass burning rate, and mass burning rate is proportional to the product of linear burning rate (surface regression rate) and the burning surface area. Since the known dependence of surface regression rates on pressure cannot alone account for the pressurization rates required to cause transition to detonation, then increased burning surface area must also be involved in producing the required mass burning rates, hence pressurization rates. Two requirements must be satisfied in order to transit from normal conductive burning to the abnormal convective burning: (1) the existence of extra surface area (defects) prior to combustion or its creation during combustion, and (2) the development of combustion on the increased surfaces. The correctness of the above seems to be confirmed by the lack of experimental evidence showing a consolidated charge undergoing DDT. In fact, investigators studying DDT phenomena often "shred" their samples.

Given the simple flow chart presented above and the two criteria outlined in the preceding paragraph, then one of the most important areas to be considered in trying to understand DDT is the penetration and establishment of the combustion front in propellant defects. It is the purpose of this survey to present what is known of the early development of combustion into defects - a necessary condition for the later transition to full convective burning and detonation.

Two aspects of combustion are considered: the onset of anomalous combustion and the progression of combustion into the defects. The first is primarily qualitative and relates to experimental observation of a singularity indicating whether or not convective burning occurred (go-no go type of test). Results of onset experiments are commonly displayed as a graphical relation which shows combinations of pressure and defect dimension for which combustion either does or does not penetrate the defect. The coordinates of such plots are usually referred to as critical pressure or critical defect size (crack width or pore diameter); it is actually the relation between the two which is critical, and no importance should be attributed to the variable which is so characterized. Other terms synonymous with critical pressure are: breakdown pressure, transition pressure, threshold pressure, and pressure at which stable burning is impaired. The critical pore size is sometimes referred to as the threshold crack width or pore diameter.

The second aspect of combustion is more quantitative, is not as extensively investigated, requires more sophisticated measurement techniques, and yields information on the rate of propagation of the ignition front into the propellant defect up to, but not including, generation of weak shocks.

At this point it is well to divert the discussion to define the terminology relevant to the various rates (velocities) of processes encountered in the survey.

Conductive rate. This is the rate of regression of a solid surface of propellant in cm/s. It is often called "normal" burning rate, surface regression rate, or simply burning rate. The latter term will not be used in this survey because of possible confusion with mass burning rate.

Ignition rate. This is the rate in cm/s at which a state of ignition (self sustained combustion) is propagated into a single pore or porous bed of propellant. Synonymous expressions are ignition propagation rate, convective burning rate, convective propagation rate, or convective rate.

Flow rate. This is the rate in cm/s at which hot gases flow in a single pore or porous bed, with or without ensuing ignition. As will be described in the appropriate sections of the survey, the gases always flow ahead of the ignition front during early stages of development of convective burning.

Mass burning rate. This is the rate of generation of combustion products in g/cm^2-s. As stated earlier, it is determined both by the conductive rate and the burning surface area, and is the quantity directly responsible for rate of pressure rise.

Much of the experimental and theoretical work on the early stages of convective burning has been conducted over the last 30-40 years in the Soviet Union. The work covers a broad spectrum of experimental conditions, sample geometries, and propellant types. *It is important to note that the term propellant, when used to describe Soviet work, does not imply an operational rocket propellant, but is used synonymously with such expressions as propellant powder, explosive, porous system, porous powder, porous charge, and others. Regardless of the name, a common feature of the samples used by the Soviets in porous bed experiments is that they are prepared by pressing or pouring mixtures of ingredients in powdered form. While the ingredients may include polymeric materials, no use is made of the binding properties of the polymer to prepare a monolithic sample.*

This report is primarily a survey of the Soviet literature but also includes non-Soviet literature relevant to early convective burning. The purpose is to bring together in an organized fashion the available information on the subject to serve as a point of departure for future experimental and theoretical work. In addition, answers were being sought to several broad questions.

1. What propellant characteristics are responsible for the onset and development of the early steps of convective burning?
2. To which characteristics are this onset and development most and least sensitive?
3. What tests and test conditions are suitable for determining these characteristics?
4. What tests and test results most nearly simulate operational firings of rocket motors?

The next section of the report explains the organization of the survey.

2.0 SURVEY ORGANIZATION

The literature describing the early stages of convective burning consists of both experimental (Section 3) and theoretical (Section 4) approaches to the problem. Two separate sections were chosen because, unfortunately, there is little systematic interaction between the two approaches.

2.1 ORGANIZATION OF SECTION 3: RESULTS FROM EXPERIMENTS

There are many aspects of convective burning, and experiments have been designed to understand various combinations of variables. The many variables to be controlled can be grouped as follows.

2.1.1 Sample

Composition (homogeneous and heterogeneous) and sample geometry have been widely studied. Two main geometric divisions are single pores (or channels bounded by propellant) and porous beds of propellant. A third type of sample, damaged propellant, was studied, but is not included in the morphological organization because of the limited amount of work conducted. The first is characterized by known length and cross-sectional shape. The second is an array of pores which are numerous enough that they must be described by statistical average quantities such as porosity, pore size distribution, particle size, specific surface area, and permeability to fluid flow. Methods of measuring these quantities as well as theories of flows through packed beds are presented in numerous standard references [Scheidegger (1974), Muskat and Wyckoff (1946), Bear (1972), Carman (1956)] as well as in one of the surveyed reports [Belyaev (1973), Sections 4 and 5]. Two comments on porous materials are appropriate at this point. First, the Russian theoretical approaches to early convective burning are based entirely on the permeability concept rather than on the fluidized bed concept used in many western models of the development of shock waves. Second, the single pore and the statistical porous bed represent two extremes with the actual conditions of irregularly branched cracks in between where no precise quantification of the defect has yet been devised for correlation with experimental results.

Both of the main types (single pore vs. porous bed) may be further characterized to include:

1. The embedded or built-in charge. In this case the sample is completely encased in gas impermeable material (Figure 1a, b) assuring that the defect is not prepressurized by the gases that would pressurize a closed vessel. This condition simulates rocket charge defects that are not originally open to the bore, i.e., the burning surface must regress to the defect.

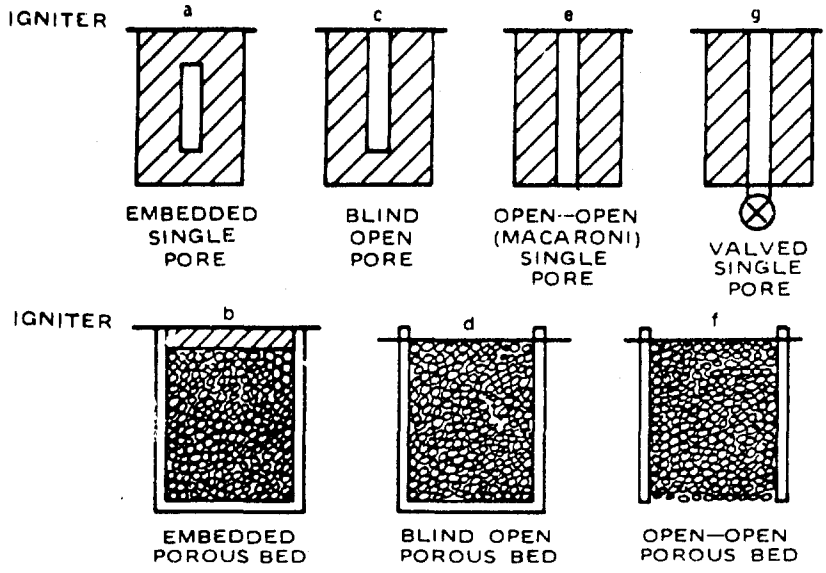

FIGURE 1. Test Sample Geometries.

2. The open defect. Here the defect is left open to the bomb pressure and the ignition event at the ignited end. This case has several subcases:

a. The unignited end is sealed (the so-called blind or closed defect shown in Figure 1c, d).
b. The unignited end is open to the bomb pressure (Figure 1e, f).
c. The unignited end is connected through a valve to a pressure less than the bomb pressure (1 atm [0.1 MPa] was used by Krasnov) (Figure 1g).

2.1.2 Environment and Stimulus

In general, convective burning is studied experimentally by burning one of the propellant samples discussed above under controlled conditions. Development of convective burning depends upon a pressure differential between the external pressure and the pressure within the defect. The external pressure may be provided by carrying out the experiment (1) in a closed bomb with only a slight pressure rise during the test, (2) in a closed bomb in which the pressure rises rapidly and significantly during the test, or (3) at ambient atmospheric pressure. In the literature reviewed, the rapid pressure rise is provided (with a single exception) by combustion of the test charge in a high loading density combustion bomb (HLDCB) with a typical loading density (grams of propellant per cubic centimeter of bomb volume) of 0.02-0.1 g/cm^3. Tests leading to small pressure rises are conducted in a low loading density combustion bomb (LLDCB) with a typical loading density less than 0.0002 g/cm^3, where the contribution of gases from the burning charge are

negligible compared with the initial gas pressure. The HLDCB (Russian equivalent: manometer bomb or bomb of rising pressure) and LLDCB (Russian equivalent: bomb of constant pressure) were discussed by Boggs (1976). In the single exception, noted above, the high rate of pressure rise is provided by admitting nitrogen gas through a regulator to the bomb during the test. It should be noted that the quantitative effect of rate of pressure rise in the HLDCB has not been studied extensively. The pressure in the LLDCB also rises during a test (the magnitude and rate may be partially offset by using a surge tank); the few atmospheric tests reported eliminate this effect. There are no tests employing pressures above atmospheric with strictly zero pressure rise rate. Such capability would be useful in exploring dynamic pressure effects but would not simulate any practical condition.

While the pressure in the HLDCB is provided primarily by sample combustion, the pressure in the LLDCB must be adjusted to the desired operating point by introducing a gas, usually nitrogen or argon, from an external source. The implications of this difference in operating mode are considerable. In addition to requiring many more tests to span a given pressure range [Boggs (1976)] the driving force causing penetration of combustion into propellant defects may be quite different in the two cases. In the HLDCB, the forcing pressure differential arises because, at the beginning of the test, the pressure external to the defect rises faster than the internal pressure. In the LLDCB, there are two possibilities. First, if the test sample is "embedded," so that its pores (at low pressure, e.g., 1 atm [0.1 MPa]) are sealed against the initial bomb pressure by an impermeable layer of auxilliary propellant, then at the instant of burnthrough of this layer, the pressure differential is set by the difference between pore pressure and the bomb pressure. Obviously this arrangement is feasible only for the blind pore or porous bed. Second, if the test sample is open to the bomb pressure, the pores are initially filled with cold, high pressure inert gas used to pressurize the bomb. Now the pressure differential responsible for convective burning originates in the slow pressure rise in the LLDCB or in the combustion process itself (dynamic pressure), which generates a slightly higher pressure at the surface of the propellant than in the surrounding volume. Moreover, the presence of the cold gases in the pore makes penetration of combustion into the pores more difficult because the initial gases must be displaced or heated before ignition of the pores can occur.

The morphology described above is graphically presented in Table 1, which also indicates references where relevant information was obtained for this survey. The columns of this matrix are concerned with the sample. This broad area is divided into single pore and porous beds. The single pore is further divided into embedded (Figure 1a), blind (Figure 1c), macaroni (open-open as shown in Figure 1e), and valved (Figure 1g). The porous bed is divided into embedded (Figure 1b), blind (Figure 1d), and open-open (Figure 1f). The rows in the matrix are

TABLE 1. Morphology of Literature on Experimental Convective Burning

O = Onset of combustion
D = Development of convective combustion

Single pore	Embedded	Blind	Open-open	Valved
p > 1 atm (0.1 MPa) $\dot{p} \approx 0$ LLDCB	Godai (1970) O	Bobolev (1965a) OD Margolin and Margulis (1969) O Belyaev (1973) D Belyaev (1969) D Prentice (1962) O Prentice (1977) O	Bobolev, (1965a) OD Margolin and Margulis (1969) O Belyaev (1969) D Payne (1969) D Prentice (1962) O Prentice (1977) O	Krasnov (1970) D
p > 1 atm (0.1 MPa) $\dot{p} >> 0$ HLDCB		Belyaev (1973) O Bobolev (1965a) O	Bobolev (1965a) O	
p = 1 atm (0.1 MPa)		Godai (1970) O	Godai (1970) O	
Porous bed	**Embedded**	**Blind**	**Open-open**	**Valved**
p > 1 atm (0.1 MPa) $\dot{p} \approx 0$ LLDCB	Belyaev (1966) O Dubovitskii (1974a) D Dubovitskii (1974b) D Frolov (1972) D	Belyaev (1966) O Margolin and Chuiko (1966) O Taylor (1962a) OD Belyaev (1973) D Andreev (1966) O Bobolev (1966) OD Andreev and Chuiko (1963) D	Taylor (1962a) OD Taylor (1962b) O	
p > 1 atm (0.1 MPa) $\dot{p} >> 0$		Belyaev (1966) O Gorbunov and Andreev (1967) O Bobolev (1965b) O Andreev and Gorbunov (1963) O		
P = 1 atm (0.1 MPa) $\dot{p} = 0$				

concerned with the environment and stimulus provided by the test apparatus. The rows include: (1) the $p > 1$ atm (0.1 MPa), $\dot{p} \approx 0$ conditions associated with LLDCBs such as a Crawford bomb, (2) the $p > 1$ atm (0.1 MPa), $\dot{p} >> 0$ conditions associated with HLDCBs, and (3) a series of tests where the environment was 1 atm (0.1 MPa) and no imposed pressure change (stimulus) was applied.

The matrix is further divided by whether the onset (O) or development (D) of convective combustion was studied.

Section 3 (Experimental Studies) will follow the organization of Table 1. That is, each column will be discussed in order in its entirety.

2.2 ORGANIZATION OF SECTION 4: RESULTS FROM THEORETICAL APPROACHES

There are two kinds of theoretical models dealing with DDT processes. The first, more complicated approach, is based on conservation laws, expressed as differential equations, augmented by empirical relationships for friction, heat transfer, and propellant ignition and combustion [Kuo (1977); Takata and Wiedermann (1976); Kuo (1973); Krier and Gokhale (1976)]. An advantage is that, assuming a correct analysis, given proper physical data, and using a high-speed computer, one may calculate meaningful detailed solutions representing growth and propagation of combustion in single channels or in porous beds. There are two disadvantages in such an attack. First, solutions do not exhibit transition from conductive to convective burning; hence no onset criterion can be established from solutions. Second, computations are expensive, so that it is not economical to carry out parameter and sensitivity studies. As a result, detailed studies of trends of solutions with relevant changes in input data have not been made.

By contrast, the other, simpler approach is characterized by several approximations in order to reduce complexity and permit solutions to be obtained without the need for extensive computer usage. While the results are not quantitatively accurate, they usually reveal qualitative trends which may be compared to experimental results if it is realized that detailed agreement is not to be expected. It is the literature concerning these simplified modeling efforts which is reviewed in Section 4 of this report.

It is convenient to separate the theoretical literature into major sections treating single pores and porous beds, as was done in the experimental section. Here the similarity ends for three reasons: (1) the scope and extent of theoretical literature is far more limited so that further categorization similar to that outlined in Section 2.1 is not warranted; (2) emphasis, in the case of simplified theories (as opposed to complex), is oriented more toward stages in the development of convective burning than toward sample boundary conditions and pressure

environment; and (3) there are miscellaneous theoretical analyses which do not even fit the experimental morphology. The emphasis on stages is really part of the simplified approach in which the overlapping (in time) phenomena are heuristically decoupled in order to enable a tractable solution of the problem.

There are three requirements for the breakdown of stable conductive (normal) burning in a single pore or porous bed. First, the hot combustion gases must flow into the defect at a velocity greater than the conductive regression rate. Otherwise the defect would not exist for the gases to penetrate. Second, the hot gases must heat the pore walls to a condition of self-sustained combustion. Third, this condition (usually called ignition) must continue to propagate into the single pore or porous bed at a velocity exceeding the conductive regression rate. The first requirement poses a hydrodynamic problem for which simplified solutions have been found for single pores and porous beds. In all instances the energy equation is either ignored or approximated by an assumption of isothermal flow. The second requirement involves heat transfer and some kind of ignition criterion, both of which are included in a non-mechanistic manner. In the literature surveyed, only single pores have been dealt with. The requirement for propagation of ignition is presented in only one paper, again limited to a single pore. The extension of single pore analyses to porous bed situations and vice versa is not exploited to any great degree because of the difficulty and uncertainty of assigning an effective pore size to a porous bed. The attempt was made, in connection with the concept of Andreev number, by Margolin and Chuiko (1966) and by Bobolev (1966). In both references, only the conditions for onset of convective burning were considered; extension of single pore analyses of ignition and propagation of ignition to porous beds is not made.

Section 4 of this report presents a review of the available theoretical literature which treats the three requirements for convective burning in single pores and porous beds. In addition, mention is made of several miscellaneous papers, dealing with melt layers, oscillatory pressure, and dynamic (combustion generated) pressure.

3.0 RESULTS FROM EXPERIMENTS

The outline and organization of this section were presented in Section 2.1.

3.1 EXPERIMENTS USING THE SINGLE PORE (OR SINGLE CHANNEL) GEOMETRY

3.1.1 Embedded Single Defect Tested in the LLDCB

Recalling the discussion of using the LLDCB to study combustion of samples having single defects (Section 2.1), two possibilities were

mentioned. If the test sample was embedded (Figure 1a), the defect (presumably having 1 atm (0.1 MPa) pressure) was sealed against the initial bomb pressure by a layer of auxilliary propellant. At the instant of burnthrough of this layer, the defect would "see" the much higher pressure of the bomb, and the required pressure differential would be established.

Only limited experimental work has been carried out using embedded, single defects in the LLDCB [Godai (1970)]. The defects consisted of narrow slits, 25 mm in length, constructed by assembling two 5 X 5 mm strands of propellant with an intervening gap varying from 0.05 to 0.5 mm. The propellant was a formulation consisting of 20% polyester and 80% trimodal AP (nominal particle sizes: 24, 160, and 480 um; no proportions given). Experiments were conducted in nitrogen and air at pressures up to 4 atm (0.4 MPa) with no noticeable effect of the gas. It was stated that tests run in helium gave slightly different results. Only the onset conditions were obtained as shown in Figure 2. Although the pressure range is quite limited, results are consistent with the trend that threshold pressure increases as defect size decreases.

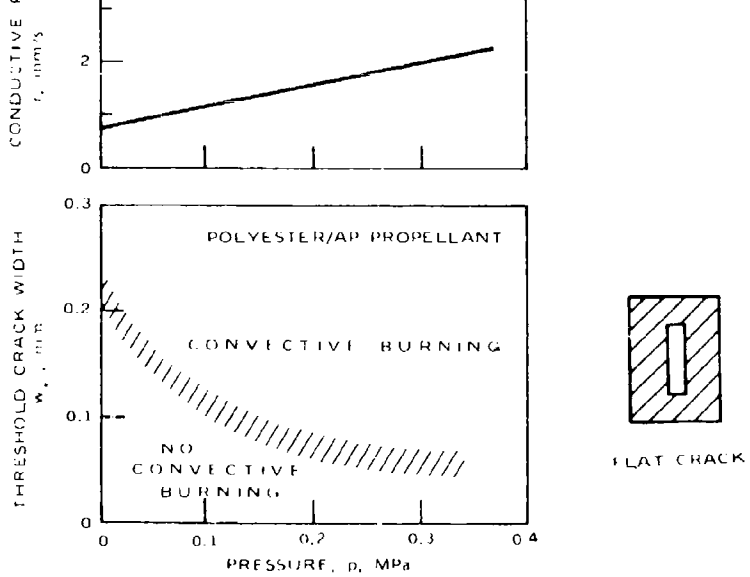

FIGURE 2. Burning Rate and Threshold Crack Width for Low Pressure Convective Burning of Polyester/AP Propellant. (Data taken from Godai [1970], Figure 5.)

3.1.2.1 The Blind Single Defect in the LLDCB

In this configuration, Figure 1c, the defect of the test sample is open to the bomb atmosphere and is intially filled with the cold, high pressure inert gas used to pressurize the bomb. The presence of the cold, inert gases in the defects makes penetration of combustion into the defects more difficult because the initial gases must be displaced or heated before ignition can occur. This is especially true for the blind defect because the only exit for gas flow (the mouth of the defect) is the entrance that the combustion front must penetrate. The slow pressure rise associated with the LLDCB compounds the difficulty of combustion penetrating the defect since the pressure differential responsible for causing convective burning comes entirely from the combustion process itself.

Results presented by Belyaev (1973) (Section 22) provide limited information on the rate of spontaneous propagation of combustion into blind flat cracks for conditions in which only a small pressure rise occurs in the crack. Two types of cracks were used: (1) two opposing "composite propellant" (no composition or formulations given) surfaces and (2) opposing "propellant" and plexiglass surfaces. The qualitative effect of pressure and crack width on convective rates is shown in Figure 3. The ordinate scale is the ratio of convective to conductive rate at the pressure involved. It is seen that the propagation rate increases with increasing pressure and with decreasing crack width until, for a minimum crack width, propagation no longer occurs. Detailed studies of the region to the right of the maxima of Figure 3 are shown in Figure 4 for a composite propellant. It is not clear which crack type was used in obtaining Figure 4 and Eq. (1). The data are represented by the expression:

$$(v_{ig}/r)w\ p^{-0.6} = 0.26\ \text{cm atm}^{-0.6} \qquad (1)$$

where

v_{ig} = ignition propagation rate
r = conductive rate
w = crack width
p = pressure

Although it is claimed that a similar result can be derived from theory, no such derivation or reference to it was given.

Without actual supportive data, the following conclusions are stated (Belyaev [1973, Section 22]) regarding propagation rates into blind channels at constant pressure:

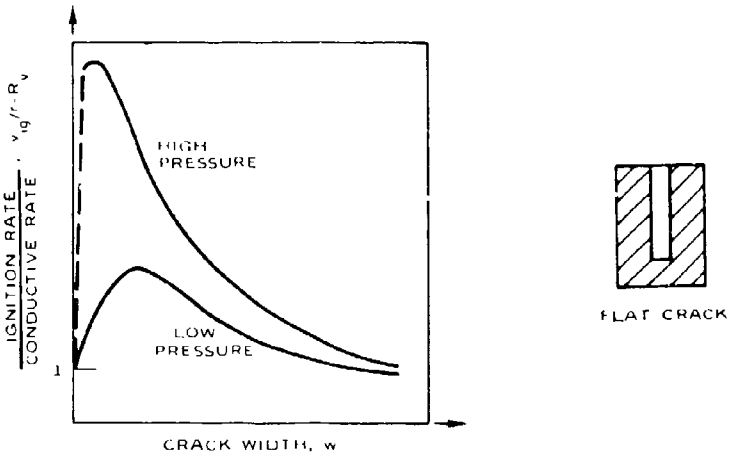

FIGURE 3. Qualitative Effect of Crack Width and Pressure on Convective Burning Rate. [Data taken from Belyaev (1973), Figure 51.]

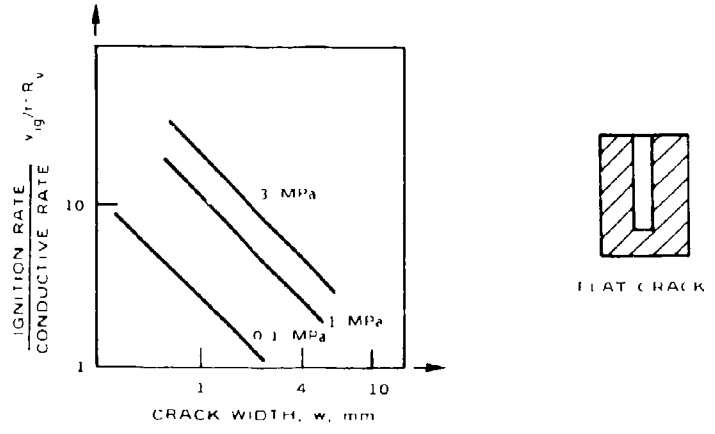

FIGURE 4. Effect of Crack Width and Pressure on Convective Burning Rate of Composite Propellant Powder. (Data taken from Belyaev (1973), Figure 52.]

1. Ignition rate increases with channel length at constant length-to-width ratio.
2. Ignition rate is greater for two opposing burning surfaces than for one inert and one burning
3. Ignition rate is increased by channel wall roughness.
4. Ignition rate is greater in a flat crack than in a circular channel with equal hydraulic diameter.

Others have also investigated the blind single pores in the LLDCB but this was only one of the configurations and apparatus combinations studied in their experiments. Rather than discuss the results here - they are more meaningful in context - only mention of the references will be made at this point. Bobolev (1965a) compared threshold conditions for open and closed flat cracks of two different lengths under conditions of constant (LLDCB) and rising (HLDCB) pressure (discussed in Section 3.1.3.2). Margolin and Margulis (1969) studied nitroglycerin powder in several configurations (discussed in Section 3.1.3.1). Belyaev (1969) conducted tests on secondary explosives, nitroglycerin powder and AP mixtures in flat, closed and open cracks of varying widths (discussed in Section 3.1.3.1). Prentice (1962 and 1977) has studied both blind and open single pores in the LLDCB (discussed in Section 3.1.3.1). Discussion of the results is deferred to the sections indicated.

3.1.2.2 Blind Single Defect in the HLDCB

The HLDCB was used to determine threshold pressure vs. pore width for several "propellants" in a narrow slit configuration [Belyaev (1973)]. Again, two types of slits were used. As described in Section 3.1.2.1, results, shown in Figure 5, were independent of the configuration. This is no contradiction of conclusion 2 of the preceding section which applies to LLDCB and ignition rate. As with many of the HLDCB tests reported, the rate of change of pressure was not recorded nor was its effect determined. It can be seen by comparing the curves presented that of the two composite propellant powders studied, the one with the higher burning rate develops convective burning at a lower pressure for a given crack width. Comparing composite and NG powders, one notes that the former are less stable. A possible explanation is the smaller flame standoff distance and heterogeneity in the flame zone owing to diffusion flames of the composites, which allows hotter gases, with greater capacity for igniting the walls, to enter the crack. Simplification of an already simple theoretical approach (see Theoretical section) provides an expression connecting pore width and threshold pressure:

$$p_*^{1+2n} w^2 = \text{const} \qquad (2)$$

where

p_* = threshold pressure
n = pressure exponent in conductive rate law

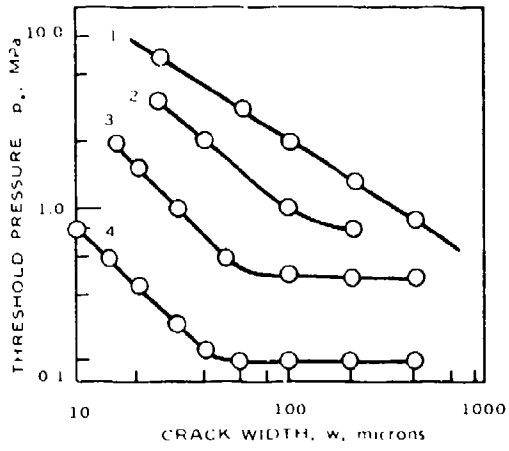

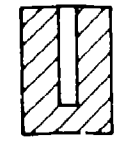

1 - RDX
2 - Nitroglycerin Powder
3 - Slow Burning Composite Propellant Powder
4 - Fast Burning Composite Propellant Powder

FIGURE 5. Dependence of Threshold Pressure on Crack Width for a Flat Crack. [Data taken from Belyaev (1973), Figure 38.]

The value of n is unity for RDX and 0.5 for the other propellants; good agreement between Eq. (2) and Figure 5 is found for small pore widths. Except for RDX, there is a break in the p_* vs. w relationship at large crack widths; this is explained as resulting from one of the simplifying assumptions (constant Nusselt number) made in deriving Eq. (2). There is no explanation offered regarding the absence of this feature in the data for RDX.

The work of Belyaev (1973) (Section 22) on blind cracks in LLDCB was summarized in Section 3.1.2.1 of this survey. When these same studies were performed in an HLDCB, the trends were similar to those of Section 3.1.2.1 but more pronounced. Effects reported include: (a) marked rise in the crack pressure, (b) large increase in propagation rate as crack width decreases, and (c) complete disappearance of the rising (small crack width) portion of the curves shown in Figure 3, even at low pressure. Conclusion (1) of Section 3.1.2.1 (ignition rate increases with channel length at constant length-to-width ratio) and effect (b) noted above could be reconciled if it were known that the HLDCB tests had been run at constant crack length.

Bobolev (1965a) studied the flashdown into a blind single pore in the HLDCB. The results are presented in Section 3.1.3.2 where the blind and open pore samples burned in LLDCB and HLDCB results are compared.

3.1.2.3 Blind Single Defect in Atmospheric Tests

In the introduction it was emphasized that convective combustion of porous charges and single defects arises from a pressure differential between the bomb and defect pressures. This differential consists of two components: (1) that imposed by the experimental conditions, and (2) that generated by combustion. In previous sections of the survey, the first contribution has always outweighed the second. An additional artifact of the high pressure experiments conducted in the LLDCB has been the dilution effect of pressurizing gases in the pores of the test sample. Elimination of this problem by using an "embedded" charge has only emphasized the experimentally created pressure difference.

Godai (1970) used two defect geometries in the atmospheric pressure blind defect pore experiments: (1) a flat crack, 5 mm wide by 25 mm long, with spacing between propellant surfaces varying from 0.05 to 0.5 mm, and (2) a round hole, 0.5 to 2.0 mm in diameter, drilled longitudinally through a propellant sample 5 x 5 x 25 mm. The propellant formulation contained 75 or 80% trimodal AP and 25 or 20% polyester binder. Effects studied included propellant temperature and propellant formulation.

The effect of propellant temperature was investigated for the flat crack at -25°C and 25°C with results shown in Table 2. Although the trend is as expected, it is questionable whether the precision of the reported results is consistent with (a) the data scatter, admitted by Godai (1970), and (b) the effect of temperature on such small dimensions The second question would be resolved if the temperature were known at which the gap measurements were made.

TABLE 2. Threshold Conditions for Propagation of Combustion into a Blind Flat Crack at Atmospheric Pressure.

Temperature, °C	Conductive rate, mm/s	Threshold crack width, mm
-25	0.77	0.24
25	0.88	0.22

The study of propellant formulation variables included: (1) oxidizer particle size and percentage, (2) addition of carbon black, and (3) substitution of polybutadiene binder. The effect of oxidizer particle size and percentage on burning rate and critical crack gap are shown

in Figure 6. While the results again show the expected decrease in threshold crack width with increasing regression rate, it is clear that burning rate alone does not control the critical conditions. Part of the increase in threshold crack width with particle size may be attributed to the increased roughness of the channel wall at larger particle size. This would have two effects: (1) increased flow resistance, and (2) either an increase or decrease in channel wall ignitability, depending on the relation between particle size and thermal wave thickness. The addition of carbon black produced no detectable effect on the relationships shown in Figure 6. It was concluded that neither radiation from carbon particles in the gas phase nor increased surface absorptivity contributes to flashdown. Substitution of polybutadiene binder for polyester resulted in lowering of the threshold crack width, which is also consistent with the increased burning rate.

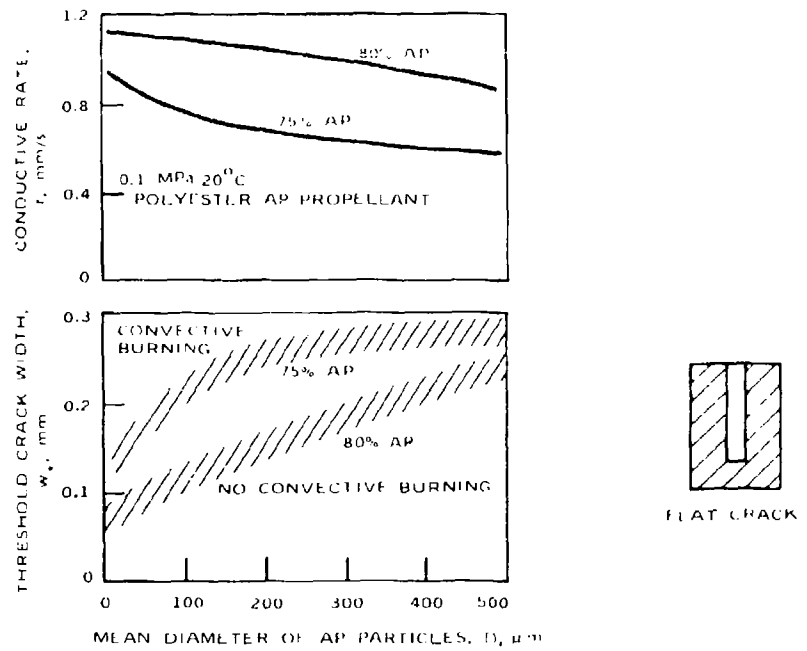

FIGURE 6. Effect of Oxidizer Particle Size and Percentage on Threshold Crack Width (Closed) at 1 atm (0.1 MPa). [Data taken from Godai (1970), Figure 6.]

When Godai conducted tests on the blind round hole, flashdown did not occur for any propellant (of those studied in the flat crack), even when 10 mm holes were used. The explanation offered was the possibility of three dimensional recirculation flows in the flat crack which could not take place in the round hole. Considering that the largest dimension in the flat crack was only 5 mm, one would expect that recirculation effects should have also been present in the 10 mm round hole.

3.1.3 Experiments Using the Open-Open Single Pore Geometry (Macaroni)

In this configuration, Figure 1c, the pore of the test sample is open at both ends thereby providing a flow channel with no stagnation region.

3.1.3.1 Macaroni Sample in the LLDCB

Although initially the pore of this sample is filled with cold inert gas, there is a vent, other than the entrance, that these gases can exit through when the combustion penetrates the pore. In this configuration the sole stimulus causing the combustion to penetrate into the pore is that generated by combustion.

Margolin and Margulis (1969) carried out experiments on nitroglycerin powder in several configurations (Figure 7). Pore size (1 mm diameter) and pressure (50 kg/cm^2) were chosen by Margolin and Margulis to give a value of An (see Section 3.2.2.1 for discussion of Andreev number criterion) which was 10-20 times that required for propagation of combustion into an open ended channel. Results for the conditions depicted in Figure 7 were:

a. No propagation
b. Propagation only as far as the side hole
c. Initial propagation into both ends, finally developing in only one side
d. Propagation after burnthrough of the blind end.

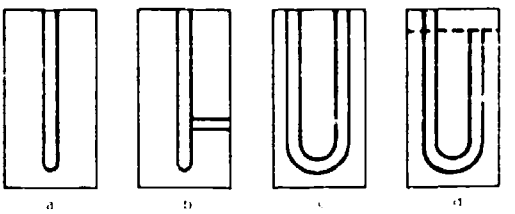

FIGURE 7. Pore Configurations Used to Study Effect of Pore Geometry on Convective Burning. [Data taken from Margolin and Margulis (1969), Figure 1.]

Additional experimental results were reported by Bobolev (1965a) comparing propagation rates into blind and open flat cracks of RDX (length 30 mm, particle size 200 μm, charge density 1.2 g/cm^3, crack width 0.1 mm). The data were fitted to the following empirical relationships:

Open crack

$$v_{ig} = 0.15\ p^{1.55} \tag{3}$$

Closed crack:

$$v_{ig} = 0.075\ p^{1.55} \tag{4}$$

where v_{ig} is ignition rate in cm/s and p is in atmospheres. The effect of crack length and width was not studied; from the available information it is seen that: (1) closing the crack halves the rate of propagation, but (2) the sensitivity of rate to pressure is not changed.

Belyaev (1969) conducted tests on secondary explosives, NC powder, and AP mixtures in closed and open flat cracks of varying widths. Belyaev chose conditions to insure penetration of combustion; however, the value of ϕ/ϕ_* (see discussion in section 3.2.2.1 relating to Figure 31) was not specified so that the margin by which conditions exceeded those for penetration was not known. Qualitative comparison of ignition rates for open and closed channels is shown in Figure 8. The ignition velocity and maximum crack pressure are shown in Figure 9 as functions of crack width. No propellant formulation was given for either figure, nor was the effect of length on ignition rate studied. Experimental results (Figure 10) (still on unknown propellant) indicate the influence of length and length-to-width ratio of a closed pore on maximum pore pressure. A simplified theoretical analysis gives trends which agree qualitatively with those shown in Figure 10.

Onset and propagation of combustion into open ended pores have been mentioned previously. Qualitatively it was noted earlier [Margolin and Margulis (1969)] that spontaneous penetration into an open pore occurs much more readily than for a closed pore, the threshold Andreev number (see Section 3.2.2.1) being 10-20 times as great for the closed pore. No length effect was reported by Margolin and Margulis (1969), however, limited data [Bobolev (1965a)] indicate (see Figure 11) that not only is the threshold pressure lower for an open channel but that it also decreases with length. Different results were obtained for rising pressures as also shown in Figure 11.

Ignition propagation rates into open channels of RDX were studied and reported [Bobolev (1965a)] (see Eq. (3)) to be double the value for closed channels. Similar qualitative results were obtained by Belyaev (1969).

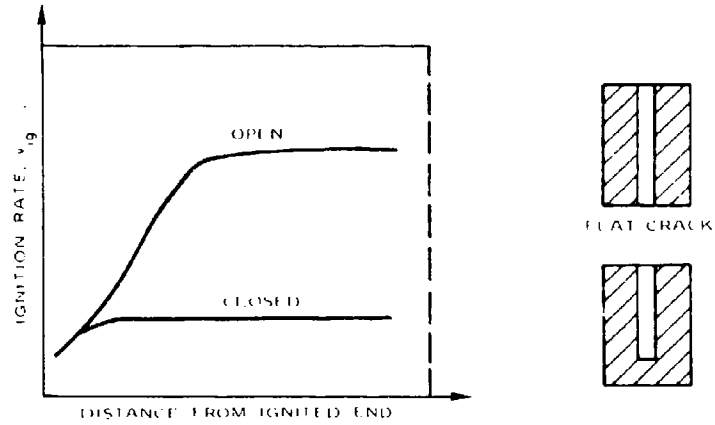

FIGURE 8. Qualitative Comparison of Convective Burning in Open and Closed Pores. [Data taken from Belyaev (1969), Figure 3.]

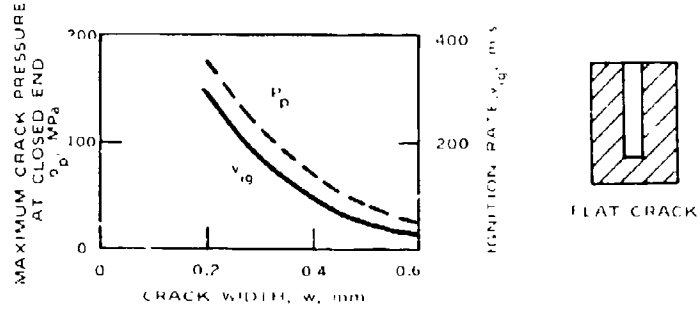

FIGURE 9. Effect of Pore Size on Maximum Channel Pressure and Ignition Rate. (Unknown propellant and channel length.) [Data taken from Belyaev (1969), tabulated data.]

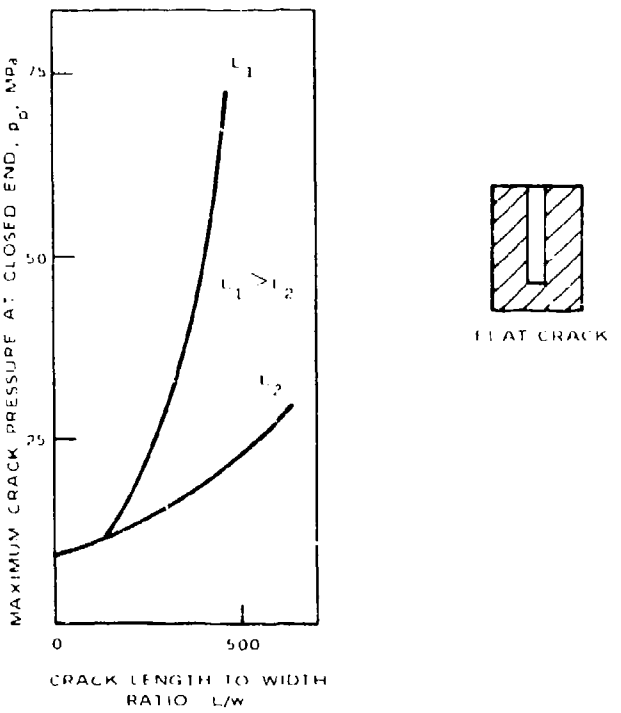

FIGURE 10. Effect of Pore Dimensions on Maximum Pressure in Closed Crack. [Data taken from Belyaev (1969), Figure 6.]

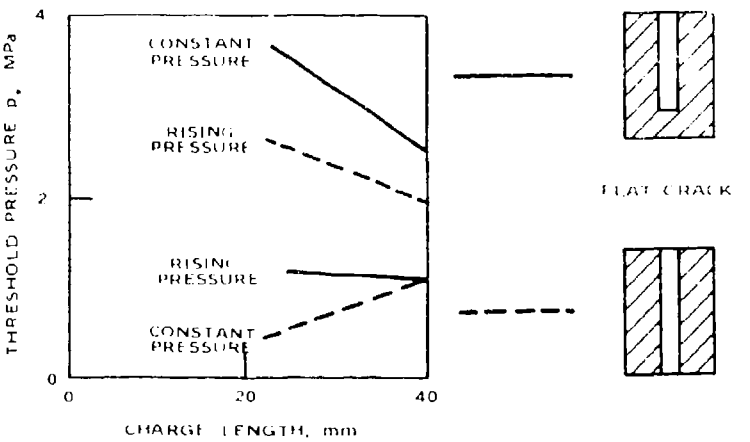

FIGURE 11. Dependence of Threshold Pressure on Length, Pressure Environment, and End Condition for 0.1 mm RDX Cracks. [Data taken from Bobolev (1965a), Table II.]

Payne (1969) ran tests on an aluminized AP composite at 700 psig (4.93 MPa) in nitrogen using cracks constructed of slabs, 0.25 in. long by 0.125 in. wide (6.4 x 3.2 mm), and having spacings ranging from 0.002-0.028 in. (0.05 x 0.7 mm). The flame entered the crack in all tests. Time required for combustion to enter the cracks increased with crack width while ignition rate increased as crack width decreased. This latter relationship, shown in Figure 12, is qualitatively similar to that found by Belyaev (1973) for closed cracks (see Figures 3 and 4).

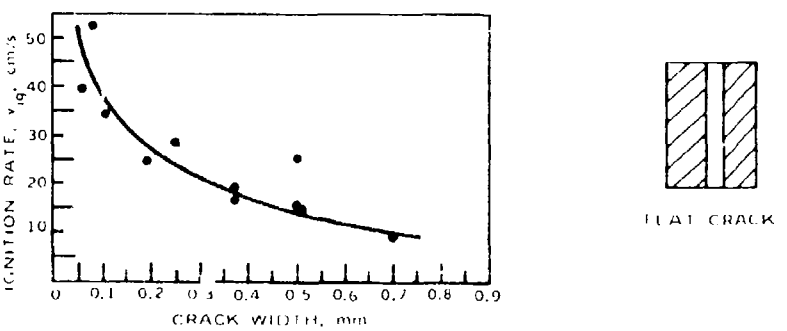

FIGURE 12. Effect of Open Crack Width on Convective Velocity for Composite Propellant at 700 psig (4.93 MPa) in Nitrogen. (Data taken from Payne (1969), Figure 4.]

Prentice (1962 and 1977) has studied both blind and open single pores in the LLDCB. In 1962 he studied nitrocellulose-petrin propellants. He found that he could not get the samples having a blind, 1/16-inch (1.6 mm) pore to flash at any pressure up to 550 psig (3.9 MPa) (the limit of his apparatus). When he burned a modified (pore ignition by burnthrough of a propellant web at ignited end of sample instead of by hot wire) open-open sample (see Figure 13) the data presented in Figure 13 were obtained. These data show flashdown at approximately 0.3 MPa bomb pressure for the open system. This dramatically shows that it is much easier to flashdown into the open-open pore than it is to flashdown into the blind pore. Prentice also found that flashdown will occur at pore diameters less than the flame stand-off distance. Additives to the nitrocellulose propellant significantly altered the flashdown: catalyzed propellants flashed more readily, while cooler propellants (1,3,5% paraformaldehyde addition) were less likely to flashdown.

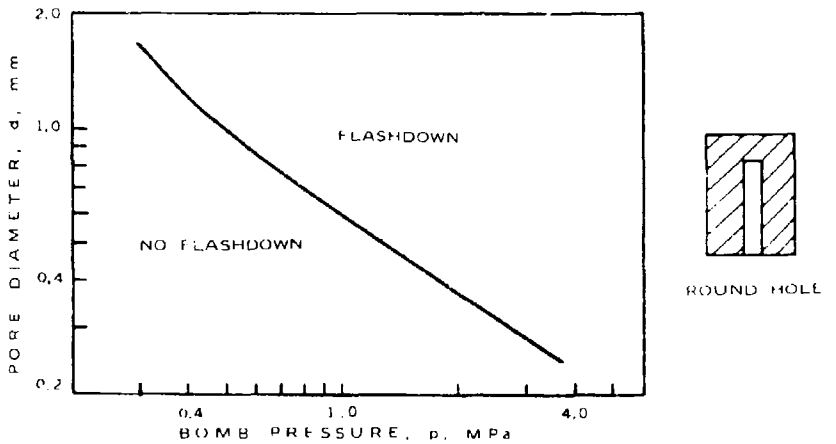

FIGURE 13. Flashdown Conditions for a Round Open Ended Hole in NC/Petrin Propellant. [Data taken from Prentice (1962), Figure 4.]

Prentice extended his earlier work to opaque composite propellants (Prentice, 1977). Both blind and open pores using previously mentioned modified ignition system were studied using the LLDCB. Flashdown was determined through the use of Vibration Response Spectroscopy (VRS). Prentice found that flashdown was facilitated by the open-ended pore as opposed to the blind pore, Figure 14. Several propellants were tested and the data are presented in Figure 15. Prentice also investigated double-base propellants having a mesa burning rate curve. The burning rate curve and flashdown curve are shown superimposed in Figure 16. From these two curves Prentice has concluded that those factors which affect the burning rate also affect the onset of flashdown.

This configuration was also considered in a comparative study by Bobolev (1965a) and is discussed in Section 3.1.3.2.

3.1.3.2 Experiments Using the Open-Open Single Pore Geometry (Macaroni) in the HLDCB

With the exception of gun propellant studies which used perforated grains burned in an HLDCB, very little work has been performed in this area. As mentioned previously, Bobolev (1965a) compared results for samples having blind and open pores burned in both LLDCB and HLDCB. This work presents brief experimental results of onset of burning in narrow slits made from RDX and lucite (0.1 mm spacing). Both rising and

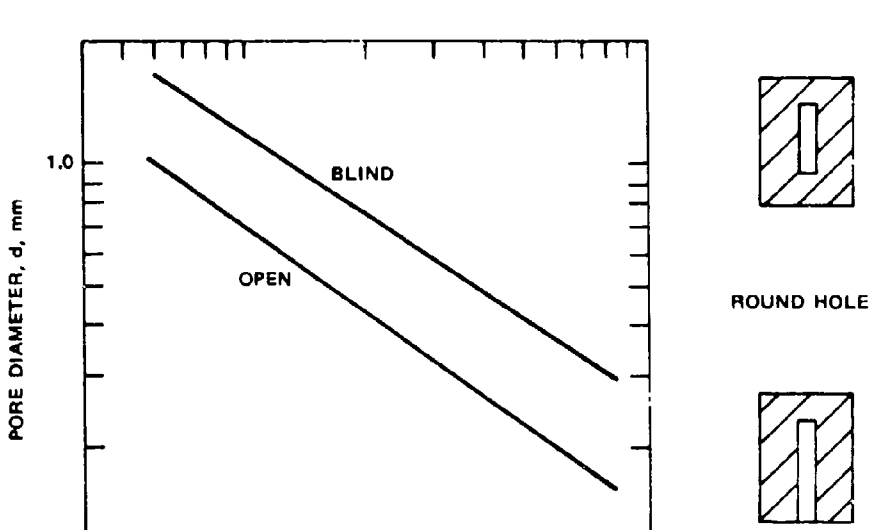

FIGURE 14. Comparison of Flashdown Conditions for Blind and Open-Ended Round Holes in Propellant A. [Data taken from Prentice (1977), Figure 20.]

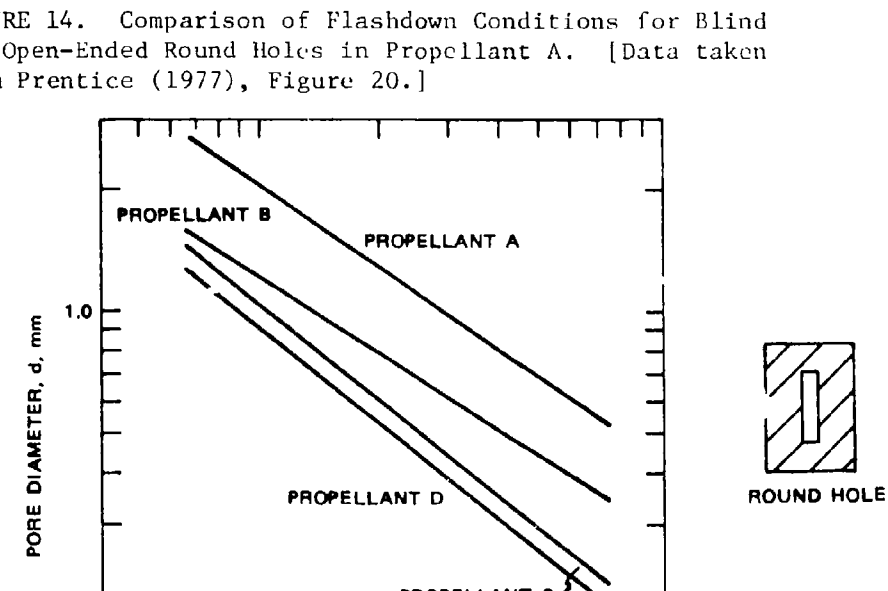

FIGURE 15. Comparison of Flashdown Conditions for a Series of Test Propellants. [Data taken from Prentice (1977), Figure 18.]

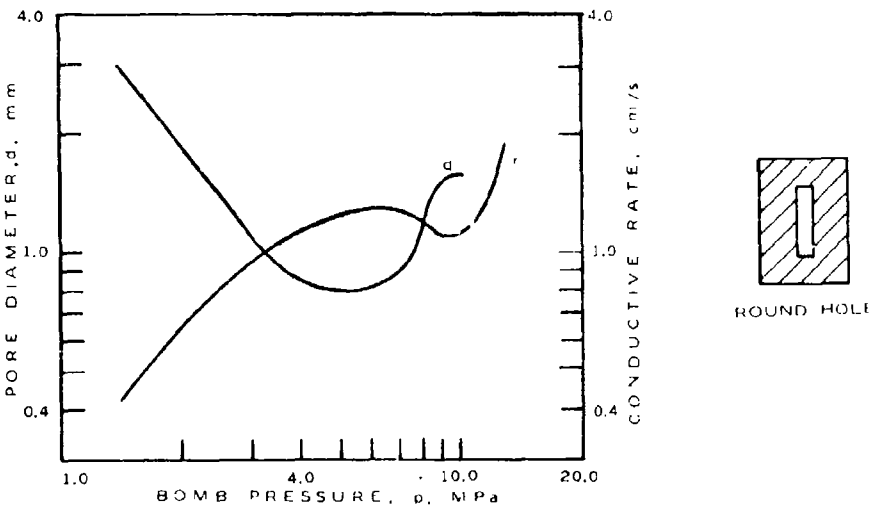

FIGURE 16. Burn Rate and Flashdown Conditions for N-5 Propellant. [Data taken from Prentice (1977), Figures 31 and 33.]

constant pressure for blind and open slots of two lengths are reported, with the results shown graphically in Figure 11. General conclusions are that, for rising pressure, combustion penetrates a closed channel more readily than an open one; on the other hand, for constant pressure, penetration is facilitated by an open channel. In addition, lengthening the channel makes penetration easier except for an open channel with constant pressure environment. Since the data given are so sparse and appear to be somewhat contradictory, with no principles elucidated to explain the results, the value of this paper is that it raises questions which should be answered by future experiments and analysis. It would be especially valuable to repeat the tests for other propellants and rates of pressure rise (none were specified by Bobolev (1965a)).

3.1.3.3 Experiments Using the Open-Open Single Pore Geometry (Macaroni) Burned at 1 Atmosphere

Whereas the blind pore experiments performed at 1 atm (0.1 MPa) were run mainly on flat cracks, nearly all the open pore tests utilized the round hole [Godai (1970)]. Effects studied were (1) oxidizer particle size and percentage (AP/polyester formulation), and (2) carbon and copper chromite F additives (AP/polybutadiene formulation). The influence of AP particle size and percentage is shown in Figure 17. The particle size dependence, noted for the blind crack, is still apparent; however, the percentage of AP has practically no effect. The effect of addition of aluminum on burning rate and critical diameter is shown in Figure 18. The interesting result here is that conductive rate is

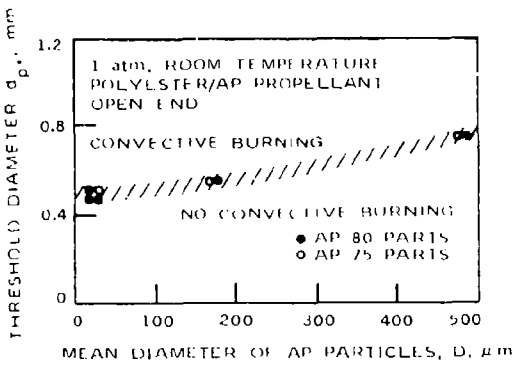

FIGURE 17. Effect of Oxidizer Particle Size and Percentage on Threshold Pore Diameter (Open) at 1 atm (0.1 MPa). [Data taken from Godai (1970), Figure 7.]

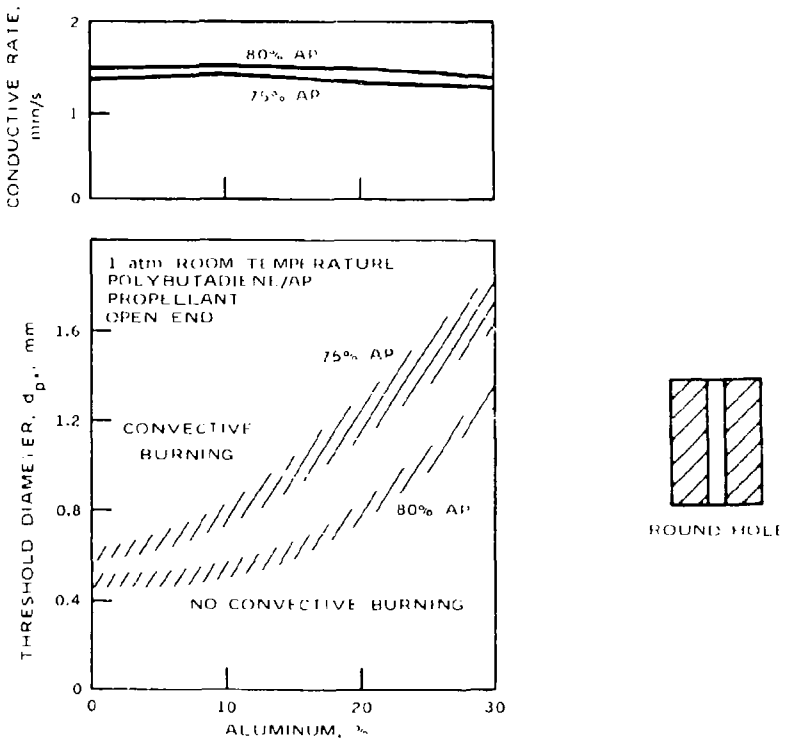

FIGURE 18. Effect of Aluminum on Conductive Rate and Threshold Pore Diameter for Open Round Pore. [Data taken from Godai (1970), Figure 8.]

virtually unaffected while flashdown diameter depends on both oxidizer and aluminum content. Again, there is clear evidence that conductive rate alone does not determine flashdown condition. The result of adding the burning rate catalyst, copper chromite F, is shown in Figure 19 and suggests that conductive rate is at least one of the contributing factors in flashdown.

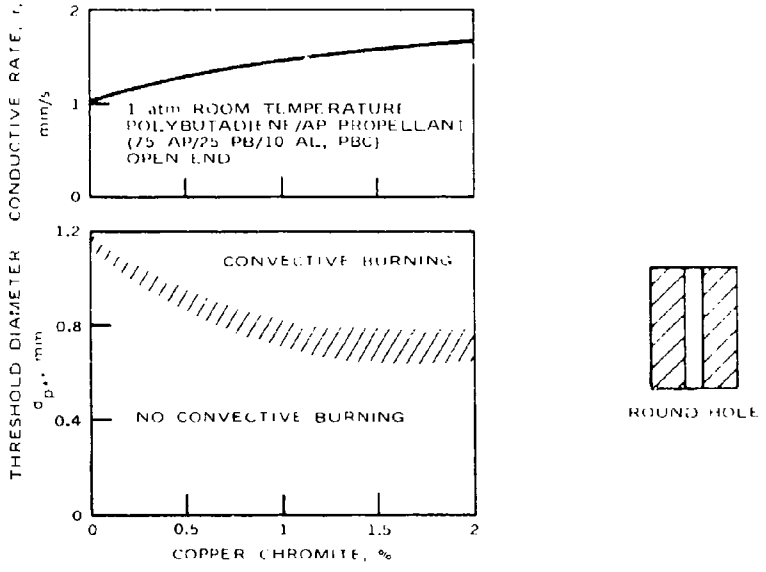

FIGURE 19. Effect of Copper Chromite on Conductive Rate and Threshold Pore Diameter for Open Round Pore. [Data taken from Godai (1970), Figure 9.]

No details were given of the results of flashdown into open flat cracks. It was noted that (1) the flame velocity accelerated more than for closed flat cracks, and (2) the threshold crack width was approximately 10% less for the open-ended case. This latter observation provides additional evidence for a recirculating flow in the closed, flat crack.

3.1.3.4 Experiments Using the Open-Open Single Pore Geometry in a Special Vented LLDCB

The development of combustion in a single pore or in a porous bed first requires the penetration of hot combustion gases evolved in the normal burning. Secondly, these flowing gases must heat the pore wall to a condition, usually called ignition, which leads to self-sustained

combustion. Because there is a time delay between penetration and ignition, the entering gases flow ahead of the ignition front.

Krasnov (1970) devised an experiment enabling the measurement of both the velocity of inflow and velocity of propagation of the ignition front. A sample of ballistite powder (double-base), containing a single cylindrical pore, 40 mm long and of varying diameters, was ignited in a constant pressure burner. The unignited end of the pore was connected to the atmosphere through a fixture containing a solenoid valve. Two different approaches were used. In one, the pore was initially filled with a liquid such as water or alcohol; upon ignition, the solenoid valve was opened and the liquid was expelled at a rate depending on the valve area. Both the liquid meniscus and ignition front were recorded by cinephotography through the relatively transparent propellant. In the other approach, a flow of nitrogen was established through the pore prior to ignition by adjusting the valve. The two methods were stated to give identical results, thereby presumably dispelling any doubts regarding inertial or cooling effects of the liquid.

Trends of experimental results are shown in Figure 20 for an unspecified pressure. The ordinate scale shows the ratio of gas flow velocity to ignition front velocity for pore sizes ranging from 1 to 4 mm. Both velocities were taken from the cinephotographs with v_{ge} being the velocity of the liquid meniscus. In general, the ignition lag increases with increasing flow velocity and decreasing pore size. For the conditions of the experiment, the ignition lag is independent of pore size above 2 mm and also of flow velocity above a critical value which increases with pore diameter. The leveling off of ignition lag with increasing pore size is shown in Figure 21, which is cross-plotted from Figure 20 for a flow velocity of 30 cm/s. It is possible to account for the effect of pore size if it is noted that the velocity of the ignition front increases for pores larger than 2 mm diameter. Auxiliary experimental results showing this effect are shown in Figure 22 for a pressure of 40 atm (4 MPa). Even though Figure 22 represents experiments relevant to a blind pore, the data are probably applicable here because, as indicated by the consistent rise in ignition velocity with pore diameter, the dead end effect is negligible in this experiment.

The underlying reason for the effect of diameter, not mentioned by Krasnov (1970), is connected with the relation between normal flame standoff distance and pore size. At constant pressure, this distance is also constant, so that larger pores permit the entry of the higher temperature gases associated wth complete combustion. It would be interesting to repeat the experiment for a composite propellant, for which the gas phase reactions are completed closer to the surface than for ballistite.

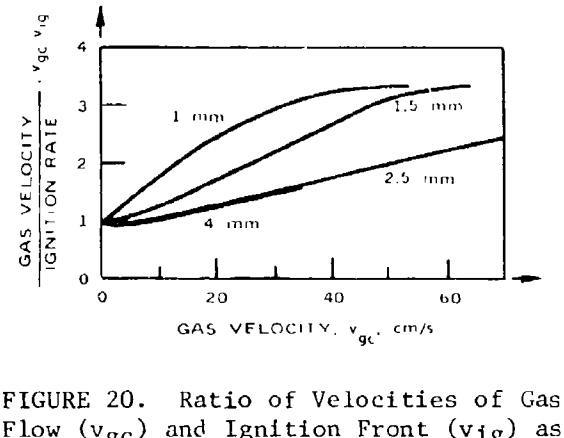

FIGURE 20. Ratio of Velocities of Gas Flow (v_{gc}) and Ignition Front (v_{ig}) as a Function of Gas Flow Velocity and Pore Diameter, d_p (Shown on Curves). [Data taken from Krasnov (1970), Figure 4.]

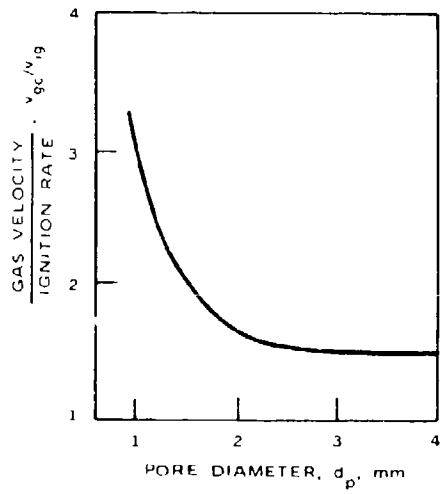

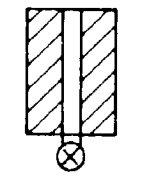

FIGURE 21. Ratio of Velocities of Gas Flow (v_{gc}) and Ignition Front (v_{ig}) as a Function of Channel Diameter, v_{gc} = 30 cm/s. [Data taken from Krasnov (1970), Figure 5.]

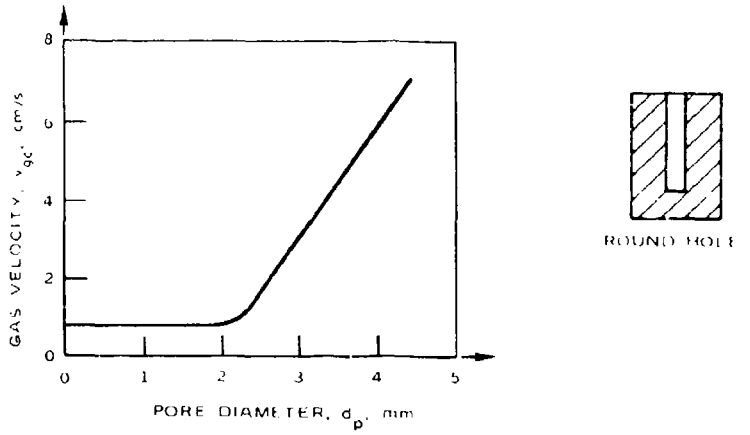

FIGURE 22. Effect of Channel Diameter on Rate of Flow Into Blind Channel at 40 atm (4 MPa). [Data taken from Krasnov (1970), Figure 7.]

This completes the survey of literature dealing with early stages of convective burning in single defects in LLDCB, HLDCB, and at atmospheric pressure. Pressure effects, but no quantitative effects of the rate of pressure rise, have been noted. The next section deals with results of experiments conducted on porous beds.

3.2 EXPERIMENTS USING THE POROUS BED GEOMETRY

While samples containing single pores may be characterized by rather precisely measured sizes such as length and cross-sectional area, the porous samples must be characterized by averaged quantities such as porosity, average particle size, specific surface area and permeability to flow. Porous beds and single pore samples differ by degree rather than kind. But since they do represent opposite ends of the increased surface area spectrum, they will be discussed separately. The samples having single pores or channels have already been discussed. The ensuing discussion will deal with porous beds.

3.2.1 Embedded Porous Bed Burned in the LLDCB

Both onset and development of convective burning have been studied for porous beds initially sealed against the bomb pressure. No detailed presentation was made of the criteria for the onset phase; instead, it was simply stated [Belyaev (1966)] that results were similar to those obtained using the HLDCB with a closed porous bed (see Section 3.2.2.2).

The implication is that the onset phase of convective burning depends only on a pressure difference between the bomb and porous bed pressures, whether the difference arises from an increasing bomb pressure or from an initially high bomb pressure. It would be expected that the rate of pressure rise for the HLDCB would influence the results, but the effect appears not to have been studied.

The rate of propagation of combustion into an embedded porous bed burned in an LLDCB was the subject of two papers [Dubovitskii (1974a) and Frolov (1972)]. In addition, a third reference [Dubovitskii (1974b)], apparently a different translation of Dubovitskii (1974a) was included in the survey in order to resolve certain translation discrepancies. Initial conditions of the experiment were chosen to ensure the onset of convective burning. Effects investigated were: propellant type, flame temperature, porosity, particle size, and sample length. The position and temperature of the advancing combustion front were measured optically and by means of thin wire thermocouples embedded at right angles to the direction of propagation.

Experiments were conducted at an initial bomb pressure of 70 atm (7 MPa) on an RDX/AP composition [Dubovitskii (1974a)] having 20% porosity. The velocity of the advancing combustion front is shown as a function of its position in Figure 23. Time also varies along each curve but is not indicated in the original reference. Two AP particle size ranges (100-125 μm and 200-250 μm) were tested but no mention was made of the size range used in obtaining the data for Figure 23; it was stated that propagation velocity increases with increasing particle size. Flame temperature was varied by changing proportion of AP and RDX. Test results can be summarized in the following statements:

1. Combustion propagation velocity is greater for longer charges, the effect becoming more pronounced at greater distances from the ignited end of the charge.

2. Combustion propagation velocity decreases as the end of the sample is approached.

3. Combustion propagation velocity in Region I is greater for higher flame temperature, increasing with distance for low flame temperature, and decreasing with increasing distance for high flame temperature.

The first two effects are a result of the counter pressure produced as the combustion front approaches the closed end. The increase in propagation velocity with combustion temperature is readily explained by the greater ease of ignition of the pore walls by the hotter gases. The reason for the increase in velocity with distance for low gas temperature compared with a decrease for high gas temperature is not explained in a satisfactory manner. It appears, however, to be the result of an

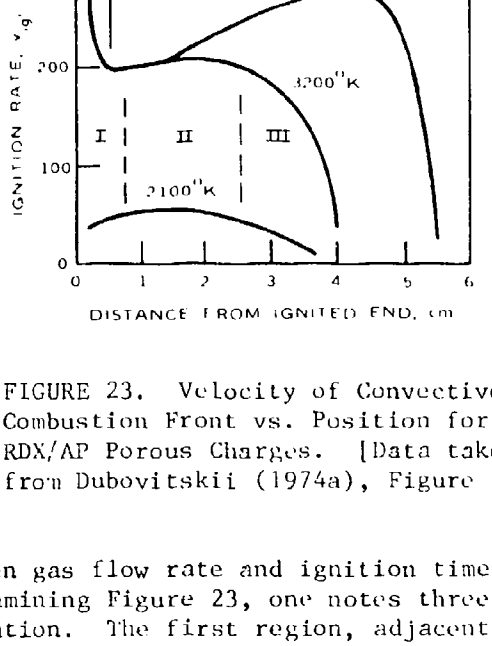

FIGURE 23. Velocity of Convective Combustion Front vs. Position for RDX/AP Porous Charges. [Data taken from Dubovitskii (1974a), Figure 1.]

interaction between gas flow rate and ignition time as gas temperature increases. In examining Figure 23, one notes three distinct regions of convective propagation. The first region, adjacent to the ignited end, is a region of decreasing velocity in which gas flow and heat transfer are the principal effects. Chemistry and ignition have not yet become important; extent of Region I appears to be insensitive to sample length (for lengths $\geq$4 cm). The second region is one of increasing velocity following ignition. The extent of Region II and acceleration of gases both increased with sample length, which determines how soon the presence of the closed end affects the progress of convective burning. Finally, in Region III, the gases slow down owing to the approach to the closed end and the development of counter pressure.

In addition to studies of the velocity of propagation of the combustion front, measurements were made of the maximum pore and bomb pressures as a function of sample length and AP particle size [Dubovitskii (1974a)]. Results are plotted in Figure 24, indicating the rather significant increase in maximum pore pressure and moderate rise in maximum bomb pressure with sample length. The pore pressure decreases with increasing particle size because, for the same porosity, the resistance to flow is less for larger particle size.

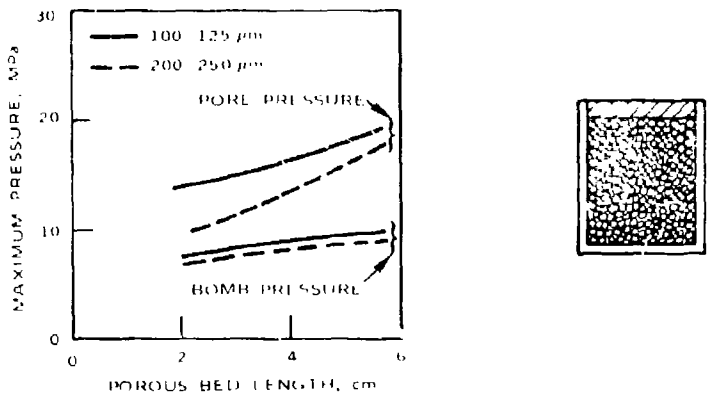

FIGURE 24. Maximum Pore and Bomb Pressures for Convective Burning in RDX/AP Porous Charges. [Data taken from Dubovitskii (1974a), Table I.]

Similar tests were conducted and reported [Frolov (1972)] for a stoichiometric mixture of AP and polystyrene (particle size ranges 60-100 μm or 100-130 μm) having a flame temperature of 2800°K. The charges were all 10 mm in diameter, 20 and 30% porosity, and were burned at an initial bomb pressure of 50-70 atm (5-7 MPa) with pressure rises of 5-10%. Velocity of the gas front as a function of position is plotted in Figure 25. The general shape of the curves is similar to those shown in Figure 23, in addition to which it is seen that propagation velocity is greater at high porosities but that the flow decelerates more rapidly in Region I for low porosities. Comparison of Figures 23 and 25 suggests that the propellant chemistry, especially ignitability which depends on kinetics, has a significant influence on the extent of Region I.

3.2.2 Blind Porous Beds

3.2.2.1 Blind Porous Bed Burned in the LLDCB. This section summarizes results obtained by burning porous beds in a Crawford type bomb (LLDCB) in which the high rates of pressure rise associated with the manometric bomb (HLDCB) are absent. Since the defect is exposed directly to the igniter, special efforts were usually made to provide a "soft" ignition, thereby avoiding the effect of a rapid pressure rise during the ignition transient. The degree of success of these attempts cannot be assessed because the effects of igniter size and brisance were not determined.

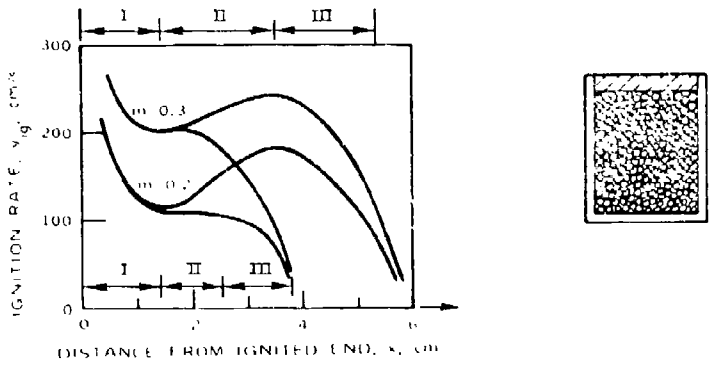

FIGURE 25. Velocity of Convective Combustion Front vs. Position Stoichiometric AP/Polystyrene Porous Charges. [Data taken from Frolov (1972), Figure 2.]

Although the experimental results to be summarized in this section relate to geometrically blind porous beds, no studies were reported of the effect of the length of the test sample. Hence it is not possible to resolve whether or not the samples were hydrodynamically blind. In a parallel effort involving rising pressure (Section 3.2.2.2) the length was adjusted so that its effect was minimized. Perhaps the same procedure was followed for the Crawford bomb tests. It is again emphasized that in these tests, the porous bed is open to the bomb pressure prior to ignition so that the pores are filled with high pressure, cold, inert gas.

Of the references found relevant to onset of convective burning in blind porous beds, one presents no experimental data; the statement is made that threshold pressures were 10-15 times as great as those obtained in experiments using the manometric bomb (Section 3.2.2.2) or the Crawford bomb with "embedded" charges (Section 3.2.1). If similar end effects are assumed in all three series of tests (all were geometrically blind) then the greater stability to onset of convective burning in the present case is explainable by the initial presence of the cold, inert, pore gases. These cold gases, at bomb pressure, both impeded the inflow of combustion products and cooled the combustion products that did flow in so that pore ignition was more difficult.

The most significant result of studies of onset of combustion in porous beds by spontaneous penetration was the confirmation of a concept which has been referred to as the "Andreev" criterion. A diversion to present a brief background of the Andreev criterion is appropriate here.

It is physically reasonable to say that combustion of a porous material will proceed in a normal manner as long as the surface irregularities, resulting from the porosity, are smaller than some dimension reflecting the combustion process. Belyaev proposed this idea in an unavailable doctoral thesis in 1946. He suggested using the ratio of pore size to standoff distance of the gaseous reaction zone as a criterion, probably with the idea of application to a single pore. The idea was quantified by Andreev in 1946 in another unavailable paper still applied to a single pore and using the solid phase thermal layer thickness as the combustion dimension. The first evidence linking the criterion to a statistically porous bed was presented by Margolin (1961) in a short theoretical note without experimental results. The current status of the Andreev number criterion is as follows:

1. Although initially developed for single pores, the Andreev number criterion has not been extensively tested experimentally for single pores. (Exceptions: see Prentice [1962 and 1977] (Section 3.1.3.1 of this survey) for single pore results.)

2. The Andreev number criterion has been applied only to spontaneous penetration of combustion into single pores and porous beds, under experimental conditions similar to those found in the LLDCB with pores prepressurized to the initial bomb pressure.

3. The Andreev number criterion has been applied to porous beds by use of an equivalent pore diameter based on permeability measurements.

4. There have been no comprehensive reports of experiments designed to determine the quantitative effects on Andreev number criterion of end condition (open or blind) or of length of single pores or porous beds.

Quantitatively, the Andreev criterion takes the form

$$\rho c_s d/\lambda_s = An > An_* \qquad (5)$$

where

ρ = bulk density of solid (mass/total volume)
c_s = specific heat of solid
d = characteristic defect size (actual or hydraulic diameter)
λ_s = thermal conductivity of solid
An = Andreev number
An_* = threshold Andreev number

Returning to specific papers in the literature survey, one finds two references dealing with spontaneous penetration of combustion into porous beds. The first [Margolin and Chuiko (1966)] represents a compendium of experimental results obtained for single component materials having a narrow particle size range and taken from many sources. Margolin and Chuiko (1966) presented Eq. (5) in the alternate form

$$\rho_s rd = \phi - \phi_* \tag{6}$$

in order to eliminate the specific heat and thermal conductivity, which are not well known, but which are stated to vary over narrow limits. It is important to note that, while An is dimensionless for consistent units, ϕ has dimensions of g/cm-s in the units chosen (ρ:g/cm^3, r:cm/s, d:cm). In applying Eq. (5) or (6) to a single pore, an appropriate value of d would be the pore diameter. In the case of a porous bed, the mean hydraulic pore diameter is used. In an article by Margolin and Chuiko (1966), where particle size varies over a narrow range for any given test, the mean hydraulic diameter is computed from

$$d_h = (2/3)D_p\ (1-\delta)/\delta \qquad \text{(see Belyaev (1973), Section 4)} \tag{7}$$

where

D_p = particle diameter

δ = relative density (one minus porosity)

Materials included in the study were TNT, picric acid, nitrocellulose, PETN, nitroglycerin powder, tetryl, RDX, HMX, AP, and mercury fulminate. Particles range in size from 20 to 850 μm with porosities of from 25.5 to 87.5%. Threshold values of mass burning rate, $(\rho r)_*$ and hydraulic diameter d_* are shown in Table 3 for two pressures, 1 and 10 MPa. Also shown for each pressure is the ratio of critical diameter to critical diameter for TNT. This number serves to rank materials according to their propensity to develop convective burning, or, in other words, to their stability of normal burning. The higher the ratio just defined, the lower the stability. It should be noted that the order of stability changes with pressure owing to the nonlinear dependence of conductive burning rate on pressure; although this method of ranking is useful, it is important to specify the pressure. It is interesting to note that both AP and HMX, coingredients of many modern high energy propellants, exhibit among the highest tendencies to develop convective burning. In addition, it has been noted [Kraeutle (March 1974)] that the exothermic decomposition temperature of HMX is significantly lowered in compositions containing AP.

TABLE 3. Threshold Conditions for Breakdown of Conductive Burning.[a]

Explosive	$\phi_* = (\rho r d)_*$ mg/cm-s	Threshold pore diameter, d_* μm		Ratio d_*/d_{*TNT}	
		1 MPa	10 MPa	1 MPa	10 MPa
TNT	8.0	850	108	1.00	1.00
Picric acid	8.5	625	90	1.36	1.20
Nitrocellulose	9.8	330	100	2.58	1.08
PETN	11.1	540	55	1.57	1.96
Nitroglycerin powder	4.35	120	40	7.08	2.70
Tetryl	7.1	235	48	3.62	2.25
RDX	6.9	163	21	5.21	5.14
HMX	6.5	140	24	6.07	4.50
AP	3.7	110	20	7.73	5.40
Mercury fulminate	11.4	115	4.3	7.39	9.39

[a]Slightly different values are given by Belyaev (1973) (Table 6).

Noting the relatively narrow range of values of ϕ_*, Margolin and Chuiko (1966) took its average value (9×10^{-3} g/cm-s), combined it with a typical value for λ_s/c_s for the condensed phase (1.5×10^{-3} g/cm-s), and so derived the threshold Andreev number ($An_* = 6$). Owing to the simplicity of the concept and to the averaging technique used in deriving the threshold constant, it is not surprising that deviations are found. Indeed, Margolin and Chuiko (1966) report variations in which ϕ_* increases by a factor of two for very smooth surfaces and decreases by a factor of one-half for very fine particles. In addition, the effect of combustion temperature and flame zone structure have been found important. For example, TNT, with the highest value of ϕ_*, also has the lowest combustion temperature of the reported secondary explosive. Certainly the implicit effects of particle size and flame temperature on the quantities which comprise ϕ_* and An_* are not completely expressed in the simplified criteria. The authors recognized this limitation when they recommended determination of An_* (or ϕ_*) for new classes of materials rather than indiscriminate application of $An_*>6$. A controversial and unresolved issue is raised by the claim that, for a pore size distribution, the appropriate value of diameter to be used in computing Andreev number should be based on maximum pore size. Other presentations, such as the one which follows [Bobolev (1966)], conclude that the average pore size is more relevant.

The other reference related to Andreev number [Bobolev (1966)] presents results of studies on RDX, AP, and mixtures consisting of RDX/AP, AP/urotropine, AP/sucrose, potassium perchlorate (KP)/ urotropine, and KP/sucrose. While Margolin and Chuiko (1966) dealt with single component systems of uniform particle size, Bobolev (1966) was concerned with establishing convective burning criteria for mixtures and multimodal particle size distributions. In addition, the effect of component melting is included in the final four mixtures since AP and urotropine do not melt,* while KP and sucrose do.

The effect of particle size and pressure on mass burning rate of RDX (theoretical maximum density = 1.80 g/cm^3) is shown in Figure 26, in which the lower curve shows the normal burning rate. The standard Russian method, given by Belyaev (1973) for calculating mass burning rate, is to multiply the observed conductive rate by sample bulk density. Since sample bulk density varied only slightly (0.996-1.038 g/cm^3) in this series of tests, Figure 26 shows mainly the effect of particle size. The high slope curves indicate convective burning rates with particle size increasing toward the left. For larger particles, the interconnecting pores are larger, thereby allowing penetration of high temperature combustion products and development of convective burning (intersection point with lower line) at lower pressures. Conditions for onset of convective burning of both pure RDX and pure AP are shown in Table 4 for different particle size ranges. The hydraulic pore diameter used in the calculation of ψ_* was computed as the mass weighted harmonic mean of the particle size distribution (see Eq. (9) below). The rationale for this approach is not explained, nor is the final value of pore diameter which lies outside the particle size range. Acceptance of the results shows that for each substance there is a near constant value of ψ_*, and that normal conductive burning of RDX is more stable than that of AP.

Additional studies were conducted on samples of RDX containing several ranges of particle sizes (bimodal and trimodal). Three alternative methods were used for computing the mean hydraulic pore diameter to be used in evaluating ψ_*:

$$d_1 = \sum a_i D_{pi} \tag{8}$$

$$d_2 = 1/d_2 = \sum a_i / D_{pi} \tag{9}$$

$$d_3 = \sqrt{2k/(1-s)} \tag{10}$$

where the a_i are weight fractions of particles with diameters, D_{pi}.

*Hightower and Price (1967 and 1968) and Boggs and Kraeutle (1969) have shown that AP has a thin liquid layer, several microns thick on the burning surface.

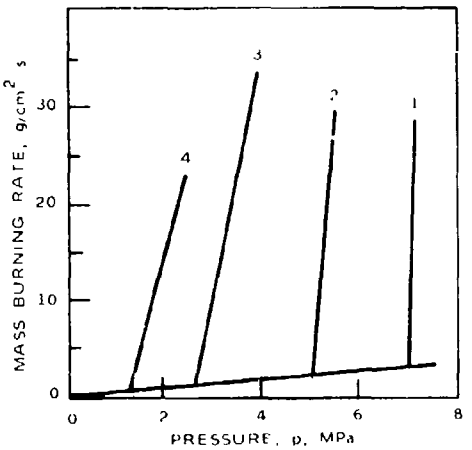

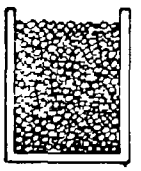

Particle diameter, μm

1 -	50 - 63
2 -	63 - 100
3 -	100 - 160
4 -	160 - 250

FIGURE 26. Mass Burning Rate of RDX as a Function of Pressure and Particle Size. [Data taken from Bobolev (1966), Figure 2.]

TABLE 4. Threshold Conditions for RDX and AP.

Particle size μm	RDX					AP				
	ρ g/cm^3	d μm	p_* MPa	$(\rho r)_*$ g/cm^2-s	Φ_* mg/cm-s	ρ g/cm^3	d μm	p_* MPa	$(\rho r)_*$ g/cm^2-s	Φ_* mg/cm-s
50-63	0.996	31	6.6	2.13	6.5	1.07	31	5.0	1.17	3.63
63-100	1.035	41	4.6	1.57	6.4	1.205	34	4.0	0.97	3.27
100-160	1.038	64	2.6	1.015	6.5	1.145	67	2.0	0.535	3.58
160-250	1.015	105	1.2	0.63	6.65	1.043	119	1.2	0.315	3.74
250-315	1.00	151	0.5	0.437	6.6	0.92	212	0.6	0.175	3.71

The origin of Eq. (8) and (9) is not provided; the pore diameters d_1 and d_2 represent arithmetic and harmonic mean mass averaged particle diameters. Neither d_1 nor d_2 leads to a constant computed value of ϕ_*. However, the hydraulic diameter d_3, determined by measurements of the gas permeability k, does yield a near constant value of ϕ_*, independent of the particle size distribution. Figure 27 compares the ϕ_* values as calculated from d_1, d_2, and d_3 for bimodal RDX containing the particle size ranges 50-63 μm and 160-250 μm. Addition of a larger size range (250-315 μm), to give a trimodal sample, does not significantly change the threshold value ϕ_* if d_3, based on permeability measurements, is used. Bobolev, and others (1966) conclude that the constant value of ϕ_* based on permeability measurements means that the pores of average diameter, being the most numerous, are the defects that influence onset of convective burning. This is in contrast to Margolin and Chuiko (1966), in which pores of maximum size were postulated as governing.

The final studies described by Bobolev (1966) concern the influence of composition on ϕ_*. Test series were run to examine the following:

1. Additivity of ϕ_* for mixtures containing the two monopropellants AP and RDX.
2. Effect of fusibility of the fuel and oxidizer components of the mixture.

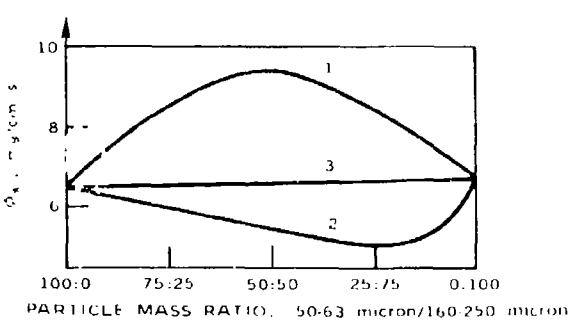

ϕ_* computed from

(1) d_1 (Eq. (8))
(2) d_2^1 (Eq. (9))
(3) d_3^2 (Eq. (10))

FIGURE 27. Threshold Quantity ϕ_* for RDX vs. Mass Ratio of Fine to Coarse Particles. (Data taken from Bobolev (1966), Figure 5.]

The AP/RDX results are summarized in Table 5, which shows the effect of mixture ratio on ϕ_* (calculated from d_3) for a particle size range of 160-250 μm. The interesting result is that ϕ_* does not seem to be an additive function of the ingredients (this would yield a linear change in ϕ_* with percent AP) but changes abruptly at that composition where the volumetric fraction of RDX exceeds 50%. No explanation of the phenomenon is offered; however, a more convincing demonstration would be provided by using monopropellant components differing more in density than AP (density = 1.95) and RDX (density = 1.8). It would also be interesting to determine ϕ_* for mixture containing two monopropellants and a fuel.

TABLE 5. Threshold Conditions for RDX/AP Mixtures.

% AP		Porosity	Pore size, μm	p_* MPa	$(\dot{r})_*$ g/cm^2-s	ϕ_* mg/cm-s
Wt.	Vol.					
100	100	0.465	119	1.20	0.315	3.74
75	73.5	0.457	115	0.35	0.350	4.05
50	48	0.456	115	0.28	0.553	6.35
25	23.5	0.438	107	0.50	0.607	6.48
0	0	0.426	106	1.20	0.630	6.65

In the tests on various oxidizer/fuel combinations, it was found that the threshold conditions for onset of convective burning (ϕ_*) were determined primarily by the oxidizer with little distinction between melting and nonmelting fuels and negligible effect of particle size or fuel fractions up to 55%. The value of ϕ_* for compositions containing the monopropellant AP varied only slightly from the value of 3.7 mg/cm-s obtained for pure AP. This near constant value of ϕ_* for AP was obtained even though the flame temperature of the AP/sucrose mixtures varied with composition by a factor of two. The higher value of $\phi_* \approx 10$ mg/cm-s for the KP mixtures agrees well with the stability limit (highest value of ϕ for which conductive burning occurs) for secondary explosives. The statement was made that no explanation could be found for the different values of ϕ_* for AP and KP. It was concluded that fuel melting is not important, however, it does not necessarily follow that oxidizer melting has no effect on burning stability.

Taylor (1962a) also introduces the melt layer concept to explain the combustion stability of fusible propellants. He points out that, at constant bomb pressure, the material with the lower melting point should have a thicker melt layer, hence should develop convective burning at a higher pressure. He cites HMX (m.p. = 278°C) which has a threshold

pressure of 1.3 MPa compared to PETN (m.p. = 140°C) with a threshold pressure of 2.8 MPa. Andreev (1966) refutes Taylor with three counter arguments:

1. Andreev believes that the melt layer thickness does not depend simply on melting but upon boiling point as well (HMX b.p. > 340°C; PETN b.p. = 270°C).

2. Taylor explains the stability of conductive burning of NC by a melt layer. Andreev does not agree that NC melts.

3. Andreev claims that at constant pressure, loss of stability of conductive burning at high pressures is a result of the higher dynamic pressure which is generated at higher static pressures. Taylor's rejoinder is that combustion of secondary explosives cannot generate a sufficiently high dynamic pressure to justify Andreev's argument.

It will be seen (Section 3.2.2.2) that the question of the role of the melt layer under conditions of rising pressure (HLDCB) is no more resolved than for the constant pressure condition just reviewed.

Thus far in this section only criteria necessary for onset of convective burning have been examined along with the effect of particle size and a limited range of compositions. Even less information is available concerning the rate of propagation of convective burning into porous beds.

Experimental observations reveal that convective burning under constant pressure (spontaneous) proceeds relatively smoothly, characterized by a plane combustion front with a definable velocity. On the other hand, convective combustion driven by a substantial pressure difference (forced penetration), such as is found in the manometric bomb or in the "embedded" charge, is marked by irregularities resulting in tongues of reaction extending deep into the porous materials. The remainder of this section will present experimental results relevant to the rate of penetration of combustion under spontaneous conditions.

Figure 26 [Bobolev (1966)], used earlier to illustrate the effect of particle size on threshold pressure, also shows the dependence of the resulting convective mass burning rate of RDX on pressure and particle size. Since a nearly constant charge density was used in obtaining the data, the steep convective burning rate curves are also representative of the linear velocity of propagation of the combustion front through the test sample. Although the slopes of the convective burning rate curves appear to increase regularly with decreasing particle size, scatter and paucity of data obviate any general conclusion. The important feature revealed by this data is the greatly increased sensitivity of mass burning rate to changes in pressure compared to the conductive mode.

Andreev and Chuiko (1963) studied the convective burning of PETN, tetryl and NC at pressures up to 100 MPa and for several porosities and particle sizes. Results, shown in Figure 28, are consistent with those for RDX; namely, stability of conductive burning increases with decreasing particle size and decreasing porosity. For large particles (Curves 1 and 2), the decrease in slope at high pressures is explained by the increased mass of inert pore gases, hence greater dilution at higher pressures. The more complicated nature of Curves 3, 4, and 5 (small particles) is attributed to competing effects of four phenomena:

1. Pore gas dilution effect is greater at high porosities and pressures.
2. Permeability to gas flow is greater at high porosities and for large particles.
3. Combustion is more complete, nearer the surface for high pressures, hence the penetrating gases represent a more energetic ignition.
4. The dynamic (combustion generated) pressure is greater at high burning rates and pressures.

For the high porosity (72%) represented by Curve 3, the dilution effect is noticeable even at comparatively low pressures; for the small particles (5 μm), dilution is not overcome even by the high pressure effect of increasing flame temperature and dynamic pressure. At lower porosity (Curve 4) the effect of dilution does not appear until a higher pressure is reached. At still higher pressures, the dilution effect is overcome by the higher combustion temperature and dynamic pressure. At the lowest porosity, the dilution effect is not obvious over the range of pressures studied. This competition among several effects is illustrated more graphically in Figure 29, which shows the mass burning rate of PETN as a function of relative density, δ, for 5 μm particles and 100 MPa pressure. The maximum in the curve arises from the tradeoff between dilution and permeability. The rising portion of the curve is attributable to the decrease in dilution as δ increases while the declining portion is caused by the decrease in permeability and penetration rate at high densities. Although further information is not available, it is expected that relationships similar to Figure 29, would be obtained for different pressures, particle sizes, and materials, depending on the interplay among the four effects mentioned above. It would be interesting to investigate (1) whether a maximum mass burning rate always exists, as in Figure 29, and (2) the character of the relation at rocket motor pressures for multimodal particle sizes and standard propellant formulations. *A significant result for the tests described by Andreev and Chuiko (1963) is that transition to detonation never occurred even at pressures up to 100 MPa, although burning rates exceeded conductive rates by factors ranging from 10 to 120.* A possible explanation is that the size of the test sample (5 mm diameter by 35 mm length) was outside the range of threshold diameter and runup length for the materials studied.

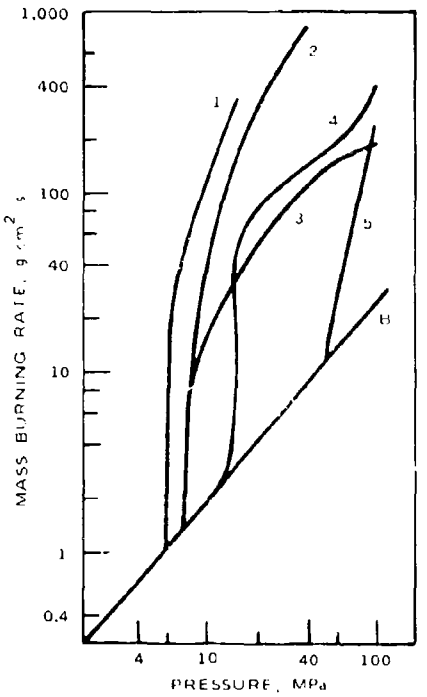

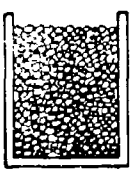

Curve	ρ (g/cm^3)	D_p, μm
1	1.08	200
2	1.17	200
3	0.5	5
4	0.71	5
5	1.17	5
B	1.77 (TMD)	...

FIGURE 28. Pressure Dependence of Mass Burning Rate of PETN at Different Relative Density and Particle Size. [Data of Andreev and Chuiko (1963), taken from Belyaev (1973), Figure 60.]

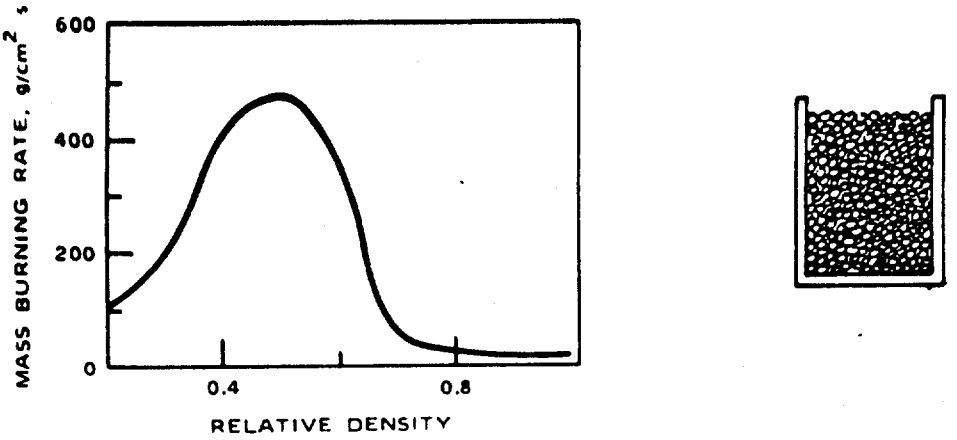

FIGURE 29. Dependence of Convective Mass Burning Rate on Relative Density for PETN (100 MPa, Particle Radius 20 μm). [Data of Andreev and Chuiko (1963) taken from Belyaev (1973), Figure 61.]

Taylor (1962a) conducted a series of tests to determine the end effect of the porous bed on propagation of the convective burning front in HMX. Conditions which remained the same throughout were: particle size range, 200-600 μm; porosity, 43.2%; bed diameter, 6 mm; bed length, 72 mm; and pressure 2.7 MPa. Progress of combustion was determined by cinephotography. The relation between time and position of the flame front is shown in Figure 30 for three different end conditions. When the end is closed (Curve c), the propagation velocity accelerates from the beginning until the counter pressure produced by the closed end causes a deceleration. For the open end (Curve b), acceleration proceeds unhindered to the end of the channel. Curve (a) shows the increase in velocity provided by a flow restriction (nozzle) and consequent pressure increase at the burning end of the charge. It is noteworthy that for the constant pressure conditions of the tests, there is no initial deceleration of inflowing gases as was reported in Section 3.2.1 dealing with an "embedded" charge. Limitations of available data do not allow an explanation of this distinction at the present time.

Belyaev (1973) presented an interesting empirical relation between propagation rate of convective combustion and conditions for its onset as shown in Figure 31. The abscissa (R_ϕ) is the ratio ϕ/ϕ_*, where ϕ is the actual value and ϕ_* is its onset value (see earlier discussion in this section). The ordinate (R_v) is the velocity of the convective front divided by the normal conductive burning rate. It is not clear whether mass or linear velocities are involved in this latter ratio; porosities are nearly constant so that the data are relatively consistent. It is seen that R_ϕ is a measure of how far conditions exceed the onset conditions while R_v measures the effect on propagation rate. There is some scatter in the data; however, considering the range of materials

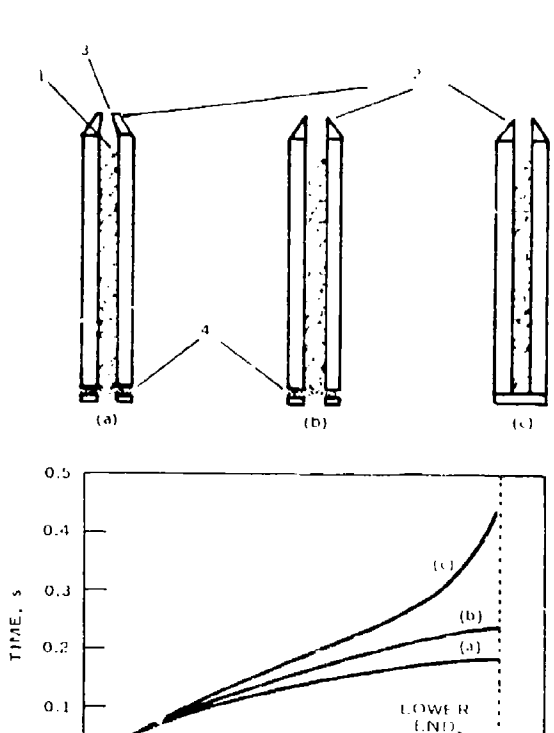

(a) Convergent nozzle
(b) Blank nozzle
(c) Blank nozzle and sealed lower end

(1) Pore diameter of Perspex tubes, 6 mm
(2) Asbestos
(3) Throat diameter, 4.3 mm
(4) Gauze support

FIGURE 30. Distance Time History of Convective Burning of HMX. [Data taken from Taylor (1962a), Figures 2 and 3.]

(HMX, RDX, PETN) and particle sizes (20-400 μm), the correlation is reasonable. An accompanying theoretical presentation is not clear. Moreover the formulas derived do not explain the slope break indicated nor do they reduce to $R_v=1$ when $R_\phi=1$.

This concludes the review of papers on convective burning in blind porous beds under conditions of constant bomb pressure.

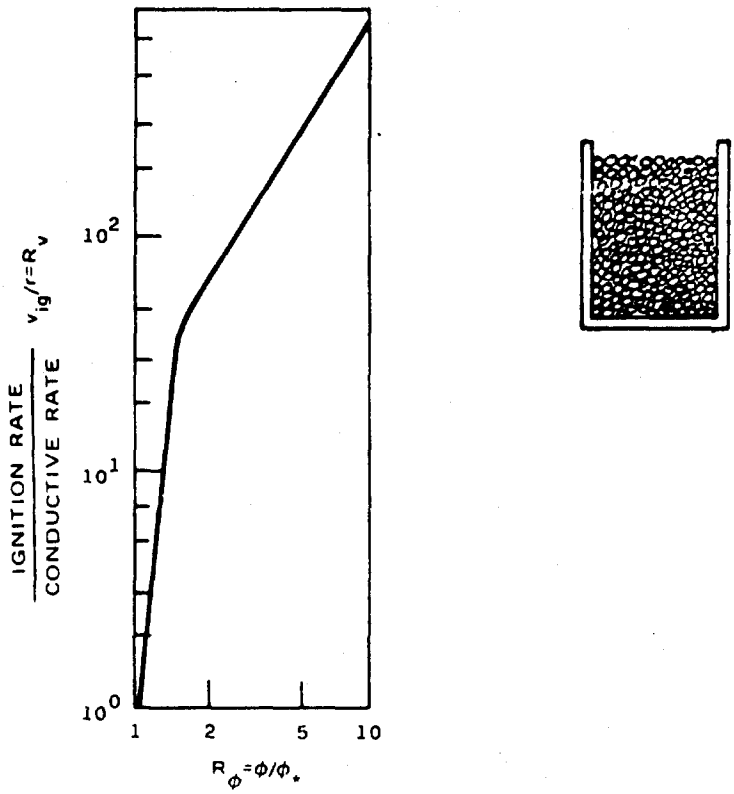

FIGURE 31. Correlation of Convective Burning Rate of Propellants With Stability Criterion. [Data taken from Belyaev (1973), Figure 63.]

3.2.2.2 Blind Porous Bed Burned in the HLDCB

Requirements for onset of convective burning in blind porous beds have been reported in five references [Belyaev (1973), Belyaev (1966), Gorbunov and Andreev (1967), Bobolev (1965b), and Andreev and Gorbunov (1963)] covering a wide range of effects. These include: propellant type, porosity, particle and pore size, permeability, charge diameter and length, and melting point. Inasmuch as theory and experiment both indicate that threshold pressure is affected by charge length and diameter, these quantities were chosen in the range where their effects were unimportant. The dependence of threshold pressure on charge diameter for PETN is shown in Figure 32. Similar considerations of length led to the choice of a specimen having a diameter of 10 mm and a length of 50-100 mm.

A series of tests was conducted [Belyaev (1966)] to compare mixed (composite) and secondary (single ingredient) explosives--a bomb loading density of 0.05 g/cm^3 was used, producing a dp/dt of 0.1-10 bar/ms. The results depicted in Figures 33 and 34, show the dependence of threshold pressure on porosity for a series of materials having a particle size

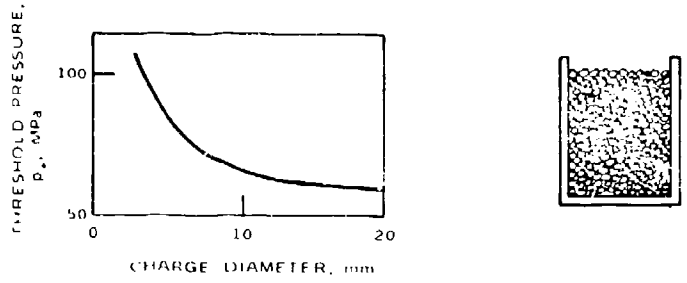

FIGURE 32. Effect of Charge Diameter on Threshold Pressure for PETN. [Data taken from Belyaev (1966), Figure 8.]

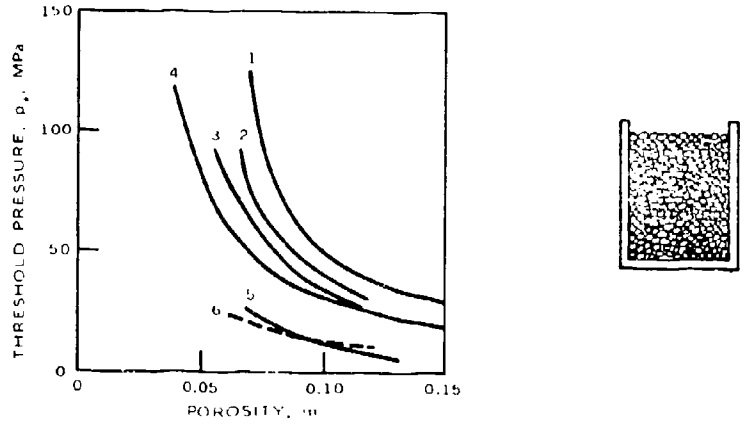

(1) TNT
(2) Picric acid
(3) DINA
(4) PETN
(5) RDX
(6) Nitrocellulose

FIGURE 33. Threshold Pressure as a Function of Porosity for Secondary Explosives (Particle Radius, 10-20 um). [Data taken from Belyaev (1966), Figure 3.]

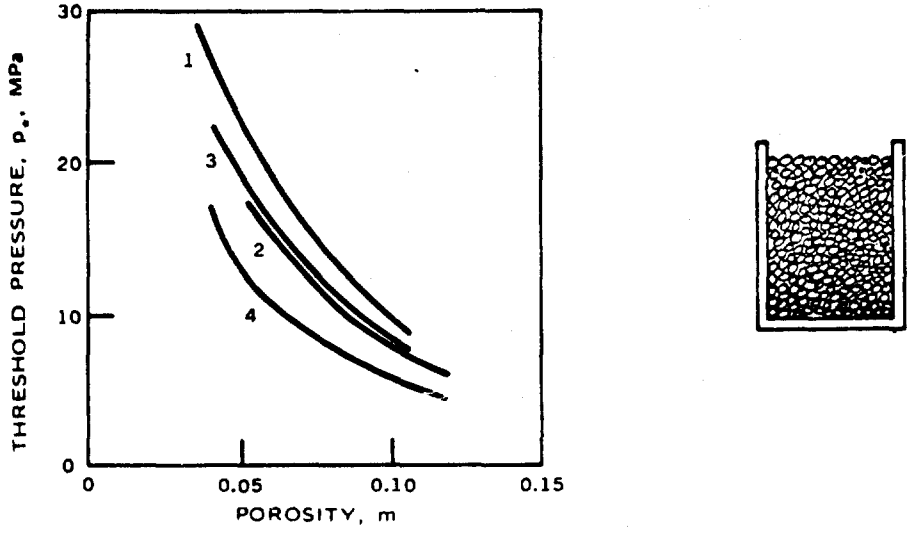

(1) Bitumen/$KClO_4$
(2) Polystyrene/$KClO_4$
(3) TNT/AP
(4) Bitumen/AP

FIGURE 34. Threshold Pressure as a Function of Porosity for Mixed Explosives (Particle Radius, 10-20 μm). [Data taken from Belyaev (1966), Figure 14.]

range of 10-20 μm. *It is noteworthy that threshold pressures are much lower for the composite materials, indicating their greater susceptibility to convective burning.* Belyaev interprets the results shown in Figure 34 as indicating that development of convective burning is governed primarily by the oxidizer properties. While there may be unreported evidence to support this claim, it should be noted that the results presented in Figure 34 suggest similar effects owing to changes in oxidizer or fuel. The important conclusion of Figures 33 and 34 are that for otherwise equivalent situations: (1) the threshold pressure decreases with increased porosity, becoming more dependent at porosities below 0.05; (2) the threshold pressure is highly sensitive to propellant type at low porosity and much less dependent at porosities exceeding 0.15. The implication is that at the low porosities most often encountered in practice, the propellant properties have a large influence on development of convective burning. Stated somewhat differently; *Figure 33 shows that homogeneous (single component) systems have a relatively high threshold pressure while Figure 34 shows that composite (heterogeneous) propellants have pressures that are of concern when compared to rocket chamber pressures where the porosities lie also in*

the area of concern. At higher porosities (>0.15) this effect decreases until propellant properties have only a minor effect. The curves of Figures 33 and 34 are approximated by the empirical relationship:

$$p_*(m - B) = A \qquad (11)$$

where

p_* = threshold pressure
m = porosity
A, B = constants dependent on propellant, with B representative of unconnected porosity

The foregoing results are for propellants with a particle size range of 10-20 μm. The results of a series of tests on PETN for different initial particle sizes are plotted in Figure 35. It is seen that large particles contributed to a lower threshold pressure and that the effect of particle size is greater at low porosity.

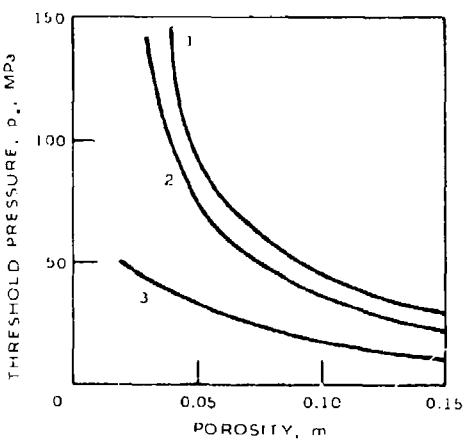

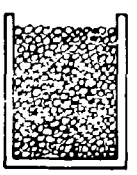

Particle radius, μm

(1) 10-20
(2) 120
(3) 550

FIGURE 35. Effect of Porosity and Particle Radius on Threshold Pressure for PETN (Charge Diameter, 5 mm). [Data taken from Belyaev (1966), Figure 5.]

The dependence of threshold pressure on gas permeability was also investigated. The permeability, k, is defined by the equation:

$$-1/A_c \; dU/dt = (k/\mu)(\partial p/\partial x) \qquad (12)$$

where

A_c = sample cross-sectional area normal to gas flow
U = volumetric throughput
k = sample gas permeability

and represents the volume flow rate per unit area for a unit fluid viscosity and pressure gradient. For A_c in cm^2, dU/dt in cm^3/s, μ in centipoise (cP), and $\partial p/\partial x$ in atm/cm, k is given in darcies. Figure 36 shows the relationship between permeability and porosity for several propellants and particle sizes. The influence of propellant type is not explained but is probably a result of different particle size distribution for the same range of particle sizes. If selected data from Figures 33 through 35 are cross-plotted with data from Figure 36, the effect of permeability on threshold pressure is obtained as shown in Figure 37. The composite propellants are well correlated by the equation

$$k \exp(p_*/D) = C \qquad (13)$$

where C and D depend weakly on the propellant formulation. The effect of particle size, other conditions remaining the same, is shown in Figure 38 for PETN. *The importance of Figures 37 and 38 is that: (1) secondary explosives such as TNT and PETN are less susceptible to convective burning and have a more complicated and sensitive dependence of threshold pressure on permeability than do the composite propellants; (2) the dependence of threshold pressure on propellant properties increases with decreasing porosity; and (3) permeability, like porosity and particle size, does not uniquely determine critical pressure.* An explanation offered for the failure of permeability to account for breakdown of surface burning is that burning penetrates the larger pores first but that permeability, a parameter which integrates the flow properties of all sizes of pores, does not reflect pore size distribution. An important deficiency in these studies is the failure to establish the effect of the rate of pressure rise on threshold pressure.

While the results just described were obtained with a geometrically blind porous bed, care was taken to choose a bed length so that the presence of the closed end did not affect the results. A difference between geometric restriction versus hydrodynamically blind needs to be kept in mind. That is, the test bed was made long enough to avoid geometric restriction. In additional auxilliary tests, the end effect

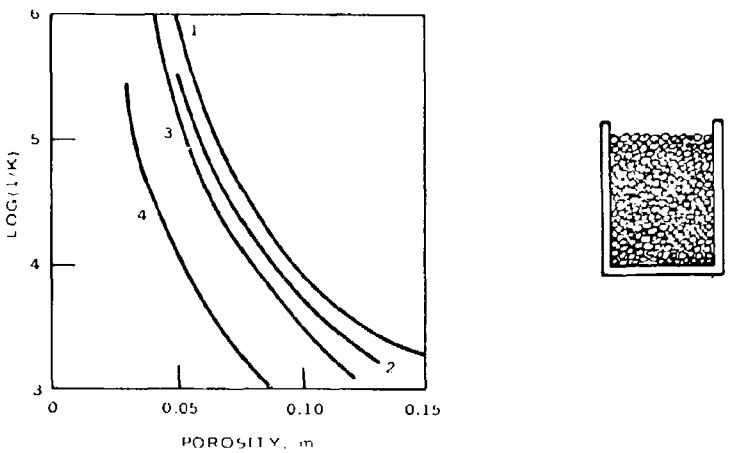

Particle radius, μm

(1) PETN (10-20)
(2) TNT/AP, stoichiometric (10-20)
(3) TNT (10-20)
(4) PETN (550)

FIGURE 36. Effect of Porosity, Particle Size, and Material on Permeability. [Data taken from Belyaev (1966), Figure 6.]

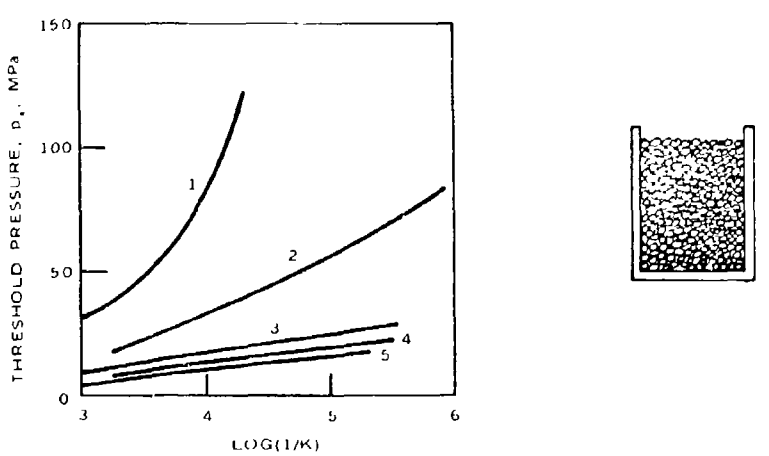

(1) TNT
(2) PETN
(3) Bitumen/$KClO_4$
(4) TNT/AP
(5) Bitumen/AP

FIGURE 37. Dependence of Threshold Pressure on Permeability and Material for Particle Radius of 10-20 μm. [Data taken from Belyaev (1966), Figure 7a.]

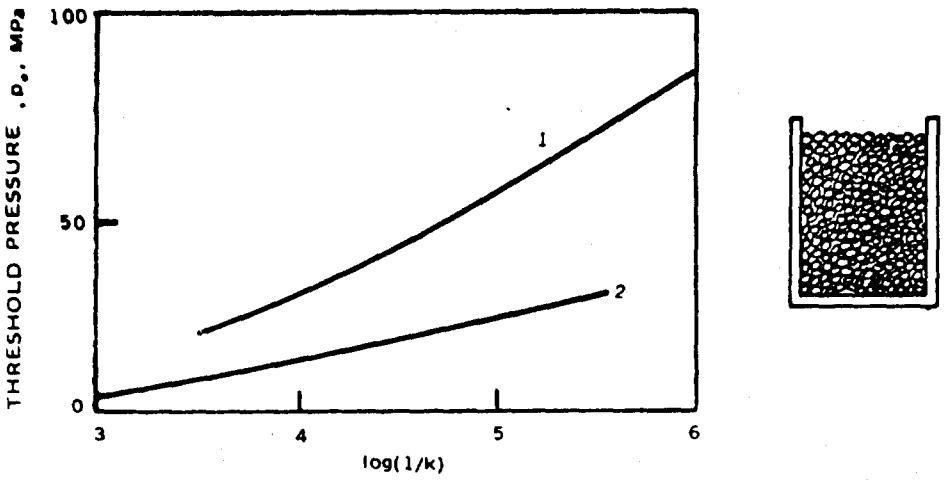

(1) 10-20 μm
(2) 550 μm

FIGURE 38. Threshold Pressure for PETN as a Function of Permeability for Two Particle Sizes. [Data taken from Belyaev (1966), Figure 7b.]

was found to be negligible if (1) the permeability was less than 10^{-3} darcy, and (2) at least 15-30 mm of unburned length remained at the time p_* was attained. For high permeability and short beds, the threshold pressure is stated to be sensitive to length [Belyaev (1966)], but no quantitative results are presented.

Andreev and Gorbunov (1963) determined the threshold porosity at which convective burning developed for TNT, picric acid, PETN, RDX, and mercury fulminate. These results, along with flow resistance (proportional to reciprocal of permeability) are indicated in Table 6. The extent to which the quantities of Table 6 are comparable is uncertain, since charge weights and dimensions varied among materials. An HLDCB was used having a volume of 50 cm^3 with an igniter consisting of 1 g of black powder which produced an initial pressure of 50 atm (5 MPa). Despite the poorer control of conditions, results show a ranking of susceptibility to convective burning similar to that indicated in Figure 33. The greater stability of PETN over RDX indicated in Table 6 may be due to the smaller particle size of the PETN. Additional experiments were conducted on PETN to show the effect of charge length and porosity. The change from normal to convective burning as charge length increased (Figure 39) indicates the stabilizing effect of the closed or blind end and is in qualitative agreement with theory (see section on theory). Figure 40 shows that convective burning is more likely to occur early in the test (at a lower pressure) if a large particle size is used. An important feature described for the tests whose pressure time records

TABLE 6. Comparative Stabilities of Conductive Burning of Explosives

Material	Threshold porosity	Threshold flow resistance (relative)	Particle size, μm
TNT	0.33	2.5	50-60
Picric acid	0.19	21	10-20
RDX	0.07	110	50-60
PETN	0.18	400	10
Mercury fulminate	0.11	1900	50-60

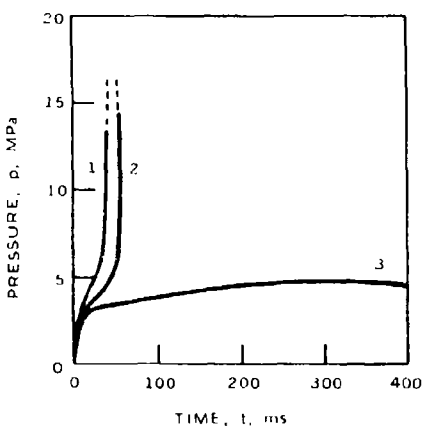

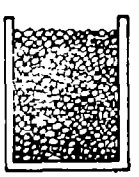

Length of charge

(1) 18 mm
(2) 13 mm
(3) 9 mm

FIGURE 39. Effect of Charge Length on Burning History of PETN (Porosity, m = 0.6; Particle Size = 10 μm). [Data taken from Andreev and Gorbunov (1963), Figure 6.]

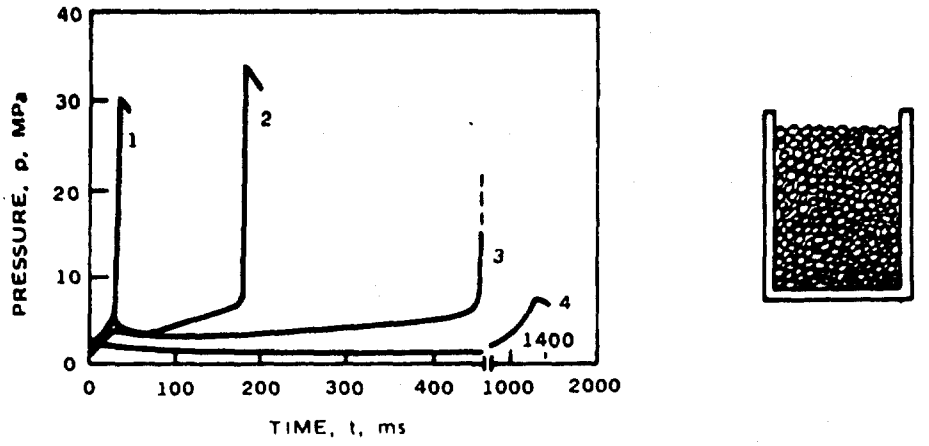

Particle size

(1) 300-400 and 460-500 μm
(2) 100-160 μm
(3) 63-100 μm (detonated)
(4) 10 μm

FIGURE 40. Effect of Particle Size on Burning History of PETN (Constant Length and Porosity). [Data taken from Andreev and Gorbunov (1963), Figure 7.]

are shown in Figure 40 is that the most violent combustion occurred for particles of intermediate size where an optimum trade-off exists between permeability (larger for large particles) and specific surface area (larger for smaller particles).

One explanation for the greater stability of conductive burning of secondary explosives, e.g., TNT, picric acid, DINA, PETN, and RDX (in order of decreasing stability) is that these materials melt during burning, forming a liquid surface layer which blocks the flow of gases into defects [Belyaev (1966)]. The criterion advanced by Belyaev for onset of convective burning is the discontinuity of the surface liquid layer, which, in turn, requires that the melt layer thickness be less than the maximum pore size. The melt layer hypothesis is supported by the fact that calculated melt layer thicknesses of the five materials listed above give values which decrease in the same order as the observed stability. An attempt was made to explore this phenomenon [Gorbunov and Andreev (1967)] by testing pairs of chemically similar materials with significantly different melting points for their propensity to develop convective burning. Particle sizes were held constant at 50-100 μm. Results, shown in Table 7, are claimed to demonstrate that the melt layer does not afford protection against onset of convective burning.

TABLE 7. Effect of Melting Properties on Stability of Conductive Burning.

	Relative threshold resistance	Threshold porosity, %	Melting point, °C
TNT	2.8	33	80
Xylyl	3.0	27	178
Trinitro benzene	29	12	121
Hezanitro biphenyl	26	18	238
RDX	110	7	203
HMX	180	6	272
DINA (15°C)	55	13	49
DINA (45°C)	55	12	49

In addition to the effect of melting point, the effect of initial temperature, hence melt layer thickness, was investigated for DINA. Results, also shown in Table 7, suggest that the thickness of the impermeable liquid layer does not govern onset of convective burning. Numerous phenomena such as reactivity of the liquid layer, boiling point, surface tension, and viscosity were not investigated. Also, results discussed in this section of the report are for rapidly rising pressures. The effect of a melt layer in a near constant pressure environment was reported in Section 3.2.2.1.

The final paper dealing with porous beds under conditions of rising pressure [Bobolev (1965b)], considers the effect of addition of paraffin to RDX (phlegmatization). Comparison was made of burning of pure RDX (particle size, 200 μm) and phlegmatized RDX (particle size range, 50-360 μm). Results are shown in Figure 41 for levels of paraffin varying from zero (pure RDX) to 10%. For this series of experiments, the addition of paraffin has no significant effect on the relation between relative density and breakdown pressure; however, even 0.5% paraffin prevents the buildup of convective burning into detonation. The essence of the explanation is that the paraffin acts both as a heat barrier, preventing heat transfer to the active component (RDX), and as a coolant (endothermic melting) for the combustion products. Thus, the role of the phlegmatizer is confined to stages of DDT following onset of convective burning, involving accelerated combustion and formation of weak shocks.

This concludes the review of experimental papers on burning in blind porous beds under conditions of rising pressure.

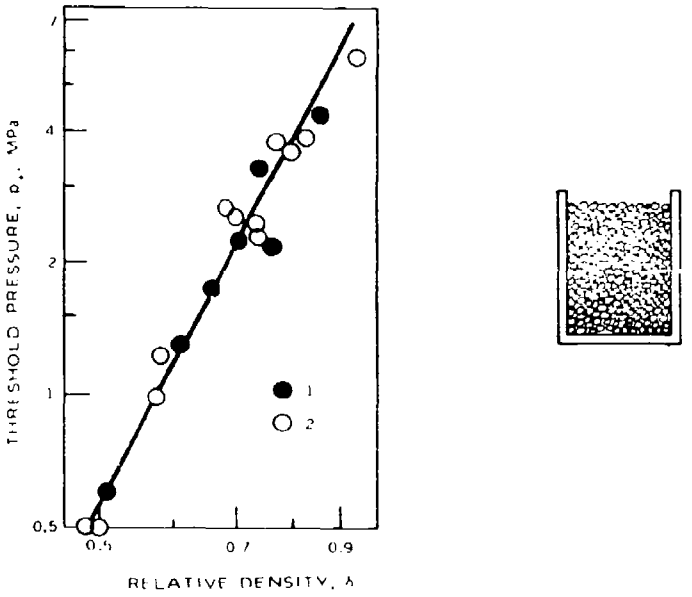

(1) Pure RDX
(2) 10% Paraffin

FIGURE 41. Effect of Addition of Paraffin on Threshold Pressure of RDX (Particle Radius, 200 μm). [Data of Bobolev (1965b) taken from Belyaev (1973), Figure 32.]

3.2.3.1 Open Porous Bed Burned in the LLDCB

Taylor (1962a) determined the effect of pressure and particle size on mass burning rate of HMX. His samples, which were burned in a Crawford bomb, consisted of 6 mm diameter paper tubes of 7.8 cm length filled with the granular material. A plug of plastic, cemented into the lower end of the tube to retain the sample, was not believed to provide a gas tight seal. Experimental results are shown in Figure 42 which shows no convective burning for small particles (5 μm) even at high pressures. Although bulk density (porosity) varied somewhat (1.02-1.20 g/cm^3) throughout the particle size range, it is clear that (1) onset of convective burning shifts to lower pressures for large particles, and (2) convective burning rates are at least an order of magnitude greater than conductive and much more sensitive to pressure. Similar trends

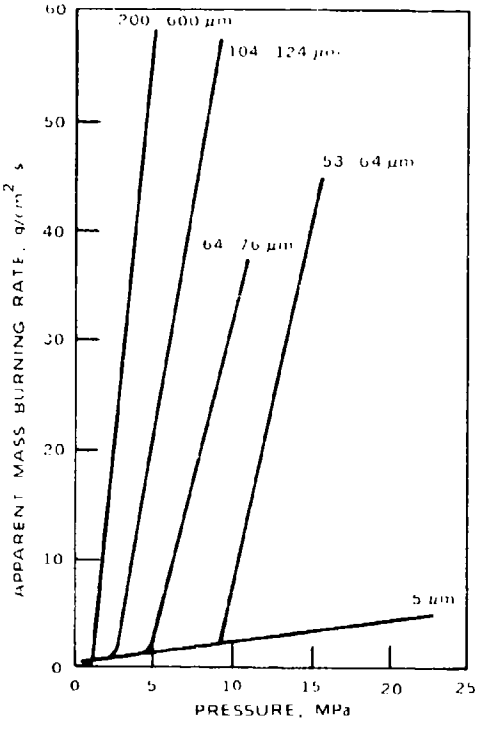

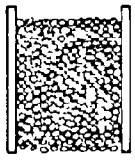

FIGURE 42. Convective Mass Burning Rate of HMX as a Function of Particle Size and Pressure. [Data taken from Taylor (1962a), Figure 1.]

have been noted and reported for other experimental conditions and materials. Effect of the end condition has been presented in Section 3.2.2.1 (see Figure 30) and shows the effect of the closed end in making development of convective burning more difficult.

In a separate investigation, Taylor (1962b), using similar techniques, measured the effect of pressure and HMX particle size on mass burning rate. The effect of pressure is shown in Figure 43 for two different combinations of density and particle size. Not only is mass burning rate nearly independent of particle size (density varying) but conductive burning prevails over the entire pressure range, as may be verified by comparison with the 5 μm curve of Figure 42. At the same time, the linear burning rate varies, approximately inversely with density (density varying from 1.02-1.66 g/cm^3). The effect of particle

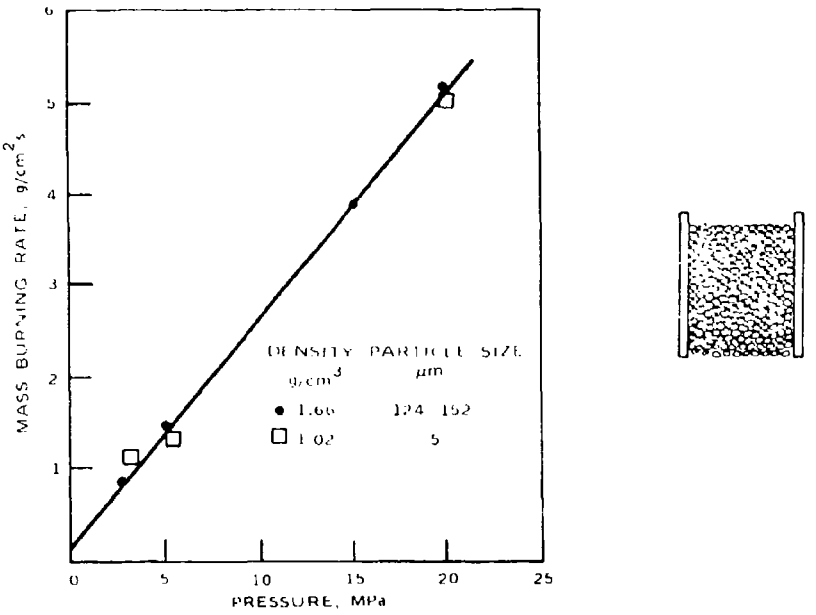

FIGURE 43. Effect of Pressure, Density, and Particle Size on Mass Burning Rate of HMX (Conductive Region). [Data taken from Taylor (1962b), Table 2.]

size on mass burning rate is shown in Figure 44 for the relatively low pressure of 12.6 atm (1.26 MPa) where convective burning does not develop over the range of conditions studied. It is seen that, although convective burning is absent, the mass burning rate increases slightly (compared to effect of particle size on convective burning) with particle size. Similar results were obtained with PETN, showing that in the conductive mode, mass burning rate is relatively insensitive to particle size and density.

Two alternate explanations are offered for the above phenomena. Taylor attributes the insensitivity of mass burning rate to particle size to a smooth melt layer which comprises a pressure dependent source of material fed to the gas phase. It is only at pressures, hence burning rates and melt layer thicknesses, which permit the melt layer to conform to surface irregularities without losing continuity that the burning rate is affected by pore size. At even higher pressures, the protection afforded by the melt layer disappears, leading to convective burning.

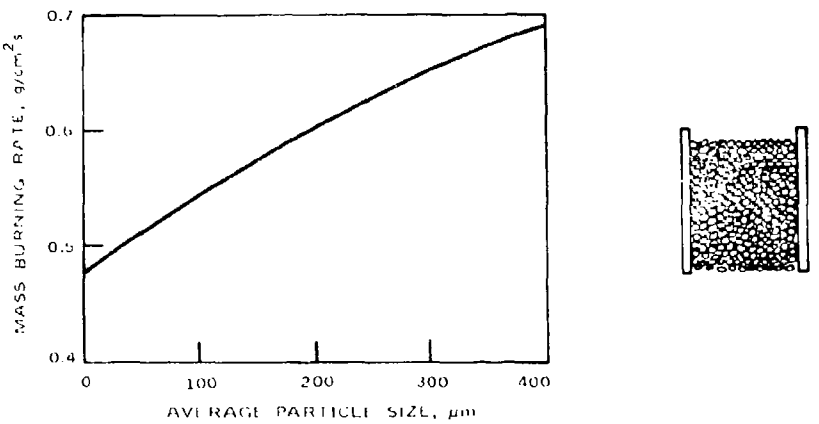

FIGURE 44. Effect of Particle Size on Mass Burning Rate of HMX at 1.26 MPa (Conductive Region) for Nearly Constant Density. [Data taken from Taylor (1962b), Table 4.]

Andreev's explanation is more tenuous and less complete, depending on his claim that heat transfer from the gas to the solid surface is independent of porosity. Without invoking a melt layer, Andreev explains the results on the basis of gas penetration which would occur at a higher rate for larger particles. The issue is not yet resolved.

3.3 DAMAGED PROPELLANT BURNED IN THE LLDCB

The combustion of damaged propellants was studied at the Naval Weapons Center. Two different series of tests were performed: one in which the propellant was strained before and during the combustion and one in which the propellant was strained until severe damage occurred but the imposed force was removed prior to the sample's being burned. Boggs, Zurn, and Derr (1976) studied the first case. Their results (Figures 45 and 46) showed some augmentation of burn rate at some values of strain and pressure.

Two propellants were used: a composite propellant with inert rubber base binder (Figure 45), and a high energy cross-linked double-base propellant (Figure 46). These propellants were placed in sample holders as shown in Figure 47. A small piece of microscope slide was placed against the sample sides to prevent the cold bomb gases from filling the voids produced by the subsequent straining accomplished

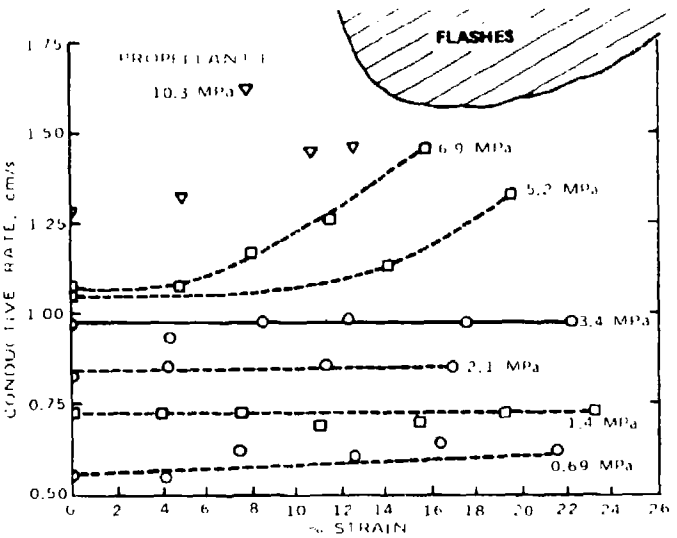

FIGURE 45. Effect of Strain and Gas Pressure on Conductive Burning Rate of Composite Propellant with Inert Binder.

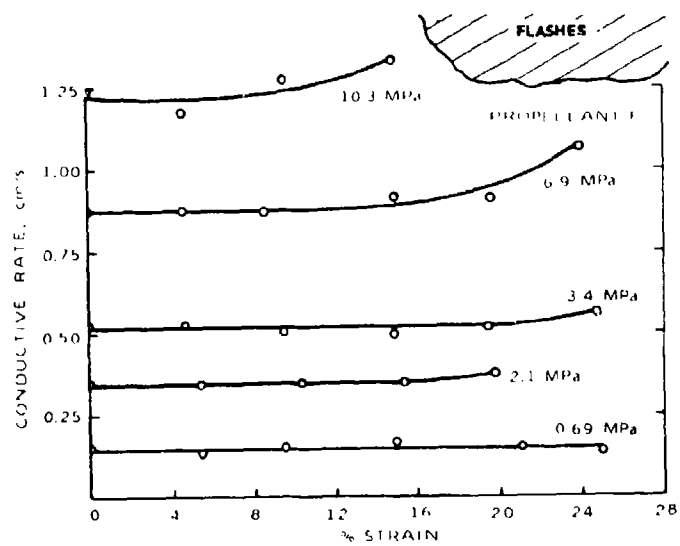

FIGURE 46. Effect of Strain and Gas Pressure on Conductive Burning Rate of a High Energy Crosslinked Double-Base Propellant.

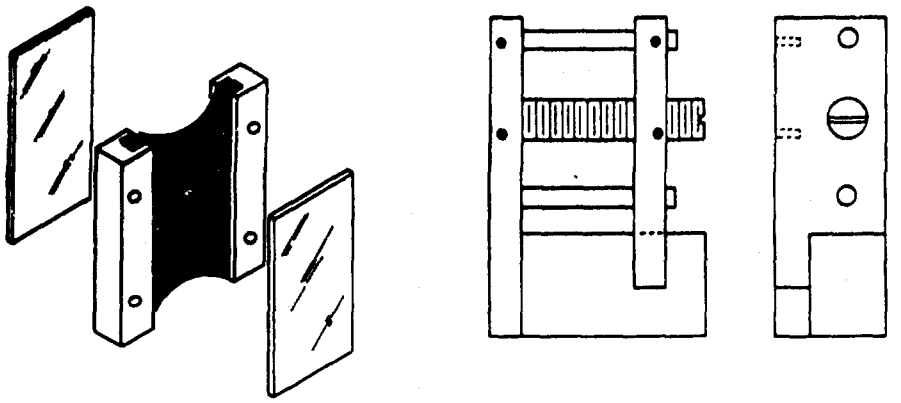

FIGURE 47. Sample Holder Used in Measuring Conductive Burning Rate of Strained Propellants.

using the device of Figure 47. The sample, under strain in the fixture, was burned in a window bomb (loading density less than 0.001 g/cm^3). Burn rates were determined from the films.

Data for both types of propellants (composite and cross-linked double-base high energy propellants) show burn rate increase at pressures and strains greater than some threshold values. It was emphasized that both threshold values have to be exceeded, exceeding just one was not sufficient. For example high strain but low pressure did not cause augmentation nor did high pressure but low strain.

The mechanical response of the propellants to strain was studied using a binocular microscope. These studies showed, using Propellant A as an example, that at 4% strain, debonds (separation, on a micro-scale, of the solid particle from the polymeric binder) between ingredients occurs. Between 9-11% strain, these debonds are often fully developed cracks, with the walls of the crack in close proximity. At approximately 16% these cracks are open voids; that is, the walls of the crack are no longer in contact with one another. At approximately 24% the sample is often riddled with large cracks and the sample fails.

The authors provided a mechanistic explanation for the burn rate augmentation due to strain and pressure. At low strain values the propellant was not significantly damaged and so regardless of the flame stand-off, augmentation did not occur. When the propellant was highly strained and fissured, augmentation occurred if the flames penetrated into these fissures. At low pressures the flame stood too far from the surface to allow penetration, but at high pressures the flame was close enough to the surface to penetrate the fissures and cause burn rate augmentation.

The above tests were conducted on samples with imposed strain (that is, the voids were open). Another series of tests was conducted on propellant samples which were heavily damaged but the imposed strain was released prior to burning. Samples of propellant were subjected to tensile strains which caused significant damage. The sample was strained to 25% and then allowed to relax to zero strain. The sample was then strained to approximately 35% where the stress/strain characteristics indicated severe damage. These damaged samples were burned at pressures up to 34.5 MPa. The results are presented in Figure 48. It was found that damaged and undamaged propellants had the same burn rate, indicating that damaged propellant tends to burn normally if the strain induced voids are allowed to close (a debond condition existed, but there was no open pore).

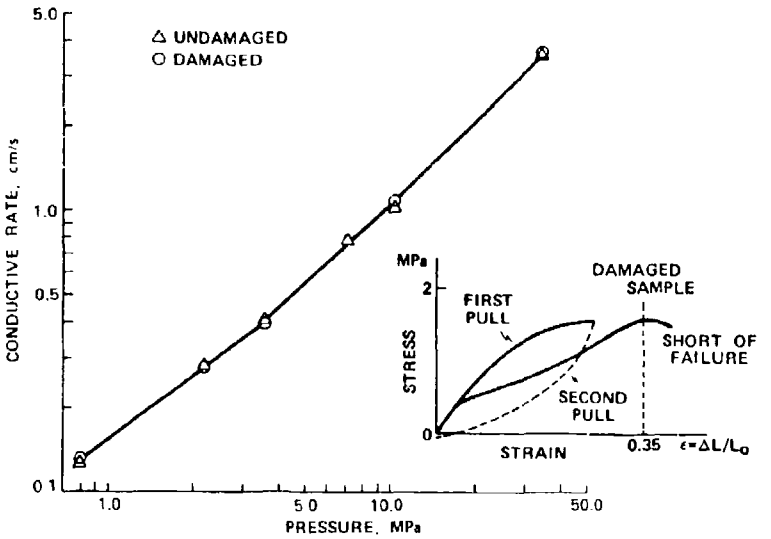

FIGURE 48. Effect of Damage on Conductive Burning Rate of a High Energy Cross-Linked Double-Base Propellant.

4.0 THEORY

As outlined earlier (Section 2.2), the literature on the simplified theory of early convective burning falls into two principal categories: single pore and porous bed. Further subdivision is according to the three requirements for convective burning, viz., fluid dynamic, heat

transfer, and propagation of an ignition front. The first and second subsections which follow present the available analyses relevant to single pore and porous bed situations. In addition, a third section is included of miscellaneous results which do not fit into the general morphological pattern.

4.1 SINGLE PORE

All three requirements for single pore convective burning have been analyzed theoretically using simplified concepts. The fluid dynamic criterion considers only a blind pore with a rising external pressure and is based on conservation of mass; hence frictional effects are ignored. The criteria of ignition and propagation of ignition include a simplified energy balance but again omit the momentum equations.

4.1.1 Fluid Dynamics

The fluid dynamic requirement of gas penetration into a single channel can be represented by the expression

$$v_g > r \tag{14}$$

where v_g is the rate of gas flow into the channel and r is the normal (conductive) regression rate. The condition is necessary but insufficient for the propagation of an ignition front into the pore. Since r is a reasonably well-known function of environmental pressure (less well-known as a function of dp/dt and gas velocity) and propellant temperature, it remains to calculate v_g for the appropriate conditions. Ideally, this calculation would involve application of transient conservation equations and would require knowledge of transient friction and heat transfer in the entrance section of the channel. The only known simplified approaches [Bobolev (1965a) and Belyaev (1973)] ignore these complications and consider the situation depicted in Figure 49. A closed end channel of length L and unit cross-sectional area is initially filled with gas at temperature T_o and pressure p. External gas at temperature T_g and pressure p, equal initially to pore gas pressure, flows in under the action of an external pressure rise dp/dt. The following assumptions are made in the analysis:

1. The incoming gases mix with the pore gases, the mixture temperature remaining constant at the initial pore temperature, T_{go}.
2. The pore is not "too" wide. This would seem to imply one dimensional flow (no recirculation).
3. Relaxation time of pore pressure is less than relaxation time of external pressure. In other words the pore process is quasi-steady.

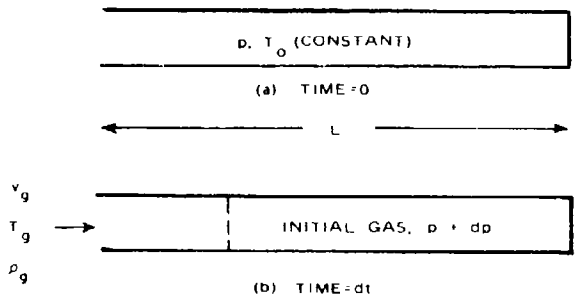

FIGURE 49. Simplified Model of Gas Flow into Blind Channel Under Rising Pressure Conditions.

4. The product Ldp/dt is "not too large." This is related to assumption 3 since the relaxation time of the pore increases with L while the relaxation time of the external pressure increases with decreasing dp/dt. An expression for v_g can be derived by equating the quantity of incoming gas

$$\dot{m}_{in} = v_g \rho_g = v_g p/bT_g \tag{15}$$

to the increase in gas in the pore

$$\dot{m}_{pore} = L\ \dot{p}/bT_{go} \tag{16}$$

during the time dt. The specific gas constant is denoted by b. Equation (16) depends upon assumption 1. Equating $\dot{m}_{in}$ to $\dot{m}_{pore}$ provides the required result:

$$v_g = (L/p)(dp/dt)(T_g/T_{go}) \tag{17}$$

Recalling Eq. (14), one notes that the hydrodynamic condition for inflow is facilitated (subject to the restrictions mentioned) by: (1) deeper channels, (2) low pressures, (3) high rate of pressure rise, (4) hot combustion products, and (5) cool propellant. The effects of low propellant temperature and low pressure are twofold: they not only increase the left-hand side but decrease the right-hand side of Eq. (14), thereby improving conditions for inflow. It should be stressed that Eq. (17) was derived for conditions simulating a blind pore, open at the

ignited end to a rising pressure. Simplified expressions giving v_g in a single pore for other conditions have not been found in the current survey.

4.1.2 Ignition of the Wall of a Single Pore

Satisfaction of the inequality (Eq. (14)) is no guarantee that the inflowing hot gases will heat the pore wall sufficiently to achieve a condition for self-sustained reaction, usually called ignition. An analysis to establish conditions for ignition of pore walls by hot gas flow is concerned with two broad problem areas: (1) definition of ignition, and (2) calculation of conditions resulting from the hot gas flow. The simplest ignition criterion is an ignition temperature which is unique to the material. Such a concept ignores the variation of ignition temperature with experimental conditions such as heating history and nature of the surrounding atmosphere. Zeldovich (1942) pointed out that attainment of a critical surface temperature alone is insufficient to assure ignition, but that the entire temperature profile (variation of temperature with distance from the heated surface) should resemble that under steady-state burning conditions for the substance being ignited. It is convenient to characterize the thermal profile by the depth of penetration of the heat introduced at the surface; it is the dual requirement of surface temperature and thermal profile depth which serves as ignition criteria in the analysis by Margolin and Chuiko (1965).

The second problem area in pore wall ignition is the calculation of surface temperature and thermal profile depth in the pore wall which results from inflowing hot gases. To simplify the calculations, Margolin and Chuiko (1965) introduced several approximations. Actually, the inflowing gases cool gradually, simulataneously heating the wall. It is assumed that

1. The gas, at constant temperature, T_g, gives up its heat to the pore wall at constant temperature, T_w. This heat transfer takes place over a cooling length, L_c, and with constant rate of heat transfer.

2. All flow variables such as temperature, velocity, and gas density are timewise and spacewise constant over the distance, L_c.

3. The gas flow is laminar and satisfies the inequality

$$\frac{x/d_p}{RePr} > 0.1 \qquad (18)$$

for which the Nusselt number is constant, given by

$$Nu = h\, d_p/\lambda_g = 3.66 \qquad (19)$$

where x is the distance from the pore entrance, h is the film coefficient for heat transfer, d_p is the pore hydraulic diameter, and λ_g is the thermal conductivity of the gas. An essential step in the establishment of ignition conditions is the calculation of the length of the cooling section L_c. In unit time, the heat lost from the gas to the wall is

$$q_{loss} = (v_g - r)\rho_g c_g (T_g - T_w)\pi d_p^2/4 \tag{20}$$

This same heat must be transferred across the gas film

$$q_{trans} = \pi d_p L_c h(T_g - T_w) \tag{21}$$

Equating the two expressions permits solving for L_c.

$$L_c = \rho_g c_g d_p (v_g - r)/4h = (v_g - r)d_p^2/4Nu\alpha_g \tag{22}$$

where the thermal diffusivity of the gas, α_g, is defined as

$$\alpha_g = \lambda_g/\rho_g c_g \tag{23}$$

The next step in applying Zeldovich's criteria consists of the evaluation of several quantities:

1. The time, τ, available for heating the pore wall
2. The depth, ℓ, of the heated layer at the time, τ
3. The depth, ℓ_s, of the steady-state thermal layer
4. The time, τ_s, required to establish the steady-state thermal layer
5. The time, τ_*, required to heat the pore wall from the initial temperature, T_o, to the ignition temperature, T_*.

The time available for heating the pore wall is simply the time required to consume the heated length of the pore, approximated by L_c, at the conductive rate r. Hence

$$\tau = L_c/r \tag{24}$$

The thermal penetration depth is actually infinite since the temperature profile at any instant is asymptotic to the initial temperature, T_o. However, at the time τ, the temperature at depth $(\alpha_s\tau)^{1/2}$ has dropped by 90% of the difference T_s-T_o; this distance is commonly used as the depth of the thermal layer. Therefore we may write approximately

$$\ell = (\alpha_s\tau)^{1/2} \tag{25}$$

$$\ell_s = (\alpha_s\tau_s)^{1/2} \tag{26}$$

The time required to establish the steady-state thermal layer is again infinite, with a reasonable approximation being provided by

$$t_s = x_s/r \tag{27}$$

which states that the steady-state profile will be attained by the time the surface has regressed a distance equal to the steady-state penetration distance.

The time required to heat the pore wall to the ignition temperature (T_*) is obtained by equating the heat flowing across the gas film to the heat absorbed by the solid, assuming spacewise constant temperature in the solid.

$$hL_c d_p (T_g - T_*) t_* = \rho_s c_s L_c (T_* - T_o)[d_p(\alpha_s t_*)^{1/2} + a\alpha_s t_*] \tag{28}$$

Solving for t^* gives

$$t_* = \frac{d_p^2}{\alpha_s}\left(\frac{\beta}{Nu - a\beta}\right)^2 \tag{29}$$

where the subscript s refers to solid phase. The quantity a is a geometric parameter with the value of zero for rectangular slits and unity for circular pores, while β is given by

$$\beta = \lambda_s(T_* - T_o)/\lambda_g(T_g - T_*) \tag{30}$$

Zeldovich's criteria are given by

$$t/t_* > 1 \tag{31}$$

$$\ell/x_s > 1 \quad \text{or} \quad t/\tau_s > 1 \tag{32}$$

Equation (31) expresses the requirement that the available pore heating time is long enough to heat the pore wall to the ignition temperature. Equation (32) states that the depth of the thermal layer should be as great as the steady-state value. The second alternative of Eq. (32) follows from Eq. (25) and (26). By combining Eq. (22) and (24) through (32), Margolin and Chuiko (1965) arrived at the following criteria for ignition of the pore wall:

From Eq. (31) (temperature criterion)

$$\boxed{\frac{v_g - r}{r}\,\frac{Nu}{4}\left(\frac{T_g - T_*}{T_* - T_o}\right)^2 \frac{\rho_g c_g \lambda_g}{\rho_s c_s \lambda_s}\left(1 - \frac{a\beta}{Nu}\right)^2 \geq 1} \tag{33}$$

From Eq. (32) (depth criterion)

$$\boxed{\frac{(v_g - r)rd_p^2}{4Nu\alpha_g\alpha_s} \geq 1} \qquad (34)$$

Both inequalities implicitly contain the hydrodynamic criterion $v_g > r$ (see Eq. (14)).

It should be noted that Eq. (33) and (34) are quite general, within the limits imposed on their derivation, because v_g and Nu depend upon unspecified experimental or model conditions. Margolin and Chuiko (1965) presented Eq. (33) and (34) in a schematic graphical display (see Figure 50) of pressure vs. pore diameter without specifying the relevant experimental or model conditions and without providing any details of the transformations required to obtain the graph. Therefore, discussion of the implications of Figure 50 must be made in the absence of any resolution of the conditions of its applicability. Curve 1, representing Eq. (33), separates the p-d_p plane into two regions, the upper one denoting conditions for which the surface is heated to the ignition temperature or above. The horizontal nature of Curve 1 suggests that pore diameter is not present, even implicitly, in Eq. (33). Actually v_g and Nu may depend on pore diameter while T_g could be influenced both by pressure and pore diameter owing to the effect of pressure on flame standoff distance and the consequent temperature of gases flowing into the pore. The effect of the variables in Eq. (33) on the position of Curve 1 cannot be estimated until the dependence of $(v_g-r)/r$ on pressure is established; this in turn, is not a general result but requires assignment of model conditions. Curve 2, representing Eq. (34), also separates two regions; the lower consisting of combinations of pressure and pore size for which the thermal layer is too thin to assure ignition. The location of Curve 2 is undetermined unless the pressure and pore size dependencies of the terms in Eq. (34) are known or assumed.

Curves 1 and 2 delineate four regions in the p-d_p plane. In Region A, both conditions for pore wall ignition are satisfied, resulting in the onset of convective burning. In Region B, neither condition is satisfied, so that combustion does not penetrate the pores. However, there is some inflow of hot gases which heat the pore walls above the ambient temperatures and lead to slight augmentation of the conductive burning rate. Region C corresponds to a hot enough but not a thick enough thermal layer. The result is known as forced pyrolysis, which would cease with removal of the stimulating source of energy. Region D represents a condition in which a thick layer of the pore wall is heated to some temperature below the ignition point. The result would be either a thermal explosion (result of synergistic interaction between temperature and rate of heat release by chemical reaction) of the thermal layer or a significant augmentation of the conductive burning rate. Region E, included in the reference, is said to represent turbulent combustion of gases which flow into the pores, but further details are sketchy.

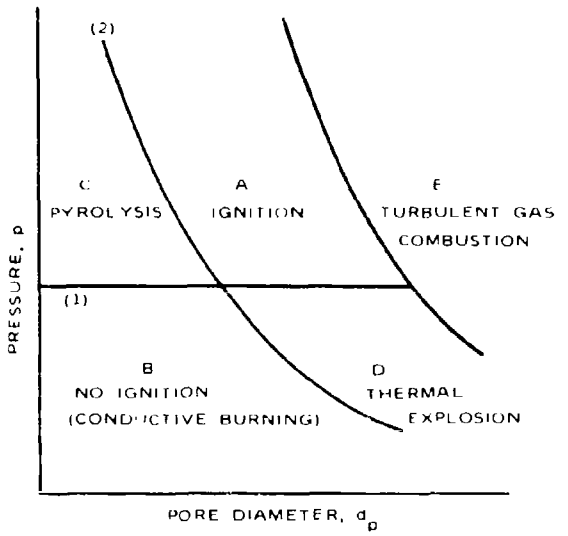

FIGURE 50. Schematic of Pore Ignition Regimes.

The foregoing analysis and remarks are strictly applicable to smooth wall pores. Brief mention of roughness of pore walls is made by Margolin and Chuiko (1965). A protuberance may serve as an ignition center if two conditions are satisfied. Define

$$\tau_p = D_c^2/\alpha_s \tag{35}$$

as the characteristic heating time of the protuberance having characteristic dimension D_c. The conditions are

$$\tau > \tau_p > \tau_s \tag{36}$$

where τ and τ_s are given by Eq. (24) and (27). The first inequality of Eq. (36) requires that the available heating time be sufficient to heat the particle to the ignition temperature while the second inequality assures the formation of a thermal layer of sufficient thickness, equal to the steady-state value. If Eq. (36) is satisfied, the ignition Region A of Figure 50 may extend into Region D.

Thus far, conditions for pore wall ignition by inflowing hot gases have been described. Margolin and Chuiko also present, without derivation, the conditions for ignition by other mechanisms, including:

1. Propagation of combustion into pores filled with combustible gases.
2. Propagation of combustion through flowing hot gases.
3. Ignition of pore walls by thermal explosion of reactive pore gases.
4. Ignition of pore walls by adiabatic compression of pore gases.

While these alternatives are viable mechanisms for pore wall ignition, neither the assumptions needed for the derivations nor the conditions of applicability are stated in the cited reference.

Despite the generality of Eq. (33) and (34), few applications have been made to particular model or experimental conditions. Margolin and Chuiko (1966) rewrote Eq. (34) as

$$\frac{1}{4Nu}\frac{v_g}{r} - \frac{d_p}{\ell_s}\frac{d_p}{\ell_g} \geq 1 \tag{37}$$

where

$$\ell_s = \alpha_s / r \tag{38}$$

$$\ell_g = \alpha_g / r \tag{39}$$

denote steady-state thermal layer thickness for the solid and gas. For the case of spontaneous penetration of combustion (pressure difference generated by combustion) the functional relationship

$$v_g = \frac{\rho_s}{\rho_g} rF\left(\frac{d_p}{\ell_i}, \frac{d_p}{D_c}, Pr_i, Le, \frac{T_g}{T_*}, \frac{T_g}{T_o}, \frac{T_m}{T_o}\right) \tag{40}$$

is presented, where ℓ_i are other, unspecified characteristic combustion zone dimensions, Pr_i are related Prandtl numbers, Le is the Lewis number, T_m is melting temperature, and the other symbols have been previously defined. Assuming

1. $v_g >> r$
2. ℓ_g is proportional to ℓ_s
3. The function F is only weakly dependent on its arguments
4. Convective burning is independent of α_s/α_g

Margolin and Chuiko (1966) combine Eq. (37) and (40) and arrive at the requirement

$$\boxed{d_p/\ell_s = \alpha_s c_s r\, d_p/\lambda_s = \text{const} = An} \tag{41}$$

Equation (41), known as the Andreev criterion, is thus seen to be related to Eq. (34), which expresses the ignition requirement of the formation of a thermal wave thickness of appropriate dimensions. It is noteworthy that the Andreev criterion does not involve a surface temperature requirement; hence, it would predict ignition of pore walls in both Regions A and D (Figure 42). The hydrodynamic criterion is satisfied by assumption (1); otherwise the Andreev criterion has limited applicability.

In the only other reference to the general ignition conditions, Belyaev (1973), in discussing results of manometer bomb tests (see Section 3.1.2.2 of this review), presents the following criterion without derivation.

$$p^{1+2n} d_p^{\,2} = \text{constant} \tag{42}$$

Equation (42) can be deduced from Eq. (34) by assuming

1. $v_g >> r$
2. v_g is proportional to r
3. α_g is proportional to 1/p, valid at low pressures
4. $r = ap^n$

Belyaev (1973) could not account for the break in the slope of the p_* (critical pressure) vs. d_p curve without attributing the phenomenon to some failure of the assumptions made in deriving Eq. (33) and (34). However, comparison of Figures 5 and 50 (see Figure 51) suggests that the break may be explained by a change in the relevant criterion. For small pores and high pressures, the experimental data fall on Curve 2, separating Regions A and C (Figure 50); hence, the criterion is the formation of a sufficiently thick thermal layer. For large pores and lower pressures, the data correspond to Curve 1, separating Regions A and D, where the criterion is the attainment of the required surface temperature. Different break points would be expected for different materials having different properties. The data for RDX (Figure 5) probably show no break simply because they do not extend to large enough pores.

Godai (1970) provides a qualitative theory to explain experimental results. By equating the rate of heat evolved in combustion of the walls of flat crack to the rate of heat lost (to these same walls) he arrives at the following relation:

$$t_* = 4\lambda_g (T_g - T_s)/r\rho_s Q_s \tag{43}$$

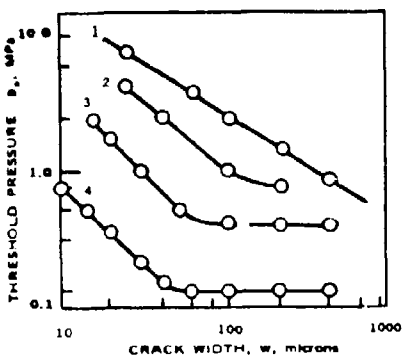

Figure 5 (Reproduced).

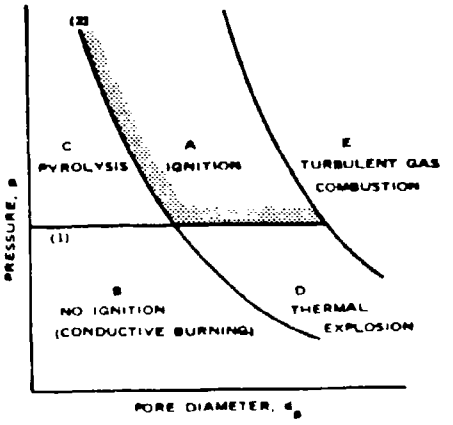

Figure 50 (Reproduced).

FIGURE 51. Comparison of Figures 5 and 50.

where

t_* = threshold crack width for penetration of combustion
λ_g = gas conductivity
T_g = gas temperature
T_s = propellant surface temperature
r = conductive burning rate
ρ_s = propellant density
Q_s = heat of combustion

Equation (43) exhibits the correct qualitative relationship between threshold crack size and burning rate and also predicts an inverse relationship between crack width and heat of combustion. However, it also predicts an increasing threshold crack size with increasing gas temperature. An additional shortcoming, stated by Godai, is the failure to explain behavior of aluminized propellants.

4.1.3 Propagation of Ignition Front in Single Pore

The preceding sections have reviewed the available literature dealing with two of the necessary conditions for transition from conductive to convective burning in a single pore: flow of hot combustion gases into the pore, and ignition of the pore walls by the hot gases. The third requirement is that the ignition front continue to propagate into the pore at a rate exceeding the normal conductive burning rate. The only available simplified model which is related to the phenomenon [Krasnov (1970)] is depicted schematically in Figure 52. The hot combustion gases with temperature T_g, velocity v_{gh}, and density ρ_{gh} flow

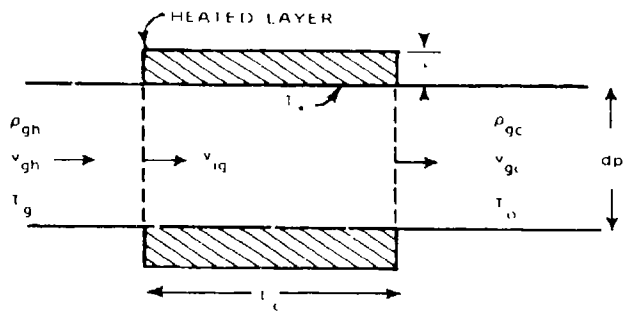

FIGURE 52. Simplified Model of Ignition Propagation into Single Pores.

into the mouth of a circular pore of diameter d_p. After traversing a cooling section of length L_c, the gas flows away at the lower temperature T_o, velocity v_{gc}, and density ρ_{gc}. The cooling process is assumed to occur at a constant temperature difference, as discussed in the previous section on ignition. Using a coordinate system moving with the ignition front with the velocity v_{ig}, energy and mass conservation for the ignition section are written

$$\rho_{gh} c_g (T_g - T_o)(v_{gh} - v_{ig})\pi d_p^2/4 = \rho_p c_p (T_* - T_o)\pi d_p v_{ig} \delta_t \quad (44)$$

$$\rho_{gh}(v_{gh} - v_{ig}) = \rho_{gc}(v_{gc} - v_{ig}) \quad (45)$$

Equation (44) equates the heat lost by the gas to the heat gained by the heated layer of propellant, whose thickness, δ_t, is assumed small compared to the pore diameter. By eliminating v_{gh} between Eq. (44) and (45), one may obtain

$$\delta_t = \frac{v_{gc} - v_{ig}}{4 v_{ig}} \frac{c_g \rho_{gc}}{c_s \rho_s} \frac{T_g - T_o}{T_* - T_o} d_p \quad (46)$$

for the thickness of the thermal layer. The cooling length may be found from

$$h(T_g - T_*)\pi L_c d_p = \rho_{gc} c_g (T_g - T_o)(v_{gc} - v_{ig})\pi d_p^2/4 \quad (47)$$

which equates the heat transferred through the gas film to the heat lost from the flowing gas. Two conditions are considered: smooth pore walls and rough pore walls with protuberances of the optimum size α_p/r (thickness of steady-state thermal layer).

Smooth Walls

The time available for wall heating is limited by the time required to burn the distance L_c at the conductive rate r (cf. Section 4.1.2)

$$\tau = L_c/r \tag{48}$$

The thermal layer thickness at time τ is*

$$\delta_t = (\alpha_s \tau)^{1/2} \tag{49}$$

Combining Eq. (46) through (49) gives the result

$$\frac{v_{gc}}{v_{ig}} = 1 + \frac{4\rho_s c_s \lambda_s (T^* - T_o)^2}{Nu\rho_g c_g \lambda_g (T_g - T_o)(T_g - T^*)} \tag{50}$$

Rough Walls

The time required to heat a particle of optimum size is

$$\tau = \alpha_p/r^2 \tag{51}$$

Combining Eq. (46) through (48) with Eq. (51) gives the result

$$\frac{v_{gc}}{v_{ig}} = 1 + \frac{4Nu\alpha_p \alpha_g}{r^2 d_p^2} \tag{52}$$

It may be concluded that for either smooth or rough wall pores, the cooled gas velocity exceeds the ignition front velocity. For smooth walls, the ratio v_{gc}/v_{ig} (referred to from here on as ignition lag) should be independent of diameter, v_{gc}, and conductive rate. Increasing the pressure should decrease the ratio since ρ_g and T_g can only increase with pressure. For rough walls, the ignition lag should be independent of v_{gc}, but should decrease with increasing values of pressure and pore diameter.

*Use of Eq. (49) is actually inconsistent with assuming a constant temperature for the thermal layer since Eq. (49) is based on a variable temperature.

Experimental results (see Section 3.1.3.4, and Figure 20 suggest that there is a dependence of ignition lag on d_p for pores smaller than 2 mm which agrees qualitatively with Eq. (52) for rough pore walls. On the other hand, experimental results for larger pores appear to be size independent as required by Eq. (50) for smooth pore walls. A possible explanation of this anomaly is that roughness, represented by a constant size protuberance, would be relatively more important in a small channel. A serious unexplained departure of experimental results from theory is the dependence of experimental ignition lag on v_{gc}. It is thus concluded that the claim of good agreement between experiment and theory by Krasnov (1970) is not well supported by the data presented.

It should be noted that the theoretical results derived in this section are not dependent on any particular model or experimental conditions, such as constant pressure (pressure is not even mentioned) or channel end condition. On the other hand, the experiment was carried out in a very specialized constant pressure apparatus in which the gas flow into the channel displaced a liquid through a valve at the unignited end.

Although the paper [Krasnov (1970)] is related to the problem of propagation rate of the ignition front, it does not present an explicit formula for v_{ig}, but only for the ratio v_{gc}/v_{ig}. The requisite analysis to determine the cool gas velocity v_{gc}, which depends on v_{gh} and thus on model conditions, has not been carried out. Thus, at this time, there is no available complete simplified analysis which leads to a criterion for fulfillment of the third requirement for convective burning in a single pore, viz., $v_{ig} > r$.

4.2 POROUS BED

The simple theories of porous bed convective burning are directed exclusively at the solution of the fluid dynamic problem of transient flow into a porous bed under several boundary conditions. Only the mass and momentum equations are involved, while the energy equation is eliminated by assuming isothermal flow. This simplification alone precludes the establishment of ignition conditions since there is no calculation of pore wall heating during the flow. The only attempt to consider ignition conditions is the heuristic extension of the Andreev criterion to porous beds by defining an equivalent average hydraulic pore diameter based on permeability measurements. The success of such a procedure has already been discussed in Section 3.2.2.1. Finally, there are no simplified theories addressing the problem of propagation of the combustion front into a porous bed.

4.2.1 Fluid Dynamics

The fluid dynamics associated with simplified modeling of convective burning in porous beds is summarized by Belyaev (1973). The analysis uses the momentum equation in the form of Darcy's law

$$u = 1/A_c \; dU/dt = - k/\mu \; \partial p/\partial x \tag{53}$$

where

u = volumetric flow rate per unit cross-sectional area of the bed (not the pores)
k = proportionality constant called permeability
μ = fluid viscosity
$\partial p/\partial x$ = pressure gradient

The conservation of mass is expressed by

$$- m \frac{\partial \rho}{\partial t} = \frac{\partial}{\partial x} (\rho u) \tag{54}$$

where

m = porosity
ρ = fluid density

The basic equation, referred to as the filtration equation by the Russians, is obtained by combining Eq. (53) and (54) to give

$$\frac{\partial \rho}{\partial t} = \frac{k}{\mu m} \frac{\partial}{\partial x} \left(\rho \frac{\partial p}{\partial x}\right) \tag{55}$$

In the derivation of Eq. (55) it is assumed that k and μ are constants. In general, the energy equation and equation of state would be used to eliminate either p or ρ from Eq. (55); however, in the simplified approach, a polytropic relation

$$\rho = C_1 p^{1/n} \tag{56}$$

is assumed. Elimination of ρ between Eq. (55) and (56) yields the following equation for pressure

$$\frac{\mu m}{nkp} \frac{\partial P}{\partial t} = \frac{\partial^2 P}{\partial x^2} \tag{57}$$

where

$$P = p^{\frac{n+1}{n}} \tag{58}$$

The only known analytical solution of Eq. (57) is when p is nearly constant (small pressure gradient), in which case P satisfies the diffusion equation. Belyaev makes no further use of this solution but turns to the solutions of Eq. (57) for large pressure gradients. Two additional assumptions are made:

1. The initial pore pressure may be neglected in comparison to the external pressure.
2. The process is isothermal (n=1)

The ensuing equation

$$\frac{\partial p}{\partial t} = \frac{k}{2\mu m} \frac{\partial^2 p^2}{\partial x^2} \tag{59}$$

is solved for an infinite porous medium and for a porous medium of length L. Exact analytical solutions of the non-linear equation (Eq. (59)) are not known but approximate solutions may be obtained.

Infinite Medium. The approximate solution of Eq. (59) for a constant external pressure p_o is

$$p(x,t) = p_o\left(1 - \frac{x}{2.29\ C_2\sqrt{p_o t}}\right) \tag{60}$$

where

$$C_2^2 = k/2m\mu \tag{61}$$

and the pressure is seen to decrease linearly with increasing distance. The position of the advancing gas front is found by equating the expression in parentheses to zero. Hence

$$X(t) = 1.62\sqrt{kp_o t/m\mu} \tag{62}$$

The velocity of the leading edge of the penetrating gas is found by differentiating Eq. (62) with respect to time

$$v_g(t) = 0.81\sqrt{kp_o/m\mu t} \tag{63}$$

The fluid dynamic criterion for gas penetration (Eq. (14)) can be stated in an alternate manner: gas must penetrate to a depth exceeding the steady-state thermal layer thickness (α_s/r) in the time required for this layer to burn (α_s/r^2). Hence, substituting $X=\alpha_s/r$ and $t=\alpha_s/r^2$ into Eq. (62) gives the fluid dynamic criterion

$$kp_o/m\mu\alpha_s > 0.38 \tag{64}$$

A numerical example, with $k=10^{-6}$ darcy (10^{-14} cm^2), m=0.05, $\mu=3\times10^{-4}$ poise, $\alpha_s=10^{-3}$ cm^2/s, and p_o=50 atm (5 MPa) indicates that gases will, in fact, penetrate porous beds having very low permeabilities. Ignition is of course not implied.

Finite Medium of Length L. The solution of Eq. (59) for an impermeable boundary at x=L is given by Eq. (60) until the gas reaches the boundary. At that instant (t'), the boundary condition $\partial p/\partial x=0$ must be imposed, leading to the approximate solution

$$p(x,t) = p_o\left\{1 - \frac{2Lx - x^2}{L^2}\exp[-3kp_o(t - t')/m\mu L^2]\right\} \tag{65}$$

At the boundary (x=L), Eq. (65) becomes

$$p(L,t) = p_o\left\{1 - \exp[-3kp_o(t - t')/m\mu L^2]\right\} \tag{66}$$

for times greater than t'. The time required for the gas to reach the boundary is found from Eq. (60) by setting x=L and p(x,t)=0.

$$t' = \frac{m\mu L^2}{2.62\ kp_o} \tag{67}$$

An experiment was conducted to verify the above analysis. A propellant charge was prepared from a mixture of 90% AP and 10% polystyrene. Conditions of the test (pressure=25 atm [2.5 MPa], m=0.15, $k=10^{-3}$ darcy, μ=0.03 cP) were such that convective burning was precluded. Measurement of pressure at the closed end of charges of lengths 1 and 2 cm confirmed that the filtration time t' is given with reasonable accuracy by Eq. (67). This agreement is taken to justify the assumptions made in deriving Eq. (67). There are two additional applications of the analysis. Both depend on the definition of pressure relaxation time for a closed channel as

$$t_r = \frac{m\mu L^2}{3kp_o} \tag{68}$$

In this additional time after the arrival of the gas at the closed end, the end pressure increases such that

$$\frac{p_L}{p_o} = 1 - 1/e = 0.63 \tag{69}$$

One application is the statement, without further analysis, that the presence of the closed end restricts the inflow of gases and may prevent convective burning if ignition of the pores does not occur before pressure relaxation. Although not stated, this relaxation time would be the total time required for the flow to reach the end plus the additional time t_r. The other application relates to the application of Eq. (17) to a porous bed for the case of rising pressure. The limitation of Eq. (17) is the equality of the relaxation time of the bomb pressure $(p/\dot{p})$ and the time, t_r. Thus, the use of Eq. (17) to calculate velocity of the gases flowing into a blind porous bed is limited by

$$\frac{dp}{dt} < \frac{3kp^2}{m\mu L^2} \tag{70}$$

Using the values p=50 atm (5 MPa), $k=10^{-3}$ darcy, m=0.15, L=5 cm, μ=0.03 cP gives a limiting value of dp/dt of 50 atm/s.

4.3 MISCELLANEOUS

Sections 4.1 and 4.2 have summarized the available literature dealing with theoretical approaches to early stages of convective burning in single pores and porous beds. This final section presents several theoretical results which do not fit the fluid dynamic, ignition, or propagation requirements of convective burning. Nevertheless they are a part of the body of theoretical knowledge and are included for completeness.

4.3.1 Effect of Melt Layer

The issue of effectiveness of the melt layer in hindering the development of convective burning is still controversial. Two theoretical efforts to approach the problem have been reported by Belyaev (1973). In the first, the solution of the steady-state heat conduction equation for a moving solid is applied to the calculation of the melt layer thickness

$$x_{melt} = \frac{\lambda}{\rho c r} \ln \frac{T_x - T_o}{T_m - T_o} \tag{71}$$

where

λ, ρ, c = properties of the melt
T_{melt} = melting temperature
T_o = initial propellant temperature
T_x = critical temperature

Although not defined, T_x is probably the highest temperature at which the melt can exist either because of boiling or decomposition. Melt layer thicknesses were calculated from E (71) (parameter values not provided) and compared with experimentally determined critical pressures for breakdown of conductive burning. The experimental conditions involved blind, non-embedded porous beds with diameters of 10 mm, lengths ranging from 40-70 mm, permeability of 10^{-5} darcy, and loading density of 0.05 g/cm^3 (HLDCB). Results, shown in Table 8 indicate that breakdown pressure increases with calculated melt layer thickness. Moreover, the non-fusible materials such as NC, AP-based composite propellants (AP is regarded as non-fusible even though contrary evidence exists [Hightower and Price (1967 and 1968) and Boggs and Kraeutle (1969)], mercury fulminate, and lead azide, exhibit lower critical pressures than shown in Table 8. It is concluded that the melt layer is effective in impeding convective burning.

TABLE 8. Comparison of Breakdown Pressure and Melt Layer Thickness for Fusible Substances.

Substance	Melt layer thickness, μm		Critical pressure, atm (MPa)
	100 atm 10 (MPa)	300 atm 30 (MPa)	
TNT	50	18	2,000 (200)
Picric acid	35	12	800 (80)
PETN	13	3	550 (55)
RDX	5	2	250 (25)

The second theoretical approach involving the melt layer states without derivation that the threshold burning rate of a fusible propellant is given by

$$r_* = \frac{12(1 - m)(\rho - \rho')r_1}{m\bar{k}\rho} \qquad (72)$$

where

ρ = solid density
ρ' = melt density

r_1 = conductive burning rate at a pressure of 1 atm (0.1 MPa)
m = porosity
R = characteristic particle size (radius?)

No application is made to evaluation of experimental data; indeed, it is not even clear which type of experiment is relevant to Eq. (72). A final comment is made that in evaluating the Andreev number for fusible propellants, the pertinent dimension to use is the melt layer thickness.

4.3.2 Dynamic (Combustion Generated) Pressure

In the absence of a rising bomb pressure or of an imposed initial pressure difference between bomb and pore, penetration of combustion is dependent upon the usually small pressure difference generated by the combustion process. This pressure gradient is needed to cause the flow of gases away from the burning surface to the surrounding atmosphere. The derivation [Belyaev (1973) and Bakhman (1965)] is based on conservation of mass and momentum.

Mass:

$$\rho_p r = \rho' v' - \rho_1 v_1 \tag{73}$$

Momentum:

$$p' + \rho_p r v' = p_1 + \rho_p r v_1 \tag{74}$$

where the primes refer to conditions in the gas phase at the surface and the subscript 1 refers to conditions of the final combustion products. The solution of Eq. (73) and (74) for $\Delta p_d = p' - p_1$ gives

$$\Delta p_d = (\rho_p r)^2 \, (1/\rho_1 - 1/\rho') \tag{75}$$

which becomes, assuming $\Delta p_d << p_1$ and using the perfect gas equation of state:

$$\Delta p_d = \frac{(\rho_p r)^2}{p_1} \left(\frac{T_1}{M_1} - \frac{T'}{M'} \right) \tag{76}$$

where M is molecular weight. The dynamic pressure increases with the square of the mass burning rate, but even so, amounts to only a few torr for most combustibles. Mercury fulminate, with a burning rate ($\rho_p r$) of 5.9 g/cm^3-s, generates a Δp_d of 13 torr while lead styphnate, with burning rate of 100 g/cm^3-s detonates upon ignition. Little use is made of Eq. (75) since the pressure differentials, even in LLDCBs, exceed the usual values of Δp_d.

4.3.3 Effect of Pressure Oscillations

The possiblity that combustion oscillations (as from combustion instability) could aid the onset of porous burning in a porous bed was investigated theoretically by Margolin (1961). The analysis is based on an assumed polytropic flow using the equation of mass and momentum conservation.

Momentum:

$$\rho \frac{\partial v}{\partial t} + \rho v \frac{\partial v}{\partial x} = - \frac{\partial p}{\partial x} - \frac{m\mu v}{k} \tag{77}$$

Mass:

$$\frac{\partial \rho}{\partial t} + \frac{\partial}{\partial x} (\rho v) = 0 \tag{78}$$

where v is gas velocity and the other symbols have their usual meanings. For boundary conditions of $p=p_o$ at $x=-\infty$ and $p=p_o+p_1 \cos\omega t$ at the burning face of the porous bed, the results may be summarized as follows:

Conditions for onset of flow

$$\frac{p_1}{p_o}\sqrt{\frac{N}{2}} \geq 1 \tag{79}$$

where $N=2\omega a^2 \rho_o k/r^2 m\mu$ for isentropic flow and $N=p_o k\omega/r^2 m\mu$ for isothermal flow. In Eq. (79), a is sonic velocity, ω is frequency, and ρ_o is average gas density. Conditions for penetration to the depth $S=2\pi(v-4)/\omega$

$$\frac{p_1}{p_o}\sqrt{\frac{N}{2}} \geq 1 + \frac{S\omega}{2\pi r} \tag{80}$$

Minimum pressure amplitude and optimum frequency (ω_1) for penetration to

(a) depth S

$$\omega_1 = 2\pi r/S$$

$$\left(\frac{p_1}{p_o}\right)_{min} = \frac{2\sqrt{2}}{\sqrt{N(\omega_1)}} \tag{81}$$

(b) depth equal to thermal layer thickness α_p/r

$$\omega_1 = 2\pi r^2/\alpha_p \tag{82}$$

$$\left(\frac{p_1}{p_o}\right)_{min} = \sqrt{\frac{\alpha_p m_1}{2\pi p_o k}} \qquad (83)$$

In Eq. (81), $N(\omega_1)$ is the appropriate function N (isentropic or isothermal) evaluated at the frequency ω_1.

No experimental verification of the theory has been found; however, owing to the occurrence of combustion instability in many operational rocket motors, it would be interesting to investigate the possible relation to DDT through assisted convective burning.

5.0 CLOSURE

The previous sections summarize the literature describing the onset and development of convective combustion. This final section is devoted to general comments on the scope and character of the surveyed literature, an enumeration of aspects of propellant systems that favor development of convective burning, and identification of problem areas demanding further study.

5.1 OVERVIEW OF THE SCOPE AND CHARACTER OF SURVEYED LITERATURE

Soviet investigators have worked for several decades on the problems associated with early stages of transition from conductive to convective burning. Their investigations deal largely with model samples having characterizable defects rather than actual propellants with more random defects. Their sample ingredients and characteristics were chosen primarily to facilitate studying basic principles and not necessarily to optimize the mechanical or ballistic properties of operational rocket propellants. As explained in Section 2.1, the defects are characterizable as single pores with definite geometrical dimensions or as porous beds with specified porosity, permeability, pore size, particle size, and other statistical quantities. Porosities encountered are often higher than those that might be encountered with propellants. Polymeric materials appear to be used only as fuels with no attention given to their binding properties (fuel beads mixed with oxidizer particles).

Experiments using the sample/defect combination just described lead to results of a fundamental nature, but no means are provided for extending these results to operational propellants and operational conditions. Within the limitations imposed by the sample/defect combination, the scope of the Soviet studies is rather broad, covering many combinations of conditions. However, this coverage is not complete, as is

evident from an examination of the morphological chart (Table 1, page 9); for example, little work has been reported for the open/open sample in the HLDCB. In addition, there is an apparent lack of systematic approach. Examples of this are:

1. There is little effort to correlate experimental results with theory. Qualitative agreement is sometimes claimed, but no examples were found in which experimental and theoretical findings were compared graphically or tabularly.
2. There is no presentation of experimental data in which a given model sample is subjected to a spectrum of experimental conditions. Claims that this was done are supported only by qualitative statements as to the similarities or differences of results.
3. In the case of different model samples under the same conditions, the situation is better, but it is sometimes difficult to determine the conditions. An outstanding example is the frequent failure to report whether or not a length effect exists for a blind porous bed or single pore. Since many of the test samples are at least geometrically, if not fluid-dynamically blind (constructed by pouring or pressing granular ingredients into a dead-end container), this is a serious deficiency.

Most of the studies are addressed to the determination of the conditions required for the onset of convective burning, where the onset is identified by the appearance of a singularity in the experimental results, e.g., a break in the pressure vs. time curve. More elaborate experiments, designed for determining the rate of propagation of the convective combustion front, have been reported only for the LLDCB. Results of both types of experiments are generally shown in graphical form with an occasional empirical correlating equation.

A final comment concerns the manner of presentation in the Russian papers. While the language barrier may be involved, the style seems unusually terse, often sketchy, with insufficient information to support the conclusions presented or to enable the reader to draw the same conclusions. In certain instances, all relevant factors have not been considered, leading to unresolved controversies. An example is the discrepancies found for the effect of the melt layer on inhibiting convective burning. Here the effect of rate of change of pressure is completely ignored and no consideration is given to melt properties other than melting point. A further difficulty is the lack of documentation of controversy. Many authors not only fail to reference the work of others that conflicts with their own, but in several cases an individual has presented evidence that directly contradicts results he previously presented, yet no mention is made of the disparity.

5.2 ATTRIBUTES FAVORING CONVECTIVE BURNING

As described earlier (Section 2.2), there are general requirements for the breakdown of conductive burning of a sample. These are, assuming the existence of a defect(s),

1. Flow of gases into the defect or porous bed
2. Ignition of pore walls

(onset of convective burning)

3. Propagation of the ignition front at a rate greater than the conductive rate (acceleration of convective burning)

The above sequence describes ignition occurring as a result of flow of hot gases (ignores effects of adibiatic compression, thermal explosion of pore gases, and propagation of combustion into reactive pore gases). As one means of summarizing the literature survey, we list, with brief comments, those attributes of propellants which provide potential for convective burning through their relation to one or more of the above general requirements.

Attributes Favoring Gas Flow Into Defect

1. The open-open configuration provides a flow path for the initial gases to be displaced by the inflowing hot gases.

2. Gas may flow more readily into a flat, blind crack than into a round blind hole because of recirculation which provides an exit for initial gases.

3. Flow into the defect is facilitated by the embedded sample because of the difference between bomb and defect pressures at the instant the conductive burning front encounters the defect.

4. High rates of pressure rise in the bomb lead to pressure differentials which cause gases to flow into defects.

5. There is conflicting evidence concerning the effectiveness of a surface melt layer in preventing combustion gases from flowing into defects. Available data suggests that the melt layer is more effective under nearly constant pressure conditions (LLDCB) than under conditions of rising pressure (HLDCB). In regard to composite formulations, a controversy exists as to whether oxidizer or fuel melting is more important.

6. Large diameter particles, large diameter pores, and high porosities lead to high permeabilities to gas flow; all favor the inflow of gases but none provides a unique correlation for determination of onset of convective burning.

Attributes Favoring Ignition of Pore Walls

1. The pore walls of an embedded sample are more readily ignited because the initial cold pore gases are at low pressure and provide less dilution of the inflowing hot gases than would be the case for an open sample tested at high pressure.

2. Pore walls are more readily ignited by higher temperature inflowing gases. Since these inflowing gases originate close to the propellant surface, it is essentially the temperature profile in the gas phase which determines the temperature of the igniting, hot gases. Thus, it is important to consider the final flame temperature and the flame standoff distances (determined by gas phase reactions kinetics). Both features favor development of convective burning in composite propellants as compared to double-base propellants. High flame temperature alone is not sufficient, as is shown by the rsults of tests with AP/sucrose mixtures. In a series of experiments using different proportions of ingredients to provide widely varying flame temperatures, no difference was observed in the propensity toward convective burning.

3. Materials of high conductive burning rate generally transit more readily to convective burning, other conditions being the same. This, in part, is reflected by the Andreev criterion, which represents the requirement for establishing a thermal wave of the required thickness in the pore wall. Ease of propellant ignitability, as determined in arc-image or laser ignition tests, is also expected to favor flashdown into defects. Experimental results [Derr and Fleming (1973)] show a high degree of correlation between high burning rate and ease of ignitability. Thus there is a strong suggestion that similar factors govern burning rate, ignition, and flashdown. The Andreev criterion also predicts that ignition should be favored by low thermal diffusivities (low thermal conductivities and high heat capacities) but systematic experimental results are lacking.

4. Rough pore walls may ignite more readily than smooth ones because protrusions can serve as foci for hot spot development. Theoretically there is an optimum roughness dimension corresponding to thermal wave thickness. Smaller particles may experience a temperature rise but lack the thermal capacity to ignite the propellant substrate. Larger particles fail to heat sufficiently because of their higher heat capacity and higher heat losses to the adjoining propellant.

Attributes Favoring Acceleration of the Convective Front

Since the convective combustion front can only evolve following fulfillment of the first two requirements, all the conditions just enumerated favor acceleration. Additional observations are:

1. Two opposing burning propellant surfaces, as contrasted to be single propellant surface opposite an inert surface, contribute to acceleration of convective burning. On the other hand, it is interesting to note that onset of convective burning is the same for the two geometries.

2. The acceleration phase of convective burning occurs more readily in longer channels.

3. A pressure difference between bomb and defect may result in acceleration of convective burning. As noted by Taylor (1962a), very small pressure differentials can result in appreciable changes in the rate of advance of the combustion front.

5.3 GENERAL COMMENTS

It is important that many of the requirements for breakdown of conductive burning are to be found in the high energy composite propellants currently in use. The heterogeneous nature and high solids loading of these fuel/oxidizer mixtures means that, unless perfect bonding is attained between the components, there are incipient flaws already built in which can lead to convective burning under appropriate conditions. Further, the gas phase reactions of these propellants are completed at much higher temperatures and closer to the surface than is the case for homogeneous propellants (the traditional double-base propellants). Indeed, comparative data show the greater susceptibility of model composite propellants to convective burning at pressures and porosities likely to be encountered in operational situations.

Studies on burning of strained composite propellants show important differences in burning mode when the incipient defects are opened to the flow of hot gases. This suggests that care be exercised in interpreting the results of tests on damaged propellant if conditions leading to the damage are different from conditions of the test. Otherwise, closed bomb tests may fail to reveal a tendency toward convective burning, not because of absence of defects, but because of absence of adequate flow channels under closed bomb conditions.

5.4 PROBLEM AREAS

There are several general problem areas connected with early stages of convective burning. As previously emphasized, available Soviet work in the field has dealt mainly with model systems (pressed mixtures of granular solids). Although basic principles have evolved from these studies (see Section 5.2), the following appear to be important topics for further study:

1. Quantitative effect of rate of pressure rise on onset of convective burning
2. Resolution of the question of the effect of a melt layer. Properties other than melting point (e.g., boiling point, reactivity, product accumulation, thickness of melt, viscosity and surface tension of melt) should be considered.
3. Establishment of mixture laws; i.e., how are onset conditions for mixtures related to onset conditions for individual components.
4. Effects of defect geometry, particularly length and end condition (open or blind).

A second set of problems currently under investigation at NWC is related to real propellants with both characterizable and random defects. Characterizable defects (open and blind round holes) have been the subject of a systematic series of studies [Prentice (1962, 1977)] to determine conditions for flame propagation. Combustion in random defects is the subject of an investigation by Boggs (1976) in the strained propellant studies.

A third important area concerns questions of a more basic nature such as:

1. Methods of flame zone modification. In particular, are additives available which will delay, without preventing, final gas phase reactions so that cooler gases will flow into available defects?
2. Ignition properties of propellants including the measurement of thermal conductivity and specific heat of components and mixtures.
3. Determination of interactions among ingredients, i.e., the lowering of decomposition temperature of HMX by admixture with AP. Particle size and pressure effects should be determined on this and other candidate ingredients.

A major problem facing the investigation of propellants containing random defects is the absence of a means of uniquely characterizing these defects. Equally challenging is the need to relate such a characterization, obtained under static conditions, to the nature of the defect existing under actual dynamic conditions in an operational rocket motor.

BIBLIOGRAPHY

Andreev, K. K., and S. V. Chuiko. "Transition of the Burning of Explosives into an Explosiion. I. Burning of Powdered Explosives at Constant High Pressures," *Russian Journal of Physical Chemistry*, Vol. 37, No. 6 (June 1963), pp. 695-99.

Andreev, K. K. and V. V. Gorbunov. "Transition of the Burning of Explosives into an Explosion. II. Stability of the Normal Burning of Powdered Explosives," *Russian Journal of Physical Chemistry*, Vol. 37, No. 9 (September 1963), pp. 1061-65.

Andreev, K. K. "Thermal Decomposition and Combustion of Explosive Substances," translated from *Termicheskoye Razlozheniye i Goreniye Vzryvchatykh Veshchestv* (1966), pp. 1-11, 101-259, and 294-344.

Bakhman, N. N. "Calculation of the Pressure Rise at a Combustion Front," *Journal of Applied Mechanics and Technical Physics*, No. 1 (1965), pp. 97-99.

Bear, Jacob. *Dynamics of Fluids in Porous Media*. New York, American Elsevier Publishing Company, Inc. (1972).

Belyaev, A. F., and others. "Breakdown of Surface Burning of Gas-Permeable Porous Systems," *Combustion Explosion and Shock Waves*, Vol. 2, No. 3 (1966), pp. 28-34.

Belyaev, A. F., and others. "Development of Combustion in an Isolated Pore," *Combustion Explosion and Shock Waves*, Vol. 5, No. 1 (1969), pp. 4-9.

Belyaev, A. F., and others. *Transition From Deflagration to Detonation in Condensed Phases*, tr. by Israel Program for Scientific Translations. Springfield, Va., National Technical Information Service, 1973. (1975 translation.)

Bobolev, V. K., and others. "The Mechanism by Which Combustion Products Penetrate into the Pores of a Charge of Explosive Material," *Proc. Acad. Sci. USSR*, Vol. 162 (1965a), pp. 75-78.

Bobolev, V. K., and others. "Combustion of Porous Charges," *Combustion Explosion and Shock Waves*, Vol. 1, No. 1 (1965b), pp. 31-36.

Bobolev, V. K., and others. "Stability of Normal Burning of Porous Systems at Constant Pressure," *Combustion Explosion and Shock Waves*, Vol. 2, No. 4 (1966), pp. 15-20.

Boggs, T. L., and K. J. Kraeutle. "Role of the Scanning Electron Microscope in the Study of Solid Rocket Propellant Combustion, 1. Ammonium Perchlorate Decomposition and Deflagration," *Combustion Sciences and Technology*, Vol. 1 (1969), pp. 75-93.

Boggs, T. L., and others. *Combustion Bombs: A Review and Recommendation for Use in High Energy Propellant Safety (HEPS) Program.* China Lake, Calif., Naval Weapons Center, August 1976. (NWC TM 2922, publication UNCLASSIFIED.)

Boggs, T. L., and others. "The Effect of Strain on the Burning Rates of High Energy Solid Propellants," in *15th JANNAF Combustion Meeting, Monterey, Calif., 15-19 September 1978.* (CPIA Pub. 281, Vol. II, December 1976, publication UNCLASSIFIED.)

Carman, P. C. *Flow of Gases Through Porous Media.* New York, Academic Press Inc. (1956).

Derr, R. L., and R. W. Fleming. "A Correlation of Solid Propellant Arc-Image Ignition Data," in *10th JANNAF Combustion Meeting*, Naval War College, 6-10 August 1973. (CPIA Pub. 243, Vol. III, December 1973, publication UNCLASSIFIED.)

Dubovitskii, V. F., and others. "Combustion of Porous Condensed Systems and Powders," translated from *Akademiya Nauk SSSR* (1974a), pp. 1-12. (FTD-MT-24-0966-75.)

Dubovitskii, V. F., and others. "Burning of Porous Condensed Systems and Powders," translated from *Fizika Goreniya i Vzryva*, Vol. 10, No. 6 (1974b), pp. 730-736.

Frolov, Yu. V., and others. "Convective Combustion of Porous Explosives," *Combustion Explosion and Shock Waves*, Vol. 8, No. 3 (July-September 1972), pp. 296-302.

Godai, T. "Flame Propagation in to the Crack of Solid-Propellant Grain," *Amer. Inst. Aeronaut. Astronaut. J.*, Vol. 8, No. 7 (1970), pp. 1322-27.

Gorbunov, V. V. and K. K. Andreev. "Effect of the Fused Layer on the Stability of the Burning of Powdered Explosives," *Russian Journal of Physical Chemistry*, Vol. 41, No. 2 (February 1967), pp. 152-55.

Hightower, J. D. and E. W. Price. "Combustion of Ammonium Perchorate," *Eleventh Symposium (International) on Combustion.* Pittsburgh, Pa., The Combustion Institute (1967), pp. 463-72.

Hightower, J. D. and E. W. Price. "Experimental Studies Relating to the Combustion Mechanism of Composite Propellants," *Astronautica Acta*, Vol. 14, No. 1 (1968), pp. 11-21.

Kraeutle, K. J. Personal communication (March 1974).

Krasnov, Yu. K., and others. "Rate of Penetration of Combustion into the Pores of an Explosive Charge," *Combustion Explosion and Shock Waves*, Vol. 6, No. 3 (July-September 1970), pp. 262-65.

Krier, Herman and S. S. Gokhale. "Predictions of Vigorous Ignition Dynamics for a Packed Bed of Solid Propellant Grains," *Int. J. Heat Mass Transfer*, Vol. 19 (1976), pp. 915-23.

Kuo, K. K., R. Vichnevetsky, and M. Summerfield. "Theory of Flame Front Propagation in Porous Propellant Charges Under Confinement," *Amer. Inst. Aeronaut. Astronaut. J.*, Vol. 11, No. 4 (1973), pp. 444-51.

Kuo, K. K., and others. *Transient Combustion in Solid Propellant Cracks*. China Lake, Calif., Naval Weapons Center, October 1977. (NWC TP 5943, publication UNCLASSIFIED.)

Margolin, A. D. "The Burning Stability of Porous High Explosives," *Doklady Academii Nauk, Phys Chem Sect.*, Vol. 140, No. 1-6 (Sep/Oct 1961), pp. 741-42.

Margolin, A. D., and S. V. Chuiko. "Conditions for Ignition of the Pore Walls in the Burning of a Porous Charge," *Combustion, Explosion, and Shock Waves*, Vol. 1, No. 1 (1965), pp. 15-19.

Margolin, A. D. and S. V. Chuiko. "Combustion Instability of a Porous Charge with Spontaneous Penetration of the Combustion Products into the Pores," *Combustion Explosion and Shock Waves*, Vol. 2, No. 3 (1966), pp. 72-75.

Margolin, A. D. and V. M. Margulis. "Penetration of Combustion into an Isolated Pore in an Explosive," *Combustion Explosion and Shock Waves*, Vol. 5, No. 1 (1969), p. 10.

Muskat, M. and P. D. Wyckoff. *The Flow of Homogeneous Fluids Through Porous Media*. Ann Arbor, Mi., J. W. Edwards, Inc. (1946).

Payne, C. E. *Flame Propagation in Propellant Cracks*, Edwards, Calif., Air Force Rocket Propulsion Laboratory, April 1969. (AFRPL-TR-69-66, publication UNCLASSIFIED.)

Prentice, J. L. *Flashback in Solid Propellants*. China Lake, Calif., Naval Ordnance Test Station, December 1962. (NOTS TP 3009, publication UNCLASSIFIED.)

Prentice, J. L. *Combustion in Solid Propellant Grain Defects: A Study of Burning in Single- and Multi-Pore Charges.* China Lake, Calif., Naval Weapons Center, June 1977. (NWC TM 3182, publication UNCLASSIFIED.)

Scheidegger, Adrian E. *The Physics of Flow through Porous Media.* University of Toronto Press (1974).

Takata, A. N. and A. H. Wiedermann. *Initiation Mechanisms of Solid Rocket Propellant Detonation.* Washington, D.C., Air Force Office of Scientific Research, 15 August 1976. (IITRI Interim Report No. J6352, publication UNCLASSIFIED.)

Taylor, John Watson. "The Burning of Secondary Explosive Powders by a Convective Mechanism," *Trans. Faraday Society*, Vol. 58 (1962a), pp. 561-68.

Taylor, John Watson. "A Melting Stage in the Burning of Solid Secondary Explosives," *Combustion and Flame*, Vo. 6 (1962b), pp. 103-107.

Zeldovich, Ya. B. "On the Theory of Combustion of Powder and Explosives," *Journal of Experimental and Theoretical Physics*, Vol. 12, No. 11/12 (1942), pp. 498-524.

NOMENCLATURE

tant in Eq. (11)
s-sectional area of porous bed
eev number = $\rho C_s dr/\lambda$
etric parameter: 0 for rectangular slits, 1 for round holes
fraction of particles with diameter D_{pi}
tant in Eq. (11)
ific gas constant = R/M
tant in Eq. (13)
tant in Eq. (56)
tant in Eq. (61)
ific heat
tant in Eq. (13)
acteristic dimension of surface roughness
icle diameter
diameter
hydraulic diameter
hydraulic pore diameter based on mass averaged particle
eter (Eq. (8))
hydraulic pore diameter based on harmonic mass averaged
icle diameter (Eq. (9))
aulic pore diameter based on permeability measurement (Eq. (10))
coefficient of heat transfer
eability of porous bed to gas flow
th of propellant pore or porous bed
th of cooling section in pore flow
s number
kness of heated propellant layer beneath pore wall at time, τ
dy-state thickness of leated gas adjacent to propellant surface
acteristic dimension of ith combustion zone
dy-state thickness of heated propellant layer beneath pore wall
ecular weight
osity = $1 - \delta$
s burning rate
s flow rate of gas into pore
s accumulation rate of gas in pore
ameter used in analysis of oscillating pressure [Eq. (79) et seq]
selt number
ssure exponent in conductive rate "law". Polytropic exponent in
tion 4.2.1
$(n+1)/n$
ssure
ssure at closed end of porous bed
tial pressure external to porous bed
imum pressure developed in a propellant defect during combustion
amic pressure rise
t of combustion
e of heat loss from pore gas to pore wall
e of heat transfer across gas film in pore

R	Universal gas constant
Re	Reynolds number
R_v	v_{ig}/r
R_ϕ	ϕ/ϕ_*
r	Conductive burning rate, surface regression rate
T	Temperature
T_m	Melting temperature
T_o	Initial solid temperature
T_w	Pore wall temperature
T_*	Pore wall ignition temperature
t	Time
t'	Time required for gas flow to penetrate to closed end of porous bed
t_r	Pressure relaxation time of porous bed
U	Total volume of fluid flowing through a porous bed
u	Volumetric flux density in flow through porous bed
v	Linear gas velocity
v_{ig}	Linear propagation rate of ignition front into pore or porous bed
w	Smallest dimension between opposing propellant surface or between propellant and inert surfaces
X	Position of gas front in propellant defect
x	Distance from entrance of pore or porous bed

Symbols

α	Thermal diffusivity = $\lambda/\rho c$
β	Define by Eq. (30)
δ	Relative density = ρ/ρ_{tmd}
δ_t	Thickness of solid thermal layer assumed to be at constant temperature (not the same as ℓ_s)
λ	Coefficient of thermal conductivity
μ	Dynamic viscosity coefficient
ρ	Density
ρ_{tmd}	Theoretical maximum density; density of substance having zero porosity
τ	Time interval available for hot gases to heat pore wall
τ_p	Characteristic heating time of particle
τ_s	Time required to reach steady-state temperature distribution in pore wall
τ_*	Time required to heat pore wall to ignition temperature T_*
ϕ	= $\rho_s r d_p$ for single round pore = $\rho_s r d_h$ for porous bed where d_h is hydraulic diameter (see d_1, d_2, and d_3)
ω	Angular frequency of oscillating pressure

Subscripts (except where otherwise noted)

c	Cooled gas
g	Gas phase
h	Hot gas
o	Initial
p	Particle
s	Solid phase
*	Threshold value

INITIAL DISTRIBUTION

1 Director of Navy Laboratories
8 Naval Air Systems Command
- AIR-30212 (2)
- AIR-330 (1)
- AIR-330B, Robert H. Heitkotter (1)
- AIR-330D (1)
- AIR-536 (1)
- AIR-954 (2)

4 Chief of Naval Operations
3 Chief of Naval Material
- MAT-03 (1)
- MAT-03PB (1)
- J. Amlie (1)

8 Naval Sea Systems Command
- SEA-03 (1)
- SEA-033 (1)
- SEA-0331, Murrin (1)
- SEA-0331B, Cassel (1)
- SEA-0332 (1)
- SEA-09G32 (2)
- A. Amster (1)

11 Chief of Naval Research, Arlington
- ONR-100 (1)
- ONR-102 (1)
- ONR-401 (1)
- ONR-420 (1)
- ONR-472 (1)
- ONR-473 (1)
  - James R. Patton, Jr. (1)
- N. Basdekas (1)
- R. Miller (1)
- L. Peebles, Jr. (1)
- J. Smith (1)

4 Naval Ordnance Station, Indian Head
- Code FS71C, Alan Roberts (1)
- Code 5251K, F. Robbins (1)
- Peter L. Stang (1)
- Technical Library (1)

3 Naval Postgraduate School, Monterey
  Code 57, Fuhs (1)
  Code 57NT, Netzer (1)
  Technical Library (1)
6 Naval Research Laboratory
  Code 2021 (1)
  Code 6130, Chemistry Division (1)
  W. Bascom (1)
  W. Moniz (1)
  J. Schnui (1)
  Technical Library (1)
3 Naval Surface Weapons Center, White Oak
  WR-10, S. Jacobs (1)
  WR-13, R. Bernecker (1)
  G. B. Wilmot (1)
1 Naval Underwater Systems Center, Newport (Code 5B331, Robert S. Lazar)
1 Naval Weapons Evaluation Facility, Kirtland Air Force Base (Code 401)
3 Navy Strategic Systems Project Office
  SP-2731, Roy Kinert (1)
  NSP-2731, Throckmorton (1)
  J. Kincaid (1)
1 Army Materiel Development and Readiness Command (DRCDE-DW, Stephen R. Matos)
1 Army Missile Research and Development Command, Redstone Arsenal (DRDMI-RK, Dr. R. G. Rhoades)
4 Army Research and Development Command, Dover
  DRDAR-SCA-PE, L. Stiefel (1)
  LCWSL, C. Lenchitz (1)
  R. Walker (1)
  R. Zastrow (1)
2 Army Armament Research and Development Center
  SMUPA-TS-TS, J. Picard (1)
  J. Hershkowitz (1)
5 Army Ballistic Research Laboratories, Aberdeen Proving Ground
  DRDAR-BLP
    Austin W. Barrows (1)
    Ingo W. May (1)
  R. Frey (1)
  D. Kooker (1)
  L. Watermeier (1)
1 Rock Island Arsenal (Edward Haug)
1 Air Force Armament Laboratory, Eglin Air Force Base (DLDL, Otto K. Heiney)
1 Air Force Rocket Propulsion Laboratory, Edwards Air Force Base (DTSC, Wilbur C. Andrepont)
1 Air Force Rocket Propulsion Laboratory, Edwards Air Force Base (Daweel George)

2 Bolling Air Force Base
  NA, Thomas C. Meier (1)
  Joseph F. Masi (1)
12 Defense Documentation Center
1 National Aeronautics and Space Administration (Code RP, Frank W. Stephenson, Jr.)
3 George C. Marshall Space Flight Center
  SE-ASTN-PEA, John Q. Miller (1)
  Richard J. Richmond (1)
  B. Shackelford (1)
1 Lewis Research Center (Richard J. Priem)
1 Lyndon B. Johnson Space Center (EP, Joseph G. Thibodaux)
2 Aerojet-Solid Propulsion Company, Sacramento, CA via AFPRO
  Dept 4350, M. Ditore (1)
  A. Oberth (1)
1 Aeronautical Research Associates of Princeton, Inc., Princeton, NJ (E. S. Fishburne)
1 Aerospace Corporation, Los Angeles, CA (Ellis M. Landsbaum)
1 Allegany Ballistics Laboratory, Cumberland, MD (Roy R. Miller)
1 Analy Syn Laboratory, Paoli, PA (V. Keenan)
1 Atlantic Research Corporation, Alexandria, VA (Merrill K. King)
1 Battelle Memorial Institute, Columbus, OH (Abbott A. Putman)
1 Brigham Young University, Provo, UT (673/WldB, L. Douglas Smoot)
2 California Institute of Technology, Pasadena, CA
  N. Cohen (1)
  W. Knauss (1)
1 California State University Sacramento, Sacramento, CA (School of Engineering, Frederick H. Reardon)
1 Calspan Corporation, Buffalo, NY (Edward B. Fisher)
1 Carnegie Institute of Technology, Pittsburgh, PA (M. Gurtin)
1 Chemical Propulsion Information Agency, Applied Physics Laboratory, Laurel, MD (Thomas W. Christian)
4 Georgia Institute of Technology, Atlanta, GA
  Edward W. Price (1)
  R. Sigman (1)
  Warren C. Strahle (1)
  Ben T. Zinn (1)
1 General Applied Science Laboratory, Westbury Long Island, NY (John Erdos)
1 General Dynamics Corporation, Pomona Division, Pomona, CA (Paul L. Boettcher)
1 Gough Associates, Portsmouth, NH (P. Gough)
6 Hercules Incorporated, Bacchus Works, Magna, UT
  McK. Anderson (1)
  Merrill W. Beckstead (1)
  B. Hopkins (1)
  D. Pilcher (1)
  Ronald L. Simmons (1)
  J. Thatcher (1)

1 IIT Research Institute, Chicago, IL (T. Eichler)
1 Institute for Defense Analyses, Arlington, VA (R. C. Oliver)
2 Jet Propulsion Laboratory, Pasadena, CA
Fred E. C. Culick (1)
Leon D. Strand (1)
4 Lockheed Missiles and Space Company, Sunnyvale, CA
J. Linsk (1)
H. Marshall (1)
R. Martinson (1)
V. Orr (1)
3 Los Alamos Scientific Laboratory, Los Alamos, NM
C. Forest (1)
R. Peeters (1)
L. Smith (1)
1 Northwestern University, Evanston, IL (J. Achenback)
2 Pennsylvania State University, University Park, PA
Applied Research Lab., Gerard M. Faeth (1)
K. Kuo (1)
2 Princeton University Forrestal Campus Library, Princeton, NJ
Leonard M. Caveny (1)
Martin Summerfield (1)
1 Propulsion Sciences Incorporated, Melville, NY (Vito Agosta)
1 Purdue University, West Lafayette, IN (School of Mechanical Engineering, John R. Osborn)
2 Rockwell International Corporation, Canoga Park, CA
BA08, Joseph E. Flanagan (1)
Dept. 589-197-SS11, Carl L. Oberg (1)
1 Rockwell International Corporation, McGregor, TX (William G. Haymes)
1 Rohm and Haas Company, Huntsville Defense Contract Office, Huntsville, AL (H. Shuey)
1 Science Applications, Inc., Woodland Hills, CA (R. B. Edelman/Suite 423)
1 Shock Hydrodynamics Incorporated, Sherman Oaks, CA (W. H. Anderson)
1 Southwest Research Institute, San Antonio, TX (Fire Research Section, William H. McLain)
1 Stanford Research Institute, Menlo Park, CA (D. Curran)
1 TRW Systems, Inc., Redondo Beach, CA (A. C. Ellings)
2 Thiokol Corporation, Huntsville Division, Huntsville AL
David A. Flanigan (1)
M. Weiner (1)
2 Thiokol Corporation, Wasatch Division, Brigham City, UT
C. M. Mihlfeith (1)
John A. Peterson (1)
1 United Technologies Corporation, East Hartford. CT (R. H. W. Waesche)
3 United Technologies Corporation, Sunnyvale, CA
Chemical Systems Division, Robert S. Brown (1)
E. Francis (1)
B. Iwanciow (1)